INFLATIONARY PREDICTIONS IN EXTENSIONS TO THE STAROBINSKY MODEL

A thesis submitted to the University of Sheffield

for the degree of Doctor of Philosophy

March 2018

Laura E. Paduraru

School of Mathematics and Statistics

To my parents

Contents

The University of Sheffield

Laura E. Paduraru
For the Degree of Doctor of Philosophy
Inflationary predictions in Extensions to the Starobinsky Model
August 8, 2018

Cosmology is the science trying to understand the nature of the Universe and its evolution. Inflation, the theory proposing a period of accelerated expansion in the very early stages of the Universe, aims to answer a number of questions arising in the standard Big Bang cosmology, like the flatness problem, the horizon problem and the origin of large-scale structures.

Inflation is usually assumed to be driven by scalar fields. The aim of this thesis is to investigate predictions of the Starobinsky model and its extensions, where an inflationary phase is driven by corrections to General Relativity. First proposed in 1980 by A. Starobinsky, he showed that corrections to General Relativity could drive an accelerated expansion in the early Universe. Here we extend this theory by adding a matter field which influences the inflationary dynamics and discuss how the predictions are altered. We find that the extended model is in excellent agreement with the latest observational results by the Planck collaboration. We also study the running of the spectral index and higher orders parametrisations of the power spectrum and compare them to predictions in other inflationary models.

Finally we are investigating the theory of reheating in the extended Starobinsky model. We show that the corrections to General Relativity have an effect on the duration of reheating during perturbative reheating and that they reduce the efficiency of particle production in parametric resonance reheating. Thus it becomes clear that these effects need to be taken into account when comparing theoretical results to data.

Preface

- Chapter 1 contains introductory material and a summary of important concepts.

- Chapter 2 contains an introduction to the Starobinsky model.

- Chapter 3 is based on the published work in Physical Review D in May 2015 with Carsten van de Bruck [1]. All new analytical and numerical calculations and production of figures were done by the Author.

- Chapter 4 is based on work done in collaboration with Carsten van de Bruck and Chris Longden. All numerical calculations and figures presented in this Chapter were conducted by the Author.

- Chapter 5 is based on the published work in the International Journal of Modern Physics in June 2016 [2], done in collaboration with Carsten van de Bruck and Peter Dunsby. The numerical calculations were performed by the Author and Carsten van de Bruck. Other contributions included numerical simulations and pieces of analytical work.

- Chapter 6 is a summary of the three projects.

Acknowledgements

First of all I would like to thank my supervisor Carsten, for all the interesting conversations and for keeping my love of Cosmology alive. It is because of his immeasurable patience that I am here, still following my passion.

Thank you to my collaborators, Chris Longden and Peter Dunsby, who have brought new ideas and perspective into my path.

And I of course have to thank my mother for her relentless support and belief in me. I carry so much of her in me, this is as much her accomplishment as it is mine.

Lastly, thank you to all who have supported and tolerated me on this journey. Your help is the cornerstone of my achievements. I do not know where I would be if you had not walked alongside me.

Chapter 1

Introduction

1.1 The Beginning - General Relativity

From the first moments of awareness as a species, people have incrementally pushed the limits of their understanding. From a flat Earth, to the acceptance of a heliocentric model, any advancement in scientific understanding has meant both a deeper insight into the Universe and more questions to be answered. One such big event was the perfecting of Einstein's Theory of General Relativity [3, 4], where he introduced the Einstein field equations. In his 1917 work [5], Einstein introduces the 'cosmological constant' in an attempt to find a solution to his equations which would account for a closed, static Universe. His 'biggest mistake', as he referred to it, is introduced to counter the effects of gravity, which causes all structures in the Universe to collapse.

In order to verify the theory that marked the culmination of his work on General Relativity, Einstein described three distinct instances, where his new approach was able to explain satisfactorily what had previously been considered anomalous or inexplicable. Any and all theoretical extensions to the Theory of General Relativity are

required to satisfy these three tests.

Test One: The perihelion procession of Mercury

The first test concerns the perihelion precession of the planet Mercury. Until the advent of Einstein's new theory, Isaac Newton's *Philosophiae Naturalis Principia Mathematica*, published in 1687, provided the most comprehensive set of principles to describe the physics of both the earth and the cosmos in which it is located. This groundbreaking piece of work changed astronomy profoundly with the three famous laws of motion and the law of gravitation.

Newtonian physics was applied to the planetary motions. The French mathematician Le Verrier found in 1841 that Mercury's perihelion procession could not be explained by the laws of motion and gravitation in their current formulation. A small shift occurred in the perihelion every century; this was calculated to be about 38 arcseconds [6]. In 1895, Simon Newcomb corrected this angle slightly, adding another 10% to the unexplained shift.

Before Einstein's explanation of the anomaly in 1915, there was no widely accepted answer to the problem. The Theory of General Relativity not only provided a full working explanation for Le Verrier's anomaly with no need for a phantom planet, it also helped Einstein to further correct the angle of the perihelion shift. Still in agreement with the currently accepted value of 45 ± 5, he calculated it as 43 arcseconds per century [7].

Test Two: Deflection of light by massive bodies

Light waves travelling through space are affected by space-time curvature. A massive body affects the path of light within its area of influence, causing it to bend, due to the

way in which space-time is affected by the gravitational energy of that body. In 1804, the German physicist Johann Georg von Soldner described this phenomenon through a calculation of the deflection of solar light rays in our solar system.

Using the Theory of Relativity, Einstein corrected the deflection calculation in 1916. According to General Relativity, the effect of gravity on light was 2 times more significant than previously thought.

Test Three: Gravitational redshift due to high density massive objects

The third classic test of the Theory of General Relativity is the gravitational redshift of light close to high density massive bodies. Early on, Einstein proposed this as a test of his new theory. It was not actually until 1960, when Rebka, Snider & Pound at Harvard university examined how photons emitted by atoms are affected by the Earth's gravitational field, that the final test of Einstein's theory was verified [8].

1.2 The Universe as We See It

1.2.1 Expanding Space

From Einstein's work, studies followed in the early decades of the 20th century, which led to the understanding that the Universe is expanding. Vesto Slipher's paper from 1917 presents observational results of the red-shifting of the light coming from the majority of galaxies that he had included in his 4 year study [9]. His work is followed by that of Hubble in 1929 [10, 11], where a linear relation between galaxy distance from the Solar System and observed redshift is introduced:

$$v = H_0 d, \tag{1.1}$$

with v the recession velocity between the galaxies, d the distance between the observables and H_0 the Hubble constant.

The relation between distance and the recession velocity of galaxies had been derived by Lemaître in 1927 [12]. He combined the ideas of de Sitter and Einstein as follows. In 1917, de Sitter proposed a solution to Einstein's equations [13], which assumed no matter in the Universe and hence zero density; Einstein's model assumed a uniform distribution of matter on large scales and a static Universe and it led to a relationship between matter density and the radius of the Universe. Lemaître's work brought the two together and he derived the solution to a Universe with constant mass, that had a radius which was allowed to vary and expand without bounds. In his later work [14, 15, 16], he proposed that this variation in size meant the Universe started from a single point.

Lemaître independently obtained the same results that Friedmann had in the early 1920s. Friedmann published two papers exploring the possibilities of a space-time which could either be static, or dynamic, which could grow or contract with time. He derived the equations describing the process, in what we now refer to as the Friedmann equations [17, 18].

1.2.2 Cosmological Microwave Background

The scientific understanding of the Universe changed dramatically from a Newtonian, classically dynamical model of planetary motion, to a world where space-time-energy affect each other. Further probing into the structure of the Universe was intimately related to an increase in technological development.

First discovered by accident by Penzias and Wilson at the Bell Laboratory in 1965

[19], the CMB is left behind after the cooling of the thermal background radiation. In the original work, the CMB temperature was measured at $3.5 \pm 1K$ in all directions, indicating that we live in an isotropic Universe. The latest value of the CMB temperature is $2.73K$ with inhomogeneities of order $10^{-5}K$ [20]. Dicke was leading a group planning to measure the CMB, when the results from Penzias and Wilson came out; his group also published a paper on the same results [21] that year.

The existence of the CMB was first proposed by Alpher, Bethe and Gamow [22]. The CMB has a blackbody spectrum. This thermal radiation is the relic of a much hotter, denser time. Alongside Hubble's law, it stands as important supporting evidence to the theory proposed by Lemaître [14, 15, 16], that the Universe could have started from a singularity, later referred to as the Big Bang.

Shortly after the discovery of the CMB, Sachs and Wolfe predicted deviations from a perfect blackbody spectrum which would be caused by density perturbations on the surface of last scattering [23].

Observations done by COBE published in 1992 revealed that the background radiation has a blackbody form, but exhibits small temperature anisotropies on large scales with an amplitude of $\Delta T/T \simeq 10^{-5}$ [24],[25].

At the turn of the millennium, the WMAP satellite took on a mission to take precise measurement of the CMB, the final results after 12 years were published in [26]. The responsibility of observing the CMB was taken then by the Planck satellite, which brought us the most comprehensive measurement of the densities of matter and energy in the Universe to date [20].

1.2.3 Concordance Model in Cosmology

The current concordance model in cosmology is the **ΛCDM** model; It models the Universe after the Big Bang with a positive cosmological constant, which drives the accelerated expansion of the Universe at late times and introduces dark matter as the dominant matter component. The cosmological constant Λ represents, the dark energy in the Universe and it was originally proposed by Einstein to allow for a static solution to his field equations. Although the reason for its introduction was later invalidated by Hubble's discovery of distancing galaxies in the local group, it is now used to model the late time accelerated expansion of the Universe.

1.2.4 Cosmological Principle

Most cosmological work is done on the assumption of the Cosmological Principle - namely that the Universe is homogeneous and isotropic on large scales. Homogeneity refers to its property of translational invariance of statistical properties and isotropy to its rotational invariance. A Universe which is everywhere isotropic is also homogeneous, but the corollary does not hold true. On small scales the structure in the Universe does not appear homogeneous and isotropic - consider galaxy clusters and voids - however on scales larger than $\approx 100h^{-1}Mpc$, in ΛCDM, the matter distribution is statistically homogeneous. One way to look at this is to consider the small-scale structure as perturbations of the Universe.

The assumption of homogeneity is at the core of the ΛCDM model, together with the Friedmann-Robertson-Walker metric (which we will introduce later in equation (1.7). Combining ΛCDM with a period of accelerated expansion in the very early Universe, i.e. inflation, predicts density fluctuations which occur on all scales. The

scale dependence of these perturbations is quantified by the spectral index n_s of the primordial power spectrum - for a spectral index equal to one, the spectrum is scale invariant. The latest Planck collaboration results place the value of $n_s \approx 0.9682 \pm 0.0062$ [20]. The density fluctuations are nearly scale invariant.

1.3 Cosmological Equations

So far, we have had a qualitative look at the evolution of our understanding of what happens in the Universe. Before proceeding our discussion, let us introduce Einstein's equations, which are a fundamental instrument in talking about space and gravitation.

The beauty in the theory of relativity lies in the matching of mathematical predictions to observable effects. This is even more elegant, as we are trying to describe the very big, by starting with one of the most fundamental descriptions of space.

1.3.1 Curvature

We take a few steps into the geometric theory underlying our work in General Relativity and extensions. We start by defining a manifold space $(M, g_{\mu\nu})$, which for our purposes has dimension 4, with metric tensor $g_{\mu\nu}$ that defines distance on the manifold. The coordinate basis on M is defined by the tangent vectors at all points in that space:

$$\hat{e}_i = \frac{\partial}{\partial x^i} = \partial_i, \quad i \in \{1, 2, 3, 4\} \tag{1.2}$$

We define $g = det(g_{\mu\nu})$ to be the determinant of the metric tensor.

We will need the Christoffel coefficients, which are related to the metric by:

$$\Gamma^{\mu}_{\alpha\beta} = \frac{g^{\mu\nu}}{2} \left(\partial_\beta g_{\nu\alpha} + \partial_\alpha g_{\beta\nu} - \partial_\nu g_{\alpha\beta}\right) \tag{1.3}$$

where the upper index notation $g^{\mu\nu}$ denotes the inverse of the metric as in $g^{\mu\nu}g_{\nu\gamma} = \delta^{\mu}_{\gamma}$, where δ^{μ}_{γ} is the Kroneker delta. Using the Christoffel coefficients, we define the Ricci tensor:

$$R_{\mu\nu} = \Gamma^{\alpha}_{\nu\mu,\alpha} - \Gamma^{\alpha}_{\alpha\mu,\nu} + \Gamma^{\alpha}_{\alpha\beta}\Gamma^{\beta}_{\nu\mu} - \Gamma^{\alpha}_{\nu\beta}\Gamma^{\beta}_{\alpha\mu} \tag{1.4}$$

that we use to define the Ricci scalar:

$$R = g^{\alpha\beta}R_{\alpha\beta}, \tag{1.5}$$

which holds information about the curvature of the space.

We define a covariant derivative of T^{μ}_{ν}, a tensor of rank $(1,1)$ in our space as:

$$\nabla_{\sigma}T^{\mu}_{\nu} = \partial_{\sigma}T^{\mu}_{\nu} + \Gamma^{\mu}_{\sigma\lambda}T^{\lambda}_{\nu} - \Gamma^{\lambda}_{\sigma\nu}T^{\mu}_{\lambda}. \tag{1.6}$$

We have looked at some general geometric quantities which will help us in our analysis later. In the next section we will make a choice of metric, that will be used in the rest of this thesis.

1.3.2 FRW Metric

The line element of a space that is homogeneous and isotropic takes the following Friedmann-Robertson-Walker (FRW) form:

$$\begin{aligned} ds^2 &= g_{\mu\nu}dx^{\mu}dx^{\nu} \\ &= -dt^2 + a^2(t)\left[\frac{dr^2}{1-Kr^2} + r^2(d\theta^2 + \sin^2\theta d\phi^2)\right] \end{aligned} \tag{1.7}$$

where the metric in cartesian coordinates for the case $K = 0$ is :

$$g_{\mu\nu} = diag(-1, a^2, a^2, a^2), \tag{1.8}$$

t is cosmic time and $a(t)$, called the scale factor, is a function of cosmic time and describes the relative size of objects; an increase in the scale factor describes the expansion of the Universe, however the relative positions of cosmological objects remains

the same in the absence of external forces acting on the system. The evolution of the scale factor $a(t)$ is determined by the Einstein Equations, which we will look at in the following section.

The parameter K determines the geometry of space:

$$\begin{aligned} K > 0 \quad & for\ a\ closed\ Universe \\ K = 0 \quad & for\ a\ flat\ Universe \\ K < 0 \quad & for\ a\ open\ Universe \end{aligned} \tag{1.9}$$

In the FRW metric, the nonzero components of the Ricci tensor are:

$$\begin{aligned} R_{00} &= -3\frac{\ddot{a}}{a}, \\ R_{11} &= \frac{a\ddot{a} + 2\dot{a}^2 + 2K}{1 - Kr^2}, \\ R_{22} &= r^2(a\ddot{a} + 2\dot{a}^2 + 2K), \\ R_{33} &= r^2(a\ddot{a} + 2\dot{a}^2 + 2K)\sin^2\theta \end{aligned} \tag{1.10}$$

and the Ricci scalar is:

$$R = 6\left[\frac{\ddot{a}}{a} + \left(\frac{\dot{a}}{a}\right)^2 + \frac{K}{a^2}\right]. \tag{1.11}$$

Einstein's Equations

The Einstein field equations relate the effect of energy and momentum on space-time and take the following tensor form:

$$G_{\mu\nu} + \Lambda g_{\mu\nu} = \kappa T_{\mu\nu}. \tag{1.12}$$

Here $G_{\mu\nu}$ is the Einstein tensor defined by:

$$G_{\mu\nu} = R_{\mu\nu} - \frac{1}{2}g_{\mu\nu}R, \tag{1.13}$$

where $R_{\mu\nu}$ is the Ricci curvature tensor, R is the scalar curvature, $g_{\mu\nu}$ is the metric tensor, Λ is the cosmological constant and $T_{\mu\nu}$ is the stress-energy tensor; we use the

factor $\kappa = M_{PL}^{-2} = (8\pi G_N)/c^4$, which is related to the reduced Planck mass, with G_N the gravitational constant and c the speed of light in vacuum.

We note that the Einstein tensor has zero divergence:

$$\nabla_\mu G^{\mu\nu} = 0. \tag{1.14}$$

The Einstein equations help describe the spacetime geometry, by describing the metric tensor for a given stress-energy configuration $T_{\mu\nu}$. The Einstein field equations are non-linear partial differential equations. In order to get exact solutions to the equations, we make use of symmetry considerations.

1.3.3 Einstein-Hilbert Action and Friedmann Equations

The Einstein field equations can be derived from applying the principle of least action on the Einstein-Hilbert action. The Einstein-Hilbert action for a Universe with matter fields S_M and cosmological constant is:

$$\begin{aligned} S =& \frac{1}{2\kappa} \int d^4x \sqrt{-g} \left[R + \Lambda\right] + S_M \\ =& S_G + S_M \end{aligned} \tag{1.15}$$

where $d^4x\sqrt{-g}$ is the invariant volume element, R is the Ricci scalar and Λ is the cosmological constant. For the rest of this section we will work with natural units where $\kappa = 1$, however there will be certain analytic sections in this thesis where we will reintroduce it. In the numerical simulations done in Chapters 3, 4, 5, we work in natural units.

We derive the Einstein equations from the Einstein-Hilbert action, by setting the variation of the action in (1.15) with respect to the inverse metric $g^{\mu\nu}$ to be zero. The inverse metric $g^{\mu\nu}$ follows the relation $g^{\mu\beta}g_{\beta\nu} = \delta^\mu_\nu$ and the variation of metric

is related to the variation of the inverse metric by $\delta g_{\mu\nu} = -g_{\mu\alpha}g_{\nu\beta}\delta g^{\alpha\beta}$. We will first derive the variation of the gravitational part of the action, denoted by S_G:

$$\begin{aligned}\delta S_G &= \frac{1}{2}\int d^4x \left[\sqrt{-g}(\delta R_{\mu\nu})g^{\mu\nu} + \sqrt{-g}(R_{\mu\nu} + \Lambda g_{\mu\nu})\delta g^{\mu\nu} + R\delta(\sqrt{-g})\right], \\ &= \frac{1}{2}\int d^4x \left[\sqrt{-g}(R_{\mu\nu} + \Lambda g_{\mu\nu})\delta g^{\mu\nu} + R\left(-\frac{1}{2}\sqrt{-g}g_{\mu\nu}\delta g^{\mu\nu}\right)\right],\end{aligned} \tag{1.16}$$

In the last term we have used the fact that:

$$\delta(\sqrt{-g}) = \frac{1}{2}\sqrt{-g}g^{\mu\nu}\delta g_{\mu\nu} = -\frac{1}{2}\sqrt{-g}g_{\mu\nu}\delta g^{\mu\nu}. \tag{1.17}$$

The first term in (1.16) can be rewritten as the integral over the natural volume element of a quantity; thus it only contributes a surface term, which we set to be equal to zero.

We can see that the total variation of the gravitational action is:

$$\delta S_G = \frac{1}{2}\int d^4x\sqrt{-g}\left(R_{\mu\nu} - \frac{1}{2}Rg_{\mu\nu} + \Lambda g_{\mu\nu}\right)\delta g^{\mu\nu}. \tag{1.18}$$

Let us now turn our attention to the matter part of the action in (1.15), S_m. We define the energy-momentum tensor, with respect to the variation of the matter action:

$$T_{\mu\nu} = -\frac{2}{\sqrt{-g}}\frac{\delta S_M}{\delta g^{\mu\nu}}. \tag{1.19}$$

The energy-momentum tensor contains information about the energy density and the pressure of the matter fields in (1.15).

In the final step, we refer back to (1.15) and minimise the variation of the action with respect to the inverse of the metric, $\delta S = 0$. Using (1.18) and (1.19) leads us back to the Einstein equations defined in (1.12), written in natural units:

$$G_{\mu\nu} + \Lambda g_{\mu\nu} = T_{\mu\nu}. \tag{1.20}$$

We have included the cosmological constant for completion in our discussion so far. For the rest of this thesis we will set $\Lambda = 0$, as we are mostly concerned with the

evolution of the very early Universe, where Λ is negligible and the Einstein equations take the following form:

$$R_{\mu\nu} - \frac{1}{2} g_{\mu\nu} R = T_{\mu\nu}. \tag{1.21}$$

We now turn our attention to cosmology and we will model the behaviour of the matter-energy content in an isotropic Universe by a perfect fluid. In the perfect fluid description of the system, there are no self-interaction terms and thus it can be completely described by its density and pressure. In comoving coordinates, i.e. in the fluid rest frame, the 4-velocity of the fluid u_μ is:

$$u^\mu = (1, 0, 0, 0). \tag{1.22}$$

We will work in the FRW metric and write the energy-momentum tensor in the fluid rest frame:

$$\begin{aligned} T_{\mu\nu} &= (\rho + p)\, u_\mu u_\nu + p g_{\mu\nu}, \\ T_{\mu\nu} &= \begin{pmatrix} \rho + p & 0 & 0 & 0 \\ 0 & 0 & 0 & 0 \\ 0 & 0 & 0 & 0 \\ 0 & 0 & 0 & 0 \end{pmatrix} + \begin{pmatrix} -p & 0 & 0 & 0 \\ 0 & p & 0 & 0 \\ 0 & 0 & p & 0 \\ 0 & 0 & 0 & p \end{pmatrix} = \begin{pmatrix} \rho & 0 & 0 & 0 \\ 0 & p & 0 & 0 \\ 0 & 0 & p & 0 \\ 0 & 0 & 0 & p \end{pmatrix}, \end{aligned} \tag{1.23}$$

with trace:

$$T = T^\nu_\nu = T_{\mu\nu} g^{\mu\nu} = diag(\rho, p, p, p) \cdot diag(-1, 1, 1, 1) = -\rho + 3p. \tag{1.24}$$

As we can see, in the FRW metric the density and pressure are:

$$\begin{aligned} -T^0_0 &= \rho \\ T^i_j &= p \delta^i_j, \end{aligned} \tag{1.25}$$

Referring back to the Einstein equations (1.21), from the 00-component we get the Friedmann equation:

$$H^2 = \frac{\rho}{3} - \frac{K}{a^2}, \tag{1.26}$$

where we define the Hubble expansion rate:

$$H = \frac{\dot{a}}{a}. \tag{1.27}$$

Taking the trace of (1.21) and using (1.26) we get the acceleration equation:

$$\frac{\ddot{a}}{a} = -\frac{\rho + 3p}{6}. \tag{1.28}$$

We take a moment here to note that we can now relate the curvature of the universe to its density. To that effect we define a density parameter and the critical density respectively:

$$\Omega = \frac{\rho}{\rho_c}, \quad \rho_c = 3H^2. \tag{1.29}$$

The critical density is the density for which the universe is flat. We can rewrite the Friedmann equation (1.26) as:

$$\Omega - 1 = \frac{K}{a^2 H^2}. \tag{1.30}$$

We also derive from (1.14) and (1.20), the conservation equation:

$$\nabla_\mu T^\mu_\nu = 0. \tag{1.31}$$

We calculate at the zero-component of the conservation equation, using the definition of the covariant derivative in (1.6):

$$\begin{aligned} \nabla_\mu T^\mu_0 &= 0, \\ \partial_\mu T^\mu_0 + \Gamma^\mu_{\mu\lambda} T^\lambda_0 - \Gamma^\lambda_{\mu 0} T^\mu_\lambda &= 0, \\ \partial_0 T^0_0 + \Gamma^\mu_{\mu 0} T^0_0 - \Gamma^\lambda_{\lambda 0} T^\lambda_\lambda &= 0, \\ -\dot{\rho} - 3\frac{\dot{a}}{a}(\rho + p) &= 0, \end{aligned} \tag{1.32}$$

where we have used the fact that T^{μ}_{ν} has only diagonal elements and the Christoffel symbols (1.3) of the FRW metric $\Gamma^{\mu}_{\mu 0} = \frac{\dot{a}}{a}$. The dot derivatives are with respect to cosmological time. We have calculated the continuity equation or fluid equation:

$$\dot{\rho} + 3H(1+\omega)\rho = 0, \tag{1.33}$$

where $\omega = p/\rho$ is the equation of state of the matter in the system.

For our analysis in subsequent Chapters, we will assume the curvature of space $K = 0$ and that it does not play a role in the evolution of the Universe.

1.4 Inflation

Inflation has been proposed as a solution to a series of problems with the Big Bang theory. It was first introduced as a cosmological theory in the 1980s in [27], [28], [29], [30]. Inflation came as an extension to an already existing cosmological model.

1.4.1 Issues with the Standard Big Bang Theory

The standard Big Bang Theory produces a series of predictions about the Universe we live in that require a very high level of fine tuning to match observation. Cosmic inflation, a proposed period of accelerated expansion in the Early Universe (we will define inflation in detail later in Section 1.4.2) was originally proposed as a solution to the problems of the standard Big Bang theory. We outline them in the following subsections and discuss how inflation solves them.

Flatness Problem

In the standard big-bang theory, the acceleration of the scale factor is always negative, $\ddot{a} < 0$, implying that $\dot{a}$ becomes smaller as time progresses. This scenario implies that for $K = 0$, the density parameter in (1.29) grows further and further away from unity. However, the observational value for the density parameter Ω is very close to one. To get such a universe from standard cosmology would imply fine-tuning in the initial conditions. With inflation, the curvature term on the right hand side term of the Friedman equation (1.26) goes to zero as a increases and the universe is driven to being flat. After inflation ends, we enter a period where the energy density starts to increase, but as long as inflation lasts longer than ~ 50 e-folds, then Ω will be close to one even to the present day (we will define the concept of e-folds later in 1.42).

Horizon Problem

As we have discussed in Section 1.2.2, we observe the cosmic microwave background (CMB) with a temperature of $2.73K$ and inhomogeneities of order $10^{-5}K$ [20]. According to the Big Bang theory, these photons have traveled from the last scattering surface. The surface of last scattering is the locus of points from which the photons we are now observing have originated. The photons traveled since the time of recombination, when the universe became cool enough for protons to combine with electrons to create hydrogen, resulting in a density drop of free charged particles and allowing light to travel freely. As we would expect from thermodynamic considerations, only photons corresponding to regions in causal contact at the time of last scattering would have the same temperature today. However, we observe the same temperature in regions which, according to the standard Big Bang theory would never have been in causal

contact.

During inflation, physical wavelengths are pushed outside the Hubble radius. After inflation, they re-enter it. In other words, during inflation, causally connected regions can get stretched out of the Hubble radius, but after the end of inflation, they shrink back inside, thus potentially solving the horizon problem. The requirement is that, the comoving distance photons can travel before decoupling, needs to be much larger than that after decoupling. This is true for inflation lasting more than ~ 50 e-folds.

Origin of large-scale structure

The anisotropies in the CMB can be described in terms of the amplitude of the spherical Fourier modes of the observed sky. The fluctuations cannot be generated by causal processes in the time between the Big Bang and the time of last scattering. In other words, standard cosmology cannot explain the homogeneity and isotropy of the universe, nor the deviations from the FRW metric.

The scales of the perturbations are initially within the Hubble radius, meaning they are subject to causal physics and thus small quantum fluctuations are induced. On such small scales, the perturbations can be treated as perturbations in flat space-time. After the scales are pushed outside the Hubble radius during inflation, the Hubble expansion becomes relevant. On such long wavelengths, the fluctuations behave classically and they essentially get frozen in. After the end of inflation, the Universe follows the laws of standard Big Bang cosmology, where the Hubble radius increases. As this happens, the scales of the perturbations fall back into the Hubble radius. The perturbations seeded during inflation will have amplitudes depending on the approximately constant Hubble rate at the time of appearance, meaning that the spectrum we observe today

is almost scale-invariant, with constant amplitude on different scales. This is what we observe as the CMB anisotropies.

Relic Density Problem

According to some popular theories beyond the standard model of particle physics, breaking certain gauge symmetries leads to the prediction of topological defects, such as monopoles and cosmic strings. However, at the time of writing no observation of such defects has been recorded. In the case of magnetic monopoles, their energy density would decrease as a matter component, as a^{-3} once the temperature is below their rest mass. The radiation energy density decreases as a^{-4}, implying that these defects could become the dominant matter in the early universe.

The unwanted relic problem is solved when the period of inflation causes these particles to get redshifted away. The condition for this to hold true is for the symmetry breaking transition that produces the magnetic monopoles to occur at least 20 e-folds before inflation ends.

1.4.2 Inflationary Period

Inflation was proposed as a solution to the problems just discussed. The field, or fields that drive inflation may be found in extensions to the standard model, like string-theory, grand unified theories and supergravity. Inflation is defined as a period of accelerated expansion of the universe, in which:

$$\ddot{a} > 0. \tag{1.34}$$

This means that $\dot{a}$ increases during inflation whereas the comoving Hubble radius $(aH)^{-1}$ decreases.

To generate such a phase, we introduce a homogeneous scalar field ϕ, called the inflaton. The introduction of a scalar field, allows for the energy conditions of inflation to be satisfied and for the period of inflation to come to an end naturally. Let us consider the action for such a system:

$$S = \frac{1}{2}\int d^4x\sqrt{-g}R + S_\phi, \tag{1.35}$$

with:

$$S_\phi = \int d^4x\sqrt{-g}\left[-\frac{1}{2}g^{\mu\nu}\partial_\mu\phi\partial_\nu\phi - V(\phi)\right] = \int d^4x\mathcal{L}_\phi, \tag{1.36}$$

and $V(\phi)$ is the potential energy of the inflaton.

The energy-momentum tensor defined in (1.19) for the inflaton field is:

$$T_{\mu\nu} = \partial_\mu\phi\partial_\nu\phi + g_{\mu\nu}\frac{\mathcal{L}_\phi}{\sqrt{-g}}. \tag{1.37}$$

As defined in equations (1.25), the energy density and pressure are given by:

$$\begin{aligned} -T^0_0 =&\rho = \frac{1}{2}\dot{\phi}^2 + V(\phi) \\ T^i_j =&p\delta^i_j \Rightarrow p = \frac{1}{2}\dot{\phi}^2 - V(\phi), \end{aligned} \tag{1.38}$$

We can find the equations of motion for the inflaton field in the FRW metric by using the Euler-Lagrange equations on the action (1.35):

$$\partial_\mu\left(\frac{\partial\mathcal{L}_\phi}{\partial(\partial_\mu\phi)}\right) - \frac{\partial\mathcal{L}_\phi}{\partial\phi} = 0. \tag{1.39}$$

This calculation gives us the Klein-Gordon equation for the inflaton field:

$$\ddot{\phi} + 3H\dot{\phi} + V_\phi = 0, \tag{1.40}$$

where $V_\phi = \frac{\partial V}{\partial\phi}$.

If we substitute (1.38) in the Friedmann equation (1.26) we find:

$$H^2 = \frac{1}{3}\left[\frac{1}{2}\dot{\phi}^2 + V(\phi)\right]. \tag{1.41}$$

For equation (1.41) we recall that we neglect the curvature term K^2/a^2, as it will become exponentially small during inflation.

1.4.3 Time and Length Scales

To describe the change in the scale factor during inflation, we define a useful quantity, the number of e-folds:

$$N = \ln a \Rightarrow \frac{dN}{dt} = H \Rightarrow N = \int_{t_i}^{t_f} H dt \tag{1.42}$$

where the subscript f marks the value of the scale factor and time at the end of inflation and the subscript i that at the beginning of inflation and H is the Hubble parameter.

We will define the transformation rules of derivatives of time to derivatives of e-fold number:

$$\begin{aligned} \dot{f} &= H f', \\ \ddot{f} &= H^2 f'' + \dot{H} f', \end{aligned} \tag{1.43}$$

where the dot denotes differentiation with respect to time t, the prime is differentiation with respect to e-fold number.

For parts of the calculations in later sections, it is easier to work with conformal time, whose relationship to cosmic time is:

$$d\tau = \frac{dt}{a(t)}. \tag{1.44}$$

Under this transformation, the line element in (1.7) for $K = 0$ becomes:

$$ds^2 = a^2(\tau)[d\tau^2 - \delta_{ij} dx^i dx^j]. \tag{1.45}$$

The transformation rules of derivatives of time to derivatives of conformal time are given by:

$$\begin{aligned}\dot{f}(t) &= \frac{f^*(\tau)}{a(\tau)},\\ \ddot{f}(t) &= \frac{f^{**}(\tau)}{a^2(\tau)} - \mathcal{H}\frac{f^*(\tau)}{a^2(\tau)},\end{aligned} \tag{1.46}$$

where the dot denotes differentiation with respect to time t, the '*' notation is differentiation with respect to conformal time τ, with conformal Hubble parameter:

$$\mathcal{H} = \frac{a^*}{a}. \tag{1.47}$$

Using the simple result presented above in (1.46) we can calculate the following:

$$\begin{aligned}H &= \frac{\dot{a}}{a} = \frac{a^*}{a^2} = \frac{\mathcal{H}}{a},\\ \ddot{a} &= \frac{a^{**}}{a^2} - \frac{\mathcal{H}^2}{a},\\ \dot{H} &= \frac{\mathcal{H}^*}{a^2} - \frac{\mathcal{H}^2}{a^2},\\ H^2 &= \frac{\rho}{3} - \frac{K}{a^2} \rightarrow \mathcal{H}^2 = \frac{\rho a^2}{3} - K,\\ \dot{H} &= -\frac{(\rho+p)}{2} \rightarrow \mathcal{H}^* = -\frac{1}{6}(\rho+3p)a^2,\\ \dot{\rho} &+ 3H(\rho+p) = 0 \rightarrow \rho^* + 3\mathcal{H}(\rho+p) = 0.\end{aligned} \tag{1.48}$$

1.4.4 Slow-roll

For the period of accelerated expansion to be realised by the evolution of one or several scalar fields to their lowest energy state, the assumption of a slow trajectory must hold. Considering the inflationary condition (1.34) in the acceleration equation (1.28) we find the following to hold true:

$$\ddot{a} > 0 \Longrightarrow \rho + 3p < 0 \Longleftrightarrow 2\dot{\phi}^2 - 2V(\phi) < 0 \Longleftrightarrow \dot{\phi}^2 < V(\phi), \tag{1.49}$$

where we have used the perfect fluid approximation to utilise the explicit form of the pressure and density in (1.38). The above implies that there will be a phase of inflation

when the potential energy of the inflaton is larger than its kinetic energy. One method of fulfilling this condition is to require the potential to be nearly flat and that it has a minimum, so inflation can end.

In qualitative terms, we can think of the slow-roll regime as a time where the dynamics of the field are slowly evolving, so the following conditions must hold:

$$\frac{\dot{\phi}^2}{2} \ll V(\phi), \tag{1.50}$$

$$\ddot{\phi} \ll 3H\dot{\phi}. \tag{1.51}$$

The slow-roll approximation ignores a term in each of the equations of motion; by assuming the kinetic term is small relative to the potential term, we rewrite (1.41) as:

$$H^2 \simeq \frac{1}{3}V \tag{1.52}$$

and in the Klein-Gordon equation (1.40) using the fact that the second order derivative of the inflaton is much smaller than its first derivative we find:

$$3H\dot{\phi} \simeq -V_\phi, \tag{1.53}$$

where we use $_\phi = \frac{\partial}{\partial\phi}$ notation throughout this work.

To characterise slow-roll we define the slow-roll parameters in the following mathematical way:

$$\begin{aligned} \epsilon_H &= -\frac{\dot{H}}{H^2}, \\ \eta_H &= \frac{\dot{\epsilon}}{H\epsilon}. \end{aligned} \tag{1.54}$$

We can also define the slow-roll parameters in terms of the potential of the inflaton field:

$$\begin{aligned} \epsilon_V &= \frac{1}{2}\left(\frac{V_\phi}{V}\right)^2 \\ \eta_V &= \frac{V_{\phi\phi}}{V}, \\ \xi_V^2 &= \frac{V_\phi V_{\phi\phi\phi}}{V^2}, \end{aligned} \tag{1.55}$$

where ϵ is defined to ensure (1.50) and η is defined to ensure that (1.51). In the case of a single inflaton field the definitions (1.54) relate to the definitions in (1.55) by:

$$\begin{aligned} \epsilon_H &= \epsilon_V = \epsilon, \\ \eta_H &= 4\epsilon_V - \eta_V. \end{aligned} \tag{1.56}$$

The necessary conditions for slow-roll are :

$$\epsilon \ll 1, \quad |\eta| \ll 1, \tag{1.57}$$

with $\eta \in \{\eta_H, \eta_V\}$. Inflation ends when the two conditions in (1.57) no longer hold.

We can go further and define the Hubble flow-functions ϵ_n, which we will use later in Chapter 4:

$$\epsilon_{n+1} = \frac{\dot{\epsilon}_n}{H\epsilon_N}, n \geq 0, \tag{1.58}$$

with $\epsilon_0 = \epsilon = -\frac{\dot{H}}{H^2}$. For slow-roll all $|\epsilon_n| \ll 1$.

1.4.5 Models of Inflation

The first inflationary models were proposed by Starobinsky [31] and Guth [27]. Guth's model is now referred to as 'old inflation' as it relies on a phase transition, between a meta-stable vacuum and a true vacuum of the inflaton field. This does not happen everywhere at once, as the transition happens via quantum tunnelling and bubbles appear in the universe, some of which settle in the true vacuum and some remaining in the false vacuum. This model illustrated how inflation would solve a number of issues that the standard Big Bang picture did not; however it was not favoured due to the high level of tuning. What followed were models of 'new inflation' [28], [30], which assume that the inflaton field is in thermal equilibrium and achieve inflation through thermal corrections of its potential. Shortly afterwards, Linde proposed what

he called 'chaotic inflation' [32], which does not make assumptions about the thermal equilibrium of the inflaton field. In chaotic models, the field driving inflation usually starts at values of order several Planck masses and they have quite simple potentials.

Inflationary models can be categorised in many ways and one can find more comprehensive classifications in [33], [34]. We look briefly at the following general classes of models.

Large field models

This category includes models such as chaotic inflation with monomial potentials:

$$V(\phi) \propto M^4 \left(\frac{\phi}{M_{PL}}\right)^p, p > 0, \tag{1.59}$$

with M being a mass scale. This category also includes the exponential potential:

$$V(\phi) = M^4 e^{\frac{\phi}{M_{PL}}}. \tag{1.60}$$

Inflation ends naturally for this class of models when the slow-roll parameter $\epsilon_H = 1$. The issue with this class of models is that they are only renormalizable for $p \in \{2, 3, 4\}$.

Small field models

In these models the inflaton field is moving from a maximum to the minimum of its potential. These types of models are usually spontaneous symmetry breaking motivated and take the following potential form:

$$V(\phi) = M^4 \left[1 - \left(\frac{\phi}{M_{PL}}\right)^p\right], p > 0, \tag{1.61}$$

where again M is a normalisation constant. A feature of these models is that the tensor-to-scalar ratio (which we will define later in 1.110) is much lower than in large field models.

Hybrid models

This class of models uses two scalar fields, one that we call ϕ that is rolling to its minimum and produces inflation and a second field χ which ends inflation as it rolls to its minimum. The original model of hybrid inflation [35] has the following potential:

$$V(\phi,\chi)=\frac{1}{2}m^2\phi^2+\frac{1}{2}\lambda_1\chi^2\phi^2+\frac{1}{4}\lambda_2(M^2-\chi^2)^2, \tag{1.62}$$

where m is the mass of the ϕ field, λ_1 and λ_2 are dimensionless coupling constants and M is a mass scale. The secondary field χ is locked in a minimum at $\chi=0$, for as long as the principal field ϕ is bigger than the critical $\phi_c=M^2\frac{\lambda_2}{\lambda_1}$. During this phase, the effective potential is:

$$V_{eff}(\phi)=\frac{\lambda_2 M^4}{4}+\frac{1}{2}m^2\phi^2, \tag{1.63}$$

which allows the field ϕ to slow-roll to the critical value ϕ_c, where χ finds two new minima at $-M$ and M. The field χ then rolls down into one of the two, causing inflation to end.

Scalar-tensor models

Inflation can be driven by corrections to General Relativity as well. This type of model was first introduced by Starobinsky [31] and is one of the inflationary models with predictions in best agreement with the Planck 2015 results [20]. The Starobinsky model is a generalisation of the Einstein-Hilbert action defined in 1.15 and generalisations of this model have the following actions gravitational actions:

$$S_G=\frac{1}{2\kappa}\int d^4x\sqrt{-g}\left[R+\mu R^{2p}\right], \tag{1.64}$$

where R is the Ricci scalar, μ has units of $M_{PL}^{-2(1+p)}$, $p\geq 1$ and we continue with our assumption that $\Lambda=0$.

1.5 Perturbation Theory

We have outlined in the previous sections the motivation behind introducing the theory of cosmological inflation in the very early stages of the universe and the mechanism for it to be driven by a scalar field.

Quantum fluctuations in the scalar field exist during inflation, they would get stretched to very large scales; the associated energy density perturbations might be the seeds of structure in the universe. Quantum fluctuations during the phase of inflation could help explain the origin of density perturbations.

Wavenumbers

We will discuss how perturbations behave. We define the wavenumber of a length scale/mode, k, taking into account the expansion of space:

$$k \propto \frac{1}{\lambda}, \tag{1.65}$$

where λ is the wavelength. We also define the comoving Hubble radius:

$$R_H = (aH)^{-1}. \tag{1.66}$$

There are three regimes which can be defined by comparing the scale of modes to the Hubble radius:

$$\begin{aligned} k > aH \quad & subhorizon \\ k = aH \quad & horizon\ crossing \\ k < aH \quad & superhorizon \end{aligned} \tag{1.67}$$

The Hubble radius is the distance from the observer at which the recession velocity of the observed object is equal to the speed of light. Objects outside the Hubble radius of the observer are out of causal contact at the time of measurement.

In order to convert the number of e-folds to a measurable scale, we use the approximation proposed in [36]. But in order to look back in time, we need to outline the history of the Universe; the scenario which we shall consider is that of an inflationary phase, followed by a reheating phase, a radiation dominated era, a matter dominated era and a dark energy/cosmological constant dominated era - with the assumption that the transitions between phases are instantaneous. We can use this model to relate observable scales today re-entering the Hubble horizon, to scales inside the Hubble radius during inflation:

$$\frac{k}{a_0 H_0} = \frac{a_k}{a_{end}} \frac{a_{end}}{a_{reh}} \frac{a_{reh}}{a_{eq}} \frac{H_k}{H_{eq}} \frac{a_{eq} H_{eq}}{a_0 H_0} = e^{-N(k)} \frac{a_{end}}{a_{reh}} \frac{a_{reh}}{a_{eq}} \frac{H_k}{H_{eq}} \frac{a_{eq} H_{eq}}{a_0 H_0}, \tag{1.68}$$

where the subscript '0' refers to present day values, the subscript 'k' values of the mode at the time it crossed the horizon, 'end' refers to the end of inflation, ' reh' denotes reheating and 'eq' the matter-radiation equality era.

We consider the following factors as given in [36]:

$$\begin{aligned} \frac{a_{eq} H_{eq}}{a_0 H_0} &= 219 \Omega_0 h \\ H_{eq} &= 5.25 \times 10^6 h^3 \Omega_0^2 H_0 \\ H_0 &= 1.75 \times 10^{-61} h M_{PL}, \ with \ h \ \simeq 0.7 \end{aligned} \tag{1.69}$$

Taking the natural logarithm of (1.68) and using the slow-roll approximation for H_k, we obtain an equation for N_k:

$$N(k) = -\ln \frac{k}{a_0 H_0} + \frac{1}{3} \ln \frac{\rho_{reh}}{\rho_{end}} + \frac{1}{4} \ln \frac{\rho_{eq}}{\rho_{reh}} + \ln(\sqrt{\frac{V}{3}} \frac{1}{H_{eq}}) + \ln 219 \Omega_0 h, \tag{1.70}$$

where $h = 0.7$ and Ω_0 is the matter density and we have used the slow-roll approximation from (1.52) in (1.70) to get a working conversion of e-fold number.

In single field evolution, modes outside the Hubble horizon stay frozen for as long as they remain greater than the Hubble radius, which is why the evolution in observables

must have happened before the mode exited the horizon.

As we will show later, for single field models, density perturbations do not evolve once their wavelength has exceeded the Hubble radius, which is why structure formation via gravitational instability can only happen if fluctuations in density appeared before the modes exited the horizon. The standard Big Bang picture needs these fluctuations to be put in by hand, but inflationary theory offers a means of physically explaining their origin.

During inflation the scale factor grows quasi-exponentially, the Hubble radius remains almost constant. This means that a wavelength of a quantum fluctuation starting inside the Hubble horizon will grow beyond the Hubble radius. The amplitude of the fluctuations then becomes frozen in, it does not change in amplitude. We will show that in an exponentially expanding universe, the wavelengths of all the vacuum fluctuations of a scalar field ϕ grow exponentially. When the wavelength of any fluctuation becomes greater than the Hubble radius (H^{-1}), its amplitude $\delta\phi$ is frozen. Such a frozen fluctuation $\delta\phi$ would appear as a classical field that does not vanish when time averaged over a macroscopic time.

At the end of inflation, the scale factor grows slower than the Hubble radius, so fluctuations start to reenter the Hubble radius during radiation and matter dominated epochs.

We will start by showing that during the exponential expansion of the Universe, the inflaton will develop fluctuations.

1.5.1 Fluctuations of Scalars During Inflation

To get a better understanding of the behaviour of quantum fluctuations of fields during inflation, we follow the method presented in [37] and we look at the simplest case, that of a massless scalar field in a flat space. We start by looking at de Sitter space and then show what modifications are brought to our results when we transition to a quasi de Sitter expansion. In a de Sitter expansion H is constant and $a(\tau) = -1/(H\tau)$. Consider a massless scalar field ϕ, whose fluctuation we expand in Fourier modes:

$$\delta\phi(\mathbf{x}, t) = \int \frac{d^3\mathbf{k}}{(2\pi)^{3/2}} e^{i\mathbf{k}\cdot\mathbf{x}} \delta\phi_{\mathbf{k}}(t). \tag{1.71}$$

The following is the equation of motion for the perturbation:

$$\delta\ddot{\phi}_{\mathbf{k}} + 3H\delta\dot{\phi}_{\mathbf{k}} + \frac{k^2}{a^2}\delta\phi_{\mathbf{k}} = 0. \tag{1.72}$$

We can now look at how the solutions behave on different scales. The first case is for wavelengths inside the horizon, $\lambda \ll H^{-1} \Leftrightarrow H \ll \lambda^{-1} \Leftrightarrow aH \ll k$, the wavenumber is much larger than the Hubble scale and $3H \ll \frac{k^2}{a^2}$. In this case looking at (1.72), it becomes apparent that the second, friction term is much smaller than the third term, so the equation can be reduced to:

$$\delta\ddot{\phi}_{\mathbf{k}} + \frac{k^2}{a^2}\delta\phi_{\mathbf{k}} = 0, \tag{1.73}$$

which indicates that the fluctuations behave like a perturbation in Minkowski space-time, whose wavelength depends on the scale factor a. In other words, for scales within the horizon, the fluctuations oscillate.

The second case is that in which the wavelengths are outside the horizon, $\lambda \gg H^{-1} \Leftrightarrow aH \gg k$ and $3H \gg \frac{k^2}{a^2}$, and equation (1.72) can be approximated to:

$$\delta\ddot{\phi}_{\mathbf{k}} + 3H\delta\dot{\phi}_{\mathbf{k}} = 0 \tag{1.74}$$

which indicates that on these scales, $\delta\phi_{\mathbf{k}}$ remains constant.

With the redefinition:

$$\delta\sigma_{\mathbf{k}} = a \cdot \delta\phi_{\mathbf{k}}, \tag{1.75}$$

equation (1.72) can be written in terms of conformal time:

$$\delta\sigma_{\mathbf{k}}^{**} + \left(k^2 - \frac{a^{**}}{a}\right)\delta\sigma_{\mathbf{k}} = 0, \tag{1.76}$$

where we have introduced an effective mass term $m = -\frac{a^{**}}{a}$, with $^* = \partial/\partial\tau$ and τ conformal time.

We can expand our analysis to the de Sitter case with a massive scalar field, with mass m_ϕ, for which equation (1.76) can be written as:

$$\delta\sigma_{\mathbf{k}}^{**} + \left(k^2 + M^2(\tau)\right)\delta\sigma_{\mathbf{k}} = 0, \tag{1.77}$$

where:

$$M^2(\tau) = (m_\phi^2 - 2H^2)a^2(\tau) = \left(m_\phi^2 - 2H^2\right)\frac{1}{H^2\tau^2} = \left(\frac{m_\phi^2}{H^2} - 2\right)\frac{1}{\tau^2}. \tag{1.78}$$

Defining:

$$\nu_\phi^2 = \left(\frac{9}{4} - \frac{m_\phi^2}{H^2}\right), \tag{1.79}$$

we can rewrite (1.77) as:

$$\delta\sigma_{\mathbf{k}}^{**} + \left[k^2 - \frac{1}{\tau^2}\left(\nu_\phi^2 - \frac{1}{4}\right)\right]\delta\sigma_{\mathbf{k}} = 0. \tag{1.80}$$

For $\nu_\phi^2 \geq 0$, the solution to (1.77) is:

$$\delta\sigma_{\mathbf{k}} = \sqrt{-\tau}\left[c_1 H_{\nu_\phi}^{(1)}(-k\tau) + c_2 H_{\nu_\phi}^{(2)}(-k\tau)\right], \tag{1.81}$$

where $H^{(1)}_{\nu_\phi}$ and $H^{(2)}_{\nu_\phi}$ are Hankel functions of the first and second kind, which behave for small and large x as follows:

$$\begin{aligned} H^{(1)}_{\nu_\phi}(x \gg 1) &\simeq \sqrt{\frac{2}{\pi x}} e^{i\left(x-\frac{\pi}{2}\nu_\phi-\frac{\pi}{4}\right)}, \\ H^{(2)}_{\nu_\phi}(x \gg 1) &\simeq \sqrt{\frac{2}{\pi x}} e^{-i\left(x-\frac{\pi}{2}\nu_\phi-\frac{\pi}{4}\right)}, \\ H^{(1)}_{\nu_\phi}(x \ll 1) &\simeq \sqrt{\frac{2}{\pi}} e^{i\frac{\pi}{2}} 2^{\left(\nu_\phi-\frac{3}{2}\right)} \frac{\Gamma(\nu_\phi)}{\Gamma(3/2)} x^{-\nu_\phi}. \end{aligned} \tag{1.82}$$

To find the coefficients c_1 and c_2, we use the fact that for the ultraviolet regime, where $k \gg aH \leftrightarrow -k\tau \gg 1$, the solution (1.81) to (1.77) is the plane-wave solution $e^{-ik\tau}/\sqrt{2k}$, to match the behaviour in Minkowski space-time. This gives $c_1(k) = \frac{\sqrt{\pi}}{2} e^{i\left(\nu_\phi+\frac{1}{2}\right)\frac{\pi}{2}}$ and $c_2(k) = 0$. Substituting c_1 and c_2 into (1.81), gives the superhorizon solution:

$$\delta\sigma_{\mathbf{k}} = e^{i\frac{\pi}{2}\left(\nu_\phi-\frac{1}{2}\right)} 2^{\left(\nu_\phi-\frac{3}{2}\right)} \frac{\Gamma(\nu_\phi)}{\Gamma(3/2)} \frac{1}{\sqrt{2k}} \left(-k\tau\right)^{\left(\frac{1}{2}-\nu_\phi\right)}. \tag{1.83}$$

Revisiting the substitution in (1.75), we find:

$$|\delta\phi_k| \simeq \frac{H}{\sqrt{2k^3}} \left(\frac{k}{aH}\right)^{\left(\frac{3}{2}-\nu_\phi\right)} \tag{1.84}$$

on superhorizon scales, i.e the fluctuation of a massive field is no longer constant on the superhorizon, but it has a small time dependence. We define :

$$\eta_\phi = \frac{m_\phi^2}{3H^2} \simeq \frac{3}{2} - \nu_\phi, \tag{1.85}$$

which $\ll 1$ for $\frac{m_\phi}{H} \ll 1$.

In a quasi de Sitter expansion, we take into account the variation of the Hubble parameter, $\dot{H} = -\epsilon H^2$ (from 1.54) and analogously:

$$a(\tau) = -1/(H\tau(1-\epsilon)). \tag{1.86}$$

The mass in (1.77) is:

$$M^2(\tau) = (m_\phi^2 - \frac{a^{**}}{a^3})a^2(\tau) = m_\phi^2 a^2 - \frac{a^{**}}{a}, \tag{1.87}$$

and

$$\begin{aligned}\frac{a^{**}}{a} &= a^2\left(\frac{\ddot{a}}{a}+H^2\right)\\ &= a^2\left(\dot{H}+2H^2\right)\\ &= a^2(2-\epsilon)H^2\\ &= \frac{(2-\epsilon)}{\tau^2\left(1-\epsilon\right)^2}\\ &\simeq \frac{1}{\tau^2}\left(2+3\epsilon\right).\end{aligned} \tag{1.88}$$

So the quasi de Sitter equivalent of (1.77) is:

$$\delta\sigma_{\mathbf{k}}^{**}+\left[k^2-\frac{1}{\tau^2}\left(\nu_\phi^2-\frac{1}{4}\right)\right]\delta\sigma_{\mathbf{k}}=0, \tag{1.89}$$

with

$$\nu_\phi=\frac{3}{2}+\epsilon-\eta_\phi. \tag{1.90}$$

1.5.2 Fluctuations of the Metric and Gauge Transformations

To analyse perturbations we refer to a background state relative to which we introduce the perturbations. In this work we are interested in perturbations from the flat FRW metric. The choice of coordinates on which to define the flat metric and perturbation is not unique and when deciding on a choice of coordinate one makes a gauge choice. Performing a gauge transformation change from one system of coordinates into another.

In different coordinate systems most quantities will take different values. Physical quantities correspond to gauge invariant quantities, which have the same value in all gauge choices. In the subsequent part we follow the presentation in [38].

SVT decomposition

We want to study perturbations of the metric in the FLRW space-time. We consider splitting the metric into a background part, $\bar{g}_{\mu\nu}$, which takes the form presented in (1.7) and a perturbed part, $\delta g_{\mu\nu}$ as:

$$g_{\mu\nu}(\tau, x^i) = \bar{g}_{\mu\nu}(\tau) + \delta g_{\mu\nu}(\tau, x^i), \tag{1.91}$$

with $\delta g_{\mu\nu}(\tau, x^i) \ll \bar{g}_{\mu\nu}(\tau)$. The metric perturbations can be decomposed into scalar, vector and tensor modes, which at linear order evolve independently. It is worth noting that vector modes decay very quickly during inflation.

Scalar perturbations

In this work we will mostly use the longitudinal, or Newtonian gauge, where the scalar metric perturbations are diagonal and the line element is:

$$ds^2 = a^2(\tau)\left[-(1+2\Phi)d\tau^2 + (1-2\Psi)\delta_{ij}dx^i dx^j\right] \tag{1.92}$$

For perfect fluids, where there are no off-diagonal components in the stress-energy-momentum tensor, so $\Phi = \Psi$ (for a full derivation see [38]).

Consider the following change in coordinates:

$$\begin{aligned} t &\to t + \delta t, \\ x^i &\to x^i + \delta^{ij}\partial_j \delta x, \end{aligned} \tag{1.93}$$

where δt fixes the time slicing and δx the spatial threading.

Let us now analyse the matter perturbations. For a scalar field, its density and

pressure, the transformation rule is:

$$\begin{aligned}\tilde{\delta\phi} &= \delta\phi - \dot{\phi}\delta t,\\ \tilde{\delta\rho} &= \delta\rho - \dot{\rho}\delta t,\\ \tilde{\delta p} &= \delta p - \dot{p}\delta t.\end{aligned} \tag{1.94}$$

We introduce the gauge invariant comoving curvature perturbation on hypersurfaces orthogonal to comoving worldlines [39], [40], [41]:

$$\mathcal{R} = \Psi - \frac{H}{\rho + p}\delta q, \tag{1.95}$$

where δq is the perturbation of the momentum potential, defined as $\delta q = \delta T^0_i$, the perturbation of the $0i$ components of the energy-momentum tensor. The momentum potential perturbation transforms as:

$$\tilde{\delta q} = \delta q + (\rho + p)\delta t. \tag{1.96}$$

For a single field ϕ we find $\delta q = -\dot{\phi}\delta\phi$ and the comoving curvature perturbation becomes:

$$\mathcal{R} = \Psi + H\delta\phi, \tag{1.97}$$

1.5.3 Relating to Observables

The quantity used to compare the properties of the perturbations today is the power spectrum of perturbations. Consider a generic quantity $f(\mathbf{x}, t)$ whose Fourier space expansion is:

$$f(\mathbf{x}, t) = \int \frac{d^3\mathbf{k}}{(2\pi)^{3/2}} e^{i\mathbf{k}\cdot\mathbf{x}} f_{\mathbf{k}}(t). \tag{1.98}$$

The power spectrum $\mathcal{P}_f$ of this quantity f is defined by:

$$\langle 0| f^*_{\mathbf{k_1}} f_{\mathbf{k_2}} |0\rangle \equiv \delta^{(3)}(\mathbf{k_1} - \mathbf{k_2}) \frac{2\pi^2}{k^3} \mathcal{P}_f(k), \tag{1.99}$$

where $|0\rangle$ is the vacuum state of the system.

We are particularly interested in the power spectrum of the comoving curvature perturbation $\mathcal{R}$ defined in (1.97):

$$\mathcal{P}_{\mathcal{R}} = \langle 0|\mathcal{R}^*_{\mathbf{k_1}}\mathcal{R}_{\mathbf{k_2}}|0\rangle\delta^{(3)}(\mathbf{k_1}-\mathbf{k_2})\frac{k^3}{2\pi^2}. \tag{1.100}$$

We substitute R from (1.97) in the above equation to find:

$$\mathcal{P}_{\mathcal{R}} = H^2\mathcal{P}_{\delta\phi}, \tag{1.101}$$

where the definition (1.99) gives the power spectrum of the field perturbation $\mathcal{P}_{\delta\phi} = \delta\phi^2\frac{k^3}{2\pi^2}$. We refer back to (1.84) to find:

$$\mathcal{P}_{\mathcal{R}} = A_s\left(\frac{k}{k_0}\right)^{3-2\nu_\phi}, \tag{1.102}$$

where $k_0 = aH|_{h.c.}$ is the pivot scale when the mode leaves the horizon and A_s is the amplitude at the pivot scale k_0.

We define the power spectrum of tensor perturbations in a similar way:

$$\mathcal{P}_{\mathcal{T}} = A_T\left(\frac{k}{k_0}\right)^{n_t}, \tag{1.103}$$

The power spectrum scale dependence is given by the spectral index:

$$n_s - 1 = \frac{d\ln\mathcal{P}_{\mathcal{R}}}{d\ln k}|_{k=aH}, \tag{1.104}$$

evaluated at horizon crossing. Evaluating the spectral index of the curvature perturbation in (1.102), we find:

$$n_s - 1 = 3 - 2\eta_\phi \xrightarrow{1.90} n_s = 1 + 2\epsilon - 2\eta_\phi. \tag{1.105}$$

Similarly we can define the scale-invariant tensor spectral index:

$$n_T = \frac{d\ln\mathcal{P}_{\mathcal{T}}}{d\ln k}|_{k=aH}. \tag{1.106}$$

Another way to parametrise the power spectrum of the comoving curvature perturbation to higher order is:

$$\mathcal{P}_{\mathcal{R}} = A_s \left(\frac{k}{k_0}\right)^{n_s - 1 + \frac{\alpha_s}{2}\log\frac{k}{k_0} + \frac{\beta_s}{6}(\log\frac{k}{k_0})^2}, \tag{1.107}$$

where α_s is the running of the spectral index:

$$\alpha_{\mathcal{R}} = \frac{dn_s}{d\ln k}|_{k=aH}, \tag{1.108}$$

and β_s is the running of the running of the index:

$$\beta_s = \frac{d\alpha_s}{d\ln k}|_{k=aH}. \tag{1.109}$$

This second order parametrisation of the power spectrum will be used in Chapter 4.

Another quantity we are interested in is the tensor-to-scalar ratio, defined by:

$$r = \frac{\mathcal{P}_T}{\mathcal{P}_{\mathcal{R}}}. \tag{1.110}$$

In this section, we have only looked at single field perturbations. In the later chapters we will consider multi-field inflation, where isocurvature perturbations seed curvature perturbations on the superhorizon scale.

Chapter 2

Starobinsky Model

Inflation is usually driven by scalar fields as we have discussed in section (1.5), however there are exceptions to this trend. One such exception are $f(R)$ models and of particular interest to this work is the Starobinsky model of inflation, in which the Einstein-Hilbert action contains an R^2 correction. First introduced in [31], its predictions are in excellent agreement with the most recent cosmological observations, the Planck 2015 results [20]. For a review of $f(R)$ theories see [42], [43]. For an analysis of inflation driven by corrections to General Relativity see [44].

In this short chapter we will discuss some generalities to do with $f(R)$ theories of inflation and we will introduce the gravitational part of the model that will be of interest in later chapters. We start by showing that the extra degree of freedom in $f(R)$ theories coming from non-vanishing first derivatives of $f(R)$ can be described with the introduction of another scalar field. Then we introduce the Jordan and Einstein frames and show how a theory can be recast from one to the other using a conformal transformation. Finally we apply these techniques to the Starobinsky model and look at inflationary predictions for it.

2.1 f(R) and Scalar-Tensor Theories

$f(R)-$theories of gravity are generalisations of General Relativity. The total action for $f(R)$ gravity with matter fields is:

$$\begin{aligned} S_{metric} &= \frac{1}{2\kappa}\int d^4x\sqrt{-g}f(R) + \int d^4x\mathcal{L}_M(g_{\mu\nu},\chi_M), \\ S_{metric} &= S_G + S_M(g_{\mu\nu},\chi_M), \end{aligned} \tag{2.1}$$

where as before $\kappa = 8\pi G$, G is the gravitational constant, g is the determinant of the metric, $f(R)$ is a function of the Ricci scalar and χ_M denote all the matter fields in the theory. This class of modified gravitational actions was first studied in detail in [45]. If we look at the variation of the action with respect to the metric $g_{\mu\nu}$ we get:

$$\begin{aligned} \delta S_{metric} =& \frac{1}{2\kappa}\int d^x\sqrt{-g}\Big[F(R)R_{\mu\nu} - \frac{1}{2}f(R)g_{\mu\nu} - \\ &- \nabla_\mu\nabla_\nu F(R) + g_{\mu\nu}\Box F(R) - \kappa T_{\mu\nu}\Big]\delta g^{\mu\nu}, \end{aligned} \tag{2.2}$$

where $F(R) = \frac{\partial f(R)}{\partial R}$ and we have ignored the surface terms at infinity.

Setting the variation to zero leads to following field equations:

$$F(R)R_{\mu\nu} - \frac{1}{2}f(R)g_{\mu\nu} - \nabla_\mu\nabla_\nu F(R) + g_{\mu\nu}\Box F(R) = \kappa T^M_{\mu\nu}, \tag{2.3}$$

where $T^M_{\mu\nu}$ is defined by (1.19) and $\Box F(R) = \frac{1}{\sqrt{-g}}\partial_\mu(\sqrt{-g}g^{\mu\nu}\partial_\nu F(R))$.

Taking the trace of (2.3) we find:

$$3\Box F(R) + F(R)R - 2f(R) = \kappa T. \tag{2.4}$$

In $f(R)$ modifications to General Relativity, the term $\Box F(R)$ is non-vanishing; with a field redefinition $\phi = F(R)$, (2.3) becomes the equation describing the dynamics of the propagating scalar degree of freedom. We will use this in Chapter 5.

2.2 Equivalent Action Formulation

We now turn our attention to the action in (2.1) and ignore the matter fields:

$$S_G = \frac{1}{2\kappa}\int d^4x\sqrt{-g}f(R). \tag{2.5}$$

We can introduce a field W, to write an equivalent action to (2.5):

$$S_G^W = \frac{1}{2\kappa}\int d^4x\sqrt{-g}\left[F(W)(R-W)+f(W)\right], \tag{2.6}$$

where $F(W) = \frac{\partial f(W)}{\partial W}$. Varying (2.6) with respect to W, we find the equation of motion for W:

$$\frac{\partial \mathcal{L}}{\partial W} = 0 \quad \longleftrightarrow \frac{\partial^2 f(W)}{\partial W^2}(R-W) = 0 \quad \leftrightarrow W = R, \tag{2.7}$$

assuming $\frac{\partial^2 f(W)}{\partial W^2} \neq 0$, thus implying that the actions (2.5) and (2.6) are dynamically equivalent. The field W is the name for the additional degree of freedom in $f(R)$ coming from the derivative $\frac{\partial f}{\partial R}$.

2.3 Going from Jordan to Einstein Frame

We call the action in (2.5) the "Jordan frame" formulation of $f(R)$. With the help of a conformal transformation, the gravitational part of the action can be brought to take the standard General Relativity form, in what is called the "Einstein frame" formulation:

$$S_E = \int d^4x\sqrt{-\tilde{g}}\tilde{R} + other\ terms, \tag{2.8}$$

where $\tilde{g}$ and $\tilde{R}$ are the determinant of the metric and the Ricci scalar in the new frame. To map the theory to this frame, one performs a conformal transformation, in which one chooses the appropriate function Ω as defined in (A.1):

$$\tilde{g}_{\mu\nu} = \Omega^2 g_{\mu\nu} \quad \rightarrow \sqrt{-\tilde{g}} = \Omega^4\sqrt{-g}. \tag{2.9}$$

Under the conformal transformation above, the action (2.6) changes to:

$$S'_G = \int d^4x\sqrt{-\tilde{g}}\frac{\Omega^{-4}}{2\kappa}\left[F(W)(R(\tilde{R})-W)+f(W)\right], \tag{2.10}$$

where $R(\tilde{R})$ is using the expression for R in terms of the transformed Ricci scalar $\tilde{R}$ as given by (A.5):

$$R = \Omega^2\tilde{R} + 6\tilde{g}^{\mu\nu}\Omega(\tilde{\nabla}_\mu\tilde{\nabla}_\nu\Omega) - 12\tilde{g}^{\mu\nu}(\tilde{\nabla}_\mu\Omega)(\tilde{\nabla}_\nu\Omega). \tag{2.11}$$

To find a transformation that takes us to the Einstein frame, we need to chose Ω in such a way that the transformed Ricci scalar is only multiplied by $\sqrt{-\tilde{g}}/2\kappa$, which means:

$$\Omega^2 = F(W), \tag{2.12}$$

for $F(W) > 0$. With this choice we can rewrite the action in (2.10) as:

$$S'_G = \int d^4x\frac{\sqrt{-\tilde{g}}}{2\kappa}\left[\tilde{R}+6\tilde{g}^{\mu\nu}\frac{\tilde{\nabla}_\mu\tilde{\nabla}_\nu\Omega}{\Omega}-12\tilde{g}^{\mu\nu}\frac{(\tilde{\nabla}_\mu\Omega)(\tilde{\nabla}_\nu\Omega)}{\Omega^2}-\Omega^{-2}W+\Omega^{-4}f(W)\right] \tag{2.13}$$

After integrating by parts we find:

$$\begin{aligned} S'_G &= \int d^4x\frac{\sqrt{-\tilde{g}}}{2\kappa}\left[\tilde{R}-6\tilde{g}^{\mu\nu}\frac{(\tilde{\nabla}_\mu\Omega)(\tilde{\nabla}_\nu\Omega)}{\Omega^2}-\Omega^{-2}W+\Omega^{-4}f(W)\right] \\ &= \int d^4x\frac{\sqrt{-\tilde{g}}}{2\kappa}\left[\tilde{R}-6\tilde{g}^{\mu\nu}(\tilde{\nabla}_\mu\ln\Omega)(\tilde{\nabla}_\nu\ln\Omega)-\Omega^{-2}W+\Omega^{-4}f(W)\right] \end{aligned} \tag{2.14}$$

We now do a field redefinition in order to get the second term in the action to look like a standard kinetic term:

$$\Omega = e^{\alpha\psi}, \tag{2.15}$$

with α a constant. The redefinition transforms the second term in the action as follows:

$$\begin{gathered} \frac{6}{2\kappa}\tilde{g}^{\mu\nu}(\tilde{\nabla}_\mu\ln\Omega)(\tilde{\nabla}_\nu\ln\Omega) = \frac{6}{2\kappa}\tilde{g}^{\mu\nu}\alpha^2(\tilde{\nabla}_\mu\psi)(\tilde{\nabla}_\nu\psi) \\ \downarrow \\ \frac{6}{2\kappa}\alpha^2 = \frac{1}{2} \rightarrow \alpha = \sqrt{\frac{\kappa}{6}}, \end{gathered} \tag{2.16}$$

Ensuring that ψ takes the appearance of a scalar field with a standard kinetic term, related to the $f(R)$ theory by:

$$\psi = \sqrt{\frac{3}{2\kappa}} \ln\left(F(W)\right). \tag{2.17}$$

We refer to the field ψ as the scalaron field. We are thus left with the Einstein frame redefined gravitational action:

$$\begin{aligned} S'_G &= \int d^4x\sqrt{-\tilde{g}}\left[\frac{\tilde{R}}{2\kappa} - \frac{1}{2}\tilde{g}^{\mu\nu}(\tilde{\nabla}_\mu\psi)(\tilde{\nabla}_\nu\psi) - V(\psi)\right] \\ V(\psi) &= e^{-2\alpha\psi}W - e^{-4\alpha\psi}f(W), \end{aligned} \tag{2.18}$$

where W can be calculated from (2.12) and (2.15). We proceed to apply this line of reasoning to a specific $f(R)$ theory.

2.4 $R + \mu\kappa R^2$ Model

The model we are particularly interested in has the following gravitational action:

$$S_{ST} = -\frac{1}{2\kappa}\int d^4x\sqrt{-g}(R + \mu\kappa R^2), \tag{2.19}$$

where μ has units $mass^{-2}$. We will discuss this model in detail in Chapter 3.

In the case of $\mu = 1M_{PL}^{-2}$ the model reduces to the Starobinsky model. For this choice $f(W) = W + \kappa\mu W^2$ and with the field redefinition (3.19), the Einstein frame action for this model is:

$$S_{STS} = \int d^4x\sqrt{-\tilde{g}}\left[\frac{\tilde{R}}{2\kappa} - \frac{1}{2}\tilde{g}^{\mu\nu}(\tilde{\nabla}_\mu\psi)(\tilde{\nabla}_\nu\psi) - \frac{(1-e^{-2\alpha\psi})^2}{8\kappa^2\mu}\right]. \tag{2.20}$$

We notice that the action (2.20) looks like standard gravity with a canonical scalar field, of potential:

$$V(\psi) = \frac{(1-e^{-2\alpha\psi})^2}{8\kappa^2\mu}. \tag{2.21}$$

The field ψ is called the scalaron. The minimum of the potential is at $\psi = 0$, and we define its mass by:

$$m_\psi^2 = V_{\psi\psi}(0) = \frac{\alpha^2}{\mu}. \tag{2.22}$$

The dynamics for action (2.20) have been considered in Section 1.4.2, so we find that in an inflationary scenario, that is driven by such a transformed scalar, the slow-roll parameters in natural units are (1.55):

$$\begin{aligned} \epsilon_V &= \frac{8\alpha^2}{(e^{2\alpha\psi} - 1)^2}, \\ \eta_V &= 8\alpha^2 e^{-2\alpha\psi} \frac{2e^{-2\alpha\psi} - 1}{(1 - e^{-2\alpha\psi})^2}, \end{aligned} \tag{2.23}$$

both of which for positive values of ψ, tend upwards to 1 with decrease of ψ.

We are interested in the predictions for the spectral index in our choice of model. To that end we start by integrating (1.42) and we will use the fact that we are working in the slow-roll regime:

$$N = \int_i^f H dt = \int_i^f H \frac{d\psi}{\dot{\psi}} \overset{1.53}{=} -\int_i^f \frac{3H^2}{V_\psi} d\psi \overset{1.52}{=} -\int_i^f \frac{V}{V_\psi} d\psi. \tag{2.24}$$

Using the definition of the slow-roll parameter ϵ_V defined in (1.55) we find:

$$N = -\int_i^f \frac{1}{\sqrt{2\epsilon_V}} d\psi. \tag{2.25}$$

We use the form of ϵ_V calculated in (2.23) to relate the duration of inflation in e-folds to the starting value of the field ψ:

$$N = -\int_i^f \frac{|e^{2\alpha\psi} - 1|}{4\alpha} d\psi. \tag{2.26}$$

As we have discussed in Subsection 1.4.4, inflation ends when the slow-roll parameter $\epsilon_V = 1$, which as we can see from (2.23) happens at:

$$\psi_f = \frac{1}{2\alpha} \ln(1 + 2\alpha\sqrt{(2)}) \simeq 0.94. \tag{2.27}$$

Going back to (2.26) and using the approximation $e^{2\alpha\psi} \gg 1$ and find:

$$N = \int_i^f -\frac{1}{4\alpha} e^{2\alpha\psi} d\psi = \frac{1}{8\alpha^2} e^{2\alpha\psi_i}, \tag{2.28}$$

where in the last step we used $e^{2\alpha\psi_f} \ll e^{2\alpha\psi_i}$.

We evaluate the spectral index in this model using the standard relation [46]:

$$n_s - 1 = -6\epsilon + 2\eta = -\frac{48\alpha^2}{e^{4\alpha\psi}} - 16\alpha^2 e^{-2\alpha\psi}, \tag{2.29}$$

where we made use of the fact that $e^{2\alpha\psi} \gg 1$. Finally, using (2.28), we obtain:

$$n_s = 1 - 48\alpha^2 \left(\frac{3}{3N}\right)^2 - 16\alpha^2 \frac{3}{4N} \simeq 1 - \frac{2}{N}, \tag{2.30}$$

where we ignored the terms of order $\mathcal{O}(N^{-2})$ and we made use of (2.16) for the value $\alpha = 1/\sqrt{6}$. For $N = 50$ e-folds, the duration of inflation, the Starobinsky model prediction for the spectral index is 0.96, which is in the range favoured by the latest observational results [20]. The largest scales we observe today left the horizon 50 to 60 e-folds before the end of inflation.

In the rest of the thesis we will focus our study on the inflationary predictions for an extension of the Starobinsky model. We will consider the Starobinsky correction to General Relativity, $R + \mu\kappa R^2$ with an added scalar field χ which is present during inflation and compare the predictions for inflationary parameters to observational results.

Chapter 3

Simplest Extension to the Starobinsky Model

3.1 Modified Starobinsky Model with a Scalar Field

In this chapter, we consider one specific model for inflation, that is an extension of Starobinsky inflation with an added scalar field, denoted by χ in the action. We ask why the Universe should be devoid of matter. Our motivation is that while gravitation might not be completely described by General Relativity, matter fields might be present during inflation and play a dynamically significant role. We consider the simplest case, that of a single scalar field to understand what matter fields would do. A similar setup was studied in [56], where different energy scales were considered.

Our theory is specified by the action:

$$\begin{aligned} S &= \int d^4x\sqrt{-g}\frac{1}{2\kappa}\Big[R+\mu\kappa R^2\Big] + \int d^4x\sqrt{-g}\Big[-\frac{1}{2}g^{\mu\nu}\nabla_\mu\chi\nabla_\nu\chi - \frac{1}{2}m^2\chi^2\Big] \\ S &= S_G + S_\chi, \end{aligned} \tag{3.1}$$

where there is a gravitational part S_G and a scalar part S_χ. For generality, we will

now define:

$$b(\psi) = -\alpha\psi, \tag{3.2}$$

where α is a function of ψ, that can be a scalar, which will later allow us to compare this model to others in literature.

Using (2.20) and (A.7), we recast the action (3.1) in the Einstein frame, which is given by:

$$S_E = \int d^4x\sqrt{-\tilde{g}}\left[\frac{\tilde{R}}{2\kappa} - \frac{\tilde{g}^{\mu\nu}}{2}(\tilde{\nabla}_\mu\psi)(\tilde{\nabla}_\nu\psi) - \frac{\tilde{g}^{\mu\nu}}{2}e^{2b(\psi)}(\tilde{\nabla}_\mu\chi)(\tilde{\nabla}_\nu\chi) - V\right], \tag{3.3}$$

with:

$$V = \frac{(1-e^{2b(\psi)})^2}{8\kappa^2\mu} + \frac{1}{2}m^2e^{4b(\psi)}\chi^2. \tag{3.4}$$

From here on we will use the notation b for $b(\psi)$.

Figure 3.1 shows the potential of this extended Starobinsky model for three cases with the same initial conditions and different mass ratios.

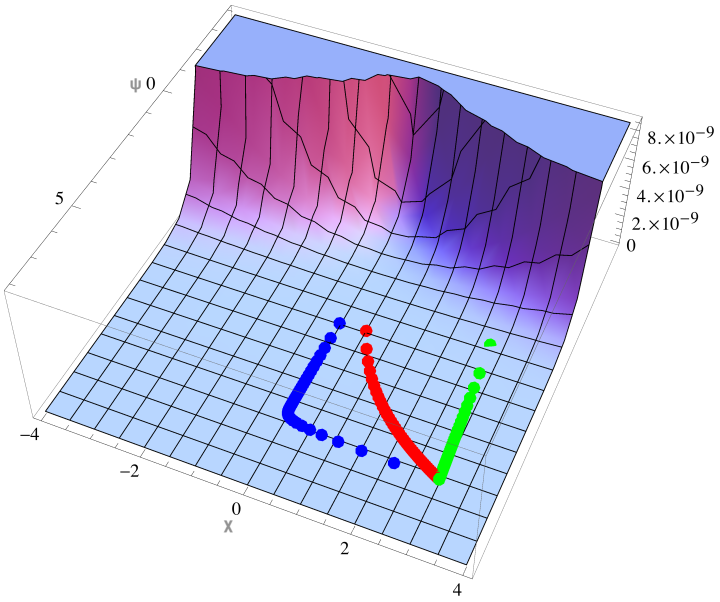

Figure 3.1: The potential of the Starobinsky model with an additional scalar field. The field trajectories illustrate three paths for the same initial starting values of the two fields, with different mass ratios. Blue corresponds to a heavier χ field, green corresponds to a heavier ψ field and red corresponds to the fields having equal masses.

3.1.1 Equations of Motion in the Einstein Frame

We find the resulting equations of motion for ψ and χ in (3.3) are:

$$\begin{aligned}\Box\psi - b_\psi e^{2b}(\tilde{\nabla}^\nu\chi)(\tilde{\nabla}_\nu\chi) - V_\psi = 0\\ \Box\chi + 2b_\psi(\tilde{\nabla}^\nu\psi)(\tilde{\nabla}_\nu\chi) - e^{-2b}V_\chi = 0,\end{aligned} \tag{3.5}$$

where $b_\psi = \partial b/\partial\psi$. We use the FRW metric $\tilde{g}_{\mu\nu} = (-1, a^2, a^2, a^2)$ and the following identity:

$$\begin{aligned}\Box\psi &= \frac{1}{\sqrt{-g}}\partial_\mu(\sqrt{-g}\partial^\mu\psi)\\ &= \frac{1}{\sqrt{-g}}\partial_\mu(\sqrt{-g}\; g^{\mu\nu}\partial_\nu\psi)\\ &= \frac{1}{a^3}\partial_\mu(a^3(-\dot{\psi}))\\ &= -\ddot{\psi} - 3H\dot{\psi}\end{aligned} \tag{3.6}$$

Working in natural units, we find the following background equations of motion:

$$\begin{aligned}\ddot{\psi} + 3H\dot{\psi} - b_\psi e^{2b}\dot{\chi}^2 + V_\psi = 0\\ \ddot{\chi} + 3H\dot{\chi} + 2b_\psi\dot{\psi}\dot{\chi} + e^{-2b}V_\chi = 0,\end{aligned} \tag{3.7}$$

where the dot represents differentiation with respect to time and the derivatives of the potential with respect to the fields are:

$$\begin{aligned}V_\psi =& -(1 - e^{2b})e^{2b}\frac{b_\psi}{2\mu} + 2m^2 b_\psi e^{4b}\chi^2,\\ V_\chi =& m^2 e^{4b}\chi.\end{aligned} \tag{3.8}$$

Solving the differential equations in terms of time can be computationally intensive, so for the purpose of solving the equations numerically, we rewrite them in terms of the e-fold number defined in (1.42) and mark the derivative with respect to N by dash, following the transformation rules defined in (1.43).

Now we will look at what the background equations (3.7) look like with respect to

e-fold number using (1.43):

$$\begin{aligned}\frac{\dot{H}}{H^2}\psi' + \psi'' + 3\psi' - b_\psi e^{2b}\chi'^2 + \frac{V_\psi}{H^2} = 0 \\ \frac{\dot{H}}{H^2}\chi' + \chi'' + 3\chi' + 2b_\psi\psi'\chi' + \frac{V_\chi}{H^2}e^{-2b} = 0\end{aligned} \tag{3.9}$$

To get the background equations in the new variable we use the Friedmann equation (1.26) assuming zero curvature:

$$H^2 = \frac{1}{3}\rho \tag{3.10}$$

with the density from (1.25):

$$\rho = \left[\frac{1}{2}\dot{\psi}^2 + \frac{1}{2}e^{2b}\dot{\chi}^2 + V\right] \tag{3.11}$$

We take the time derivative of equations (3.10), (3.11) and use the background equations of motion in (3.7). We then transform into to derivatives of e-folds to find:

$$\frac{\dot{H}}{H^2} = \frac{1}{2}\left[-\psi'^2 - e^{2b}\chi'^2\right]. \tag{3.12}$$

Substituting (3.12) in (3.9), we obtain the field background equations in terms of derivatives of e-fold:

$$\begin{aligned}\psi'' + \psi'\left[-\frac{1}{2}\psi'^2 - \frac{1}{2}e^{2b}\chi'^2 + 3\right] - b_\psi e^{2b}\chi'^2 + \frac{V_\psi}{H^2} = 0 \\ \chi'' + \chi'\left[-\frac{1}{2}\psi'^2 - \frac{1}{2}e^{2b}\chi'^2 + 3 + 2b_\psi\psi'\right] + \frac{V_\chi e^{-2b}}{H^2} = 0\end{aligned} \tag{3.13}$$

We relate the parameter μ to the mass of the scalaron field ψ as we have done in (2.22):

$$m_\psi = \sqrt{\frac{1}{6\mu}} \tag{3.14}$$

3.1.2 Perturbations and Power Spectra

In section 1.5 we discussed the perturbations of a single scalar field and found that they get frozen after the mode exits the horizon. In multi-field models this is no longer

true, as there are both adiabatic and non-adiabatic fluctuations, which we will study now following the formalism presented in [47]. Adiabatic perturbations coincide with perturbations in the metric, they are curvature perturbations, whereas non-adiabatic perturbations correspond to situations where several matter species are present, where energy exchange can happen between the matter components.

In order to study the perturbations of the model we chose to work in the longitudinal (or Newtonian) gauge. In the models considered, the matter content is formed of scalar fields, which means that the off-diagonal spatial components of the stress-energy tensor are zero. The perturbed metric element takes the following form:

$$ds^2 = -(1+2\Phi)dt^2 + a^2(1-2\Phi)\delta_{ij}dx^i dx^j, \tag{3.15}$$

where we only consider scalar perturbations.

The scalar fields are composed into the background and perturbed components respectively:

$$\begin{aligned} \psi(t,x) &= \psi(t) + \delta\psi(t,x), \\ \chi(t,x) &= \chi(t) + \delta\chi(t,x). \end{aligned} \tag{3.16}$$

In two field models, there are usually 5 slow-roll parameters defined [48] , analogous to (1.55), two which describe the slope of the potential along the directions of the fields:

$$\begin{aligned} \epsilon_\psi &\equiv \frac{1}{2}\left(\frac{V_\psi}{V}\right)^2 \\ \epsilon_\chi &\equiv \frac{1}{2}\left(\frac{V_\chi}{V}\right)^2 \end{aligned} \tag{3.17}$$

and three curvature parameters:

$$\begin{aligned} \eta_{\psi\psi} &\equiv \frac{V_{\psi\psi}}{V} \\ \eta_{\psi\chi} &\equiv \frac{V_{\psi\chi}}{V} \\ \eta_{\chi\chi} &\equiv \frac{V_{\chi\chi}}{V} \end{aligned} \tag{3.18}$$

In the formalism we will be using, it is convenient to perform a rotation in field space as done in [49]:

$$\begin{aligned}\delta\sigma &= \cos\theta\delta\psi + \sin\theta e^{b}\delta\chi,\\ \delta s &= -\sin\theta\delta\psi + \cos\theta e^{b}\delta\chi,\end{aligned} \tag{3.19}$$

with the following definitions:

$$\cos\theta = \frac{\dot{\psi}}{\dot{\sigma}} = c_\theta, \qquad \sin\theta = \frac{\dot{\chi}e^{b}}{\dot{\sigma}} = s_\theta, \qquad \text{and} \qquad \dot{\sigma} = \sqrt{\dot{\psi}^2 + e^{2b}\dot{\chi}^2}. \tag{3.20}$$

The perturbations along the background trajectory at a point are quantified by $\delta\sigma$ and the perturbations orthogonal to the background trajectory perturbations by δs. The variable $\dot{\theta}$ describes the amount of curvature. With this redefinition, the slope orthogonal to the trajectory is zero, so the slow roll parameters in the redefined directions are defined by:

$$\epsilon = -\frac{\dot{H}}{H^2} \tag{3.21}$$

$$\eta_{AB} = \frac{V_{AB}}{3H^2} \tag{3.22}$$

$$\eta_{\sigma\sigma} = \frac{V_{\psi\psi}}{V}\cos^2\theta + \frac{V_{\chi\chi}}{V}e^{-2b(\psi)}\sin^2\theta + \frac{V_{\psi\chi}}{V}e^{-b(\psi)}\sin 2\theta, \tag{3.23}$$

$$\eta_{\sigma s} = \left(\frac{V_{\chi\chi}}{V}e^{-2b} - \frac{V_{\psi\psi}}{V}\right)\sin\theta\cos\theta + \frac{V_{\chi\psi}}{V}e^{-b}\cos 2\theta, \tag{3.24}$$

$$\begin{aligned}\eta_{ss} =& \frac{V_{\psi\psi}}{V}\sin^2\theta - \frac{V_{\chi\psi}}{V}e^{-b}\sin 2\theta + \frac{V_{\chi\chi}}{V}e^{-2b}\cos 2\theta +\\ &+ \sin\theta b_{,\psi}\left(\frac{V_\psi}{V}\sin\theta + \frac{V_\psi}{V}e^{-b}\cos\theta\right),\end{aligned} \tag{3.25}$$

which are extensions to those calculated in [50] with added non-canonical contributions. Their time derivatives are given in [47] by:

$$\dot{\eta_{\sigma\sigma}} = 2H\epsilon\eta_{\sigma\sigma} - 2H\eta_{\sigma s}^2 - 2H\eta_{\sigma\sigma}\xi_1 s_\theta^2 c_\theta - 4H\eta_{\sigma s}\xi_1 s_\theta c_\theta^2 - H\alpha_{\sigma\sigma\sigma}, \tag{3.26}$$

$$\dot{\eta_{\sigma s}} = 2H\epsilon\eta_{\sigma s} + H\eta_{\sigma s}\eta_{\sigma\sigma} - H\eta_{\sigma s}\eta_{ss} - 2H\eta_{ss}\xi_1 s_\theta c_\theta^2 - H\eta_{\sigma s}\xi_1 c_\theta - H\alpha_{\sigma\sigma s}, \tag{3.27}$$

$$\dot{\eta_{ss}} = 2H\epsilon\eta_{ss} + 2H\eta_{\sigma s}^2 - 2Hc_\theta^3\xi_1\eta_{ss} - H\alpha_{\sigma ss} \quad \text{and} \tag{3.28}$$

$$\dot{\xi_1} = 2H\epsilon\xi_1 - H\xi_1\eta_{\sigma\sigma} - H\xi_1^2 s_\theta^2 c_\theta + H\xi_2 c_\theta, \tag{3.29}$$

where

$$\alpha_{IJK} \equiv \frac{V_\sigma V_{IJK}}{V^2}, \tag{3.30}$$

and [51]:

$$\xi_1 = \sqrt{2\epsilon} b_\psi, \tag{3.31}$$

$$\xi_2 = 2\epsilon b_{\psi\psi}. \tag{3.32}$$

The parameters ξ_1 and ξ_2 are treated as first and second order slow-roll parameters respectively.

Instead of working with $\delta\psi, \delta\chi$ or $\delta s, \delta\sigma$, we chose to work with the Mukhanov-Sasaki variables [52],[53] defined as:

$$Q_\sigma = \delta\sigma - \frac{\dot{\sigma}}{H}\Phi, \tag{3.33}$$

where Φ is the metric perturbation defined in (3.15) and $\delta\sigma$ is defined in (3.19). In this basis the background equations are:

$$\begin{aligned} &\ddot{\sigma} + 3H\dot{\sigma} + V_\sigma = 0 \quad \text{and} \\ &\dot{\theta} + \frac{V_s}{\dot{\sigma}} + b_\psi\dot{\sigma}\sin(\theta) = 0. \end{aligned} \tag{3.34}$$

The perturbation equations in Fourier space for the wavenumber k for the Mukhanov-Sasaki variables are:

$$\begin{pmatrix} \ddot{Q}_\sigma \\ \ddot{\delta s} \end{pmatrix} + \begin{pmatrix} 3H & \frac{2V_{,s}}{\dot{\sigma}} \\ -\frac{2V_{,s}}{\dot{\sigma}} & 3H \end{pmatrix} \begin{pmatrix} \dot{Q}_\sigma \\ \dot{\delta s} \end{pmatrix} + \left[\frac{k^2}{a^2}\mathbf{1} + \begin{pmatrix} C_{\sigma\sigma} & C_{\sigma s} \\ C_{s\sigma} & C_{ss} \end{pmatrix} \right] \begin{pmatrix} Q_\sigma \\ \delta s \end{pmatrix} = 0. \quad (3.35)$$

The coefficients, C_{AB}, are given to second order in slow-roll parameters in [47]:

$$C_{\sigma\sigma} = 3H^2 \left[\eta_{\sigma\sigma} - 2\epsilon + \xi_1 s_\theta^2 c_\theta - \frac{\eta_{\sigma s}^2}{3} - 2\epsilon^2 + \frac{4\epsilon\eta_{\sigma\sigma}}{3} + \frac{\xi_1\eta_{\sigma s}}{3}(s_\theta - 3s_\theta c_\theta^2) + \frac{5\epsilon\xi_1 s_\theta^2 c_\theta}{3} - \frac{\xi_1\eta_{\sigma\sigma}s_\theta^2 c_\theta}{3} + \frac{\xi_1^2 s_\theta^4 c_\theta^2}{3} \right], \quad (3.36)$$

$$C_{\sigma s} = 3H^2 \left[2\eta_{\sigma s} - 2\xi_1 s_\theta^3 + \frac{2\eta_{\sigma\sigma}\eta_{\sigma s}}{3} - \frac{2\epsilon\xi_1 s_\theta^3}{3} + \frac{2\xi_1^2 c_\theta^3 s_\theta^3}{3} + \frac{2\eta_{\sigma s}\xi_1 c_\theta(s_\theta^2 - c_\theta^2)}{3} \right], \quad (3.37)$$

$$C_{s\sigma} = 3H^2 \left[\frac{4\epsilon\eta_{\sigma s}}{3} - \frac{2\eta_{\sigma\sigma}\eta_{\sigma s}}{3} + \frac{2\eta_{\sigma\sigma}\xi_1 s_\theta^3}{3} - \frac{4\epsilon\xi_1 s_\theta^3}{3} - \frac{2\eta_{\sigma s}\xi_1 s_\theta^2 c_\theta}{3} + \frac{2\xi_1^2 s_\theta^5 c_\theta}{3} \right], \quad (3.38)$$

$$C_{ss} = 3H^2 \left[\eta_{ss} - \xi_1(1+s_\theta^2)c_\theta - \frac{\eta_{\sigma s}^2}{3} + \frac{\xi_1^2 c_\theta^2(s_\theta^4 - 1)}{3} + \frac{\eta_{\sigma s}\xi_1 s_\theta(1+s_\theta^2)}{3} + \frac{\eta_{\sigma\sigma}\xi_1 c_\theta(1+s_\theta^2)}{3} - \frac{\epsilon\xi_1 c_\theta(1+s_\theta^2)}{3} \right], \quad (3.39)$$

As we are interested in specific observables, we convert back to the comoving curvature perturbation and renormalised entropy perturbation, using the following relations [48]:

$$\begin{aligned} \mathcal{R} &\equiv \frac{H}{\dot{\sigma}} Q_s \\ \mathcal{S} &\equiv \frac{H}{\dot{\sigma}} \delta s. \end{aligned} \quad (3.40)$$

In order to calculate the power spectra at the end of inflation, we look at two regimes, namely horizon crossing and the subsequent evolution. The former looks at a single mode as it exits the horizon and the later follows that mode from a few e-folds after it exits the horizon to the end of inflation.

Horizon Crossing

According to [47] we calculate the power spectra for the curvature perturbation $\mathcal{P}_\mathcal{R}$ and the entropy perturbation $\mathcal{P}_\mathcal{S}$ at horizon crossing as (the $*$ denotes horizon crossing):

$$\begin{aligned}\mathcal{P}_{\mathcal{R}*} = \frac{H_*^2}{8\pi^2\epsilon_*}&(1-2\epsilon_*-11\epsilon_*^2+4\epsilon_*\eta_{\sigma\sigma*}+4\epsilon_*\xi_{1*}s_{\theta*}^2c_{\theta*})(1+k^2\tau^2)\times\\ &\left[1+\frac{2}{3}(3\epsilon_*+20\epsilon_*^2-8\epsilon_*\eta_{\sigma\sigma*}-8\epsilon_*\xi_{1*}s_{\theta*}^2c_\theta*-A_{Q*})f(x)\right.\\ &\left.+\left(\epsilon_*^2+\frac{A_{Q*}^2+B_{Q*}^2}{9}-\frac{2\epsilon_*A_{Q*}}{3}\right)g(x)\right],\end{aligned} \tag{3.41}$$

$$\begin{aligned}\mathcal{P}_{\mathcal{S}*} = \frac{H_*^2}{8\pi^2\epsilon_*}&(1-2\epsilon_*-11\epsilon_*^2+4\epsilon_*\eta_{\sigma\sigma*}+4\epsilon_*\xi_{1*}s_{\theta*}^2c_{\theta*})(1+k^2\tau^2)\times\\ &\left[1+\frac{2}{3}(3\epsilon_*+20\epsilon_*^2-8\epsilon_*\eta_{\sigma\sigma*}-8\epsilon_*\xi_{1*}s_{\theta*}^2c_\theta*-D_{Q*})f(x)\right.\\ &\left.+\left(\epsilon_*^2+\frac{D_{Q*}^2+B_{Q*}^2}{9}-\frac{2\epsilon_*D_{Q*}}{3}\right)g(x)\right],\end{aligned} \tag{3.42}$$

where τ is conformal time defined in (1.44) and:

$$\begin{aligned}A_Q &= 3\eta_{\sigma\sigma}-6\epsilon+3\xi_1s_\theta^2c_\theta+10\epsilon\eta_{\sigma\sigma}-18\epsilon^2+11\epsilon\xi_1s_\theta^2c_\theta\\ &\quad-\eta_{\sigma\sigma}\xi_1s_\theta^2c_\theta+\xi_1^2s_\theta^4-\eta_{\sigma s}\xi_1s_\theta(1+c_\theta^2),\\ B_Q &= 3\eta_{\sigma s}-3\xi_1s_\theta^3+8\epsilon\eta_{\sigma s}-9\epsilon\xi_1s_\theta^3+\eta_{\sigma\sigma}\xi_1s_\theta^3-\eta_{\sigma s}\xi_1c_\theta^3+\xi_1^2s_\theta^3c_\theta,\\ C_Q &= 3\eta_{\sigma s}-3\xi_1s_\theta^3+8\epsilon\eta_{\sigma s}-9\epsilon\xi_1s_\theta^3+\eta_{\sigma\sigma}\xi_1s_\theta^3-\eta_{\sigma s}\xi_1c_\theta^3+\xi_1^2s_\theta^3c_\theta,\\ D_Q &= 3\eta_{ss}-3\xi_1c_\theta(1+s_\theta^2)+6\epsilon\eta_{ss}-7\epsilon\xi_1c_\theta(1+s_\theta^2)+\eta_{\sigma\sigma}\xi_1c_\theta(1+s_\theta^2)\\ &\quad+\eta_{\sigma s}\xi_1s_\theta c_\theta^2+\xi_1^2(s_\theta^4-c_\theta^2).\end{aligned} \tag{3.43}$$

$$f(x) = 2-\gamma-\ln 2-\ln x \tag{3.44}$$

$$\begin{aligned}6g(x) = 16+3\pi^2-44\gamma+12\gamma^2+24\gamma\ln 2-44\ln 2+12\ln^2 2\\ +12\ln^2 x-44\ln x+24\gamma\ln x+24\ln x\ln 2\end{aligned} \tag{3.45}$$

These will be used below.

Super-Hubble Scales

Next we need to determine how these quantities evolve after horizon crossing. Working on super horizon scales, where we can neglect the $\frac{k^2}{a^2}$ term and the time derivatives (as the quantities in question are slowly evolving in time), equation (3.35) reduces to:

$$\frac{\dot{Q}_\sigma}{H} = AQ_\sigma + B\delta s, \tag{3.46}$$

$$\frac{\dot{\delta s}}{H} = D\delta s, \tag{3.47}$$

where

$$\begin{aligned} A = \Bigg(& 2\epsilon - \eta_{\sigma\sigma} - \xi_1 s_\theta^2 c_\theta - \frac{\eta_{\sigma s}^2}{3} - \frac{4\epsilon^2}{3} - \frac{\eta_{\sigma\sigma}^2}{3} + \frac{5\epsilon\eta_{\sigma\sigma}}{3} - \frac{2\xi_1^2 s_\theta^2 c_\theta^2}{3} + \frac{\xi_2 s_\theta^2 c_\theta^2}{3} \\ & - \frac{4\eta_{\sigma\sigma}\xi_1 s_\theta^2 c_\theta}{3} - \frac{4\eta_{\sigma s}\xi_1 s_\theta c_\theta^2}{3} + \frac{4\epsilon\xi_1 s_\theta^2 c_\theta}{3} - \frac{\alpha_{\sigma\sigma\sigma}}{3}\Bigg), \end{aligned} \tag{3.48}$$

$$\begin{aligned} B = \Bigg(& -2\eta_{\sigma s} + 2\xi_1 s_\theta^3 + 2\epsilon\eta_{\sigma s} - \frac{2\eta_{\sigma\sigma}\eta_{\sigma s}}{3} - \frac{2\eta_{ss}\eta_{\sigma s}}{3} + \frac{4\eta_{\sigma\sigma}\xi_1 s_\theta^3}{3} - \frac{4\epsilon\xi_1 s_\theta^3}{3} \\ & - \frac{4\eta_{ss}\xi_1 s_\theta c_\theta^2}{3} + \frac{4\xi_1^2 s_\theta^3 c_\theta}{3} - \frac{2\alpha_{\sigma\sigma s}}{3}\Bigg), \end{aligned} \tag{3.49}$$

$$\begin{aligned} D = \Bigg(& -\eta_{ss} + \xi_1 c_\theta(1 + s_\theta^2) - \frac{\eta_{\sigma s}^2}{3} - \frac{\eta_{ss}^2}{3} + \frac{\epsilon\eta_{ss}}{3} - \frac{\alpha_{\sigma ss}}{3} + \frac{4\eta_{\sigma s}\xi_1 s_\theta^3}{3} \\ & - \frac{4\xi_1^2 s_\theta^4}{3} + \frac{4\eta_{ss}\xi_1 c_\theta s_\theta^2}{3}\Bigg), \end{aligned} \tag{3.50}$$

which can then be integrated and used to find the final power spectra as in [51]:

$$\begin{aligned} \mathcal{P}_\mathcal{R}(N) &= \mathcal{P}_{\mathcal{R}*}\Bigg[1 + \left(\int_{N_*}^{N} B(N'')e^{\int_{N_*}^{N}\gamma(N')dN'}dN''\right)^2 \\ &- 2\eta_{\sigma s} f(-k\tau_*)\int_{N_*}^{N} B(N'')e^{\int_{N_*}^{N}\gamma(N')dN'}dN''\Bigg], \end{aligned} \tag{3.51}$$

$$\mathcal{P}_\mathcal{S}(N) = \mathcal{P}_{\mathcal{S}*}e^{2\int_{N_*}^{N}\gamma(N')dN'}, \tag{3.52}$$

where the '$_*$' denotes the value of the power spectra at horizon crossing and $\gamma = D - A$.

Finally, to calculate the power spectrum of tensor perturbations $\mathcal{P}_\mathcal{T}$ we use the slow-roll approximation (see [54]):

$$\mathcal{P}_\mathcal{T} = \frac{16}{\pi}\left[1 - 2(\gamma + \ln 2 - 1)\epsilon\right]\frac{H^2}{M_{PL}^2} \tag{3.53}$$

To utilise equations (3.51) and (3.53), we need to relate the e-fold number N to the scale k at which the mode exits the horizon. We implement the relation given in [55], introduced in (1.70):

$$N(k) = -\ln\frac{k}{a_0 H_0} + \frac{1}{3}\ln\frac{\rho_{reh}}{\rho_{end}} + \frac{1}{4}\ln\frac{\rho_{eq}}{\rho_{reh}} + \ln\left(\sqrt{\frac{V_k}{3}}\frac{1}{H_{eq}}\right) + \ln 219\Omega_0 h \tag{3.54}$$

3.2 Observational Results

We look at predictions of this extension of the Starobinsky model for the spectral index n_s defined in (1.104), the amplitude of the power spectrum A_s, defined by $\mathcal{P}_{\mathcal{R}}|_{k=k_0}$ and the tensor-to-scalar ratio r defined in (1.110) at a pivot scale of $k_0 = 0.05\ Mpc^{-1}$ and compare to observational results of the Planck 2015 data given in [20].

We find that there are regions of parameter space which predict observables consistent with observations. The parameters to be varied in this model are the starting points of the fields ψ and χ, the mass m_χ and the ratio of the two field masses:

$$R_m = m_\psi / m_\chi. \tag{3.55}$$

To get predictions for the observables for this model, we have solved numerically the equations of motion (3.13) and the equations for the evolution of the power spectra in (3.51).and impose that during the numerical runs, inflation lasts no less than 55 e-folds and no more than 600 e-folds, of which only the last 55 are considered. The inflationary phase is said to finish when the slow-roll parameter ϵ_H defined in (1.54) is 1.

3.2.1 Varying Field Initial Conditions

Firstly we study how robust the predictions for the observables are under variations of initial conditions of the fields. We calculate the change in the observables at the pivot scale of $k_0 = 0.05\ Mpc^{-1}$ when we fix the masses of the fields at $m_\psi = m_\chi = 10^{-5.5} M_{PL}$, but vary the initial conditions on the field starting values $\psi_{\rm ini}$, $\chi_{\rm ini}$. The analysis is done changing the initial starting point of ψ_{ini} between 5.5 M_{PL} and 8 M_{PL} in increments of 0.1 M_{PL}, whilst keeping the starting point of χ_{ini} constant. Then we repeat the analysis for the initial value of the field ψ_{ini} constant and varying χ_{ini} between 3 and 12 M_{PL}. The starting values for the analysis are chosen, so that the predictions for the observable are in the Planck 2015 accepted region [20]. We refer to these starting values of the fields for the numerical runs $\psi_{\rm ini}$ and $\chi_{\rm ini}$. In the following subsections, $\psi_{\rm ini}$ and $\chi_{\rm ini}$ are given in units of M_{PL}.

Change in Tensor-to-Scalar Ratio

We find the value of the tensor-to-scalar ratio to change very little and consistently stays below 0.055 for all $\psi_{\rm ini}$ and $\chi_{\rm ini}$ values considered.

The results are shown in Figure 3.2. The top two figures labeled $\psi_{\rm ini} = 5$ and $\psi_{\rm ini} = 7$ are for runs where $\psi_{\rm ini}$ is kept constant at 5 M_{PL} and 7 M_{PL} respectively, whilst varying the initial value of the χ field. The bottom two figures, labeled $\chi_{\rm ini} = 5$ and $\chi_{\rm ini} = 10$ are for runs where $\chi_{\rm ini}$ is kept constant at 5 M_{PL} and 10 M_{PL} respectively, whilst varying the initial value of the ψ field. Note that the upper left-hand side subplot, labeled $\psi_{\rm ini} = 5$ only showcases values for runs where $\chi_{\rm ini} > 9.5\ M_{PL}$, because of our restriction on the duration of the numerical run to last longer than 55 e-folds.

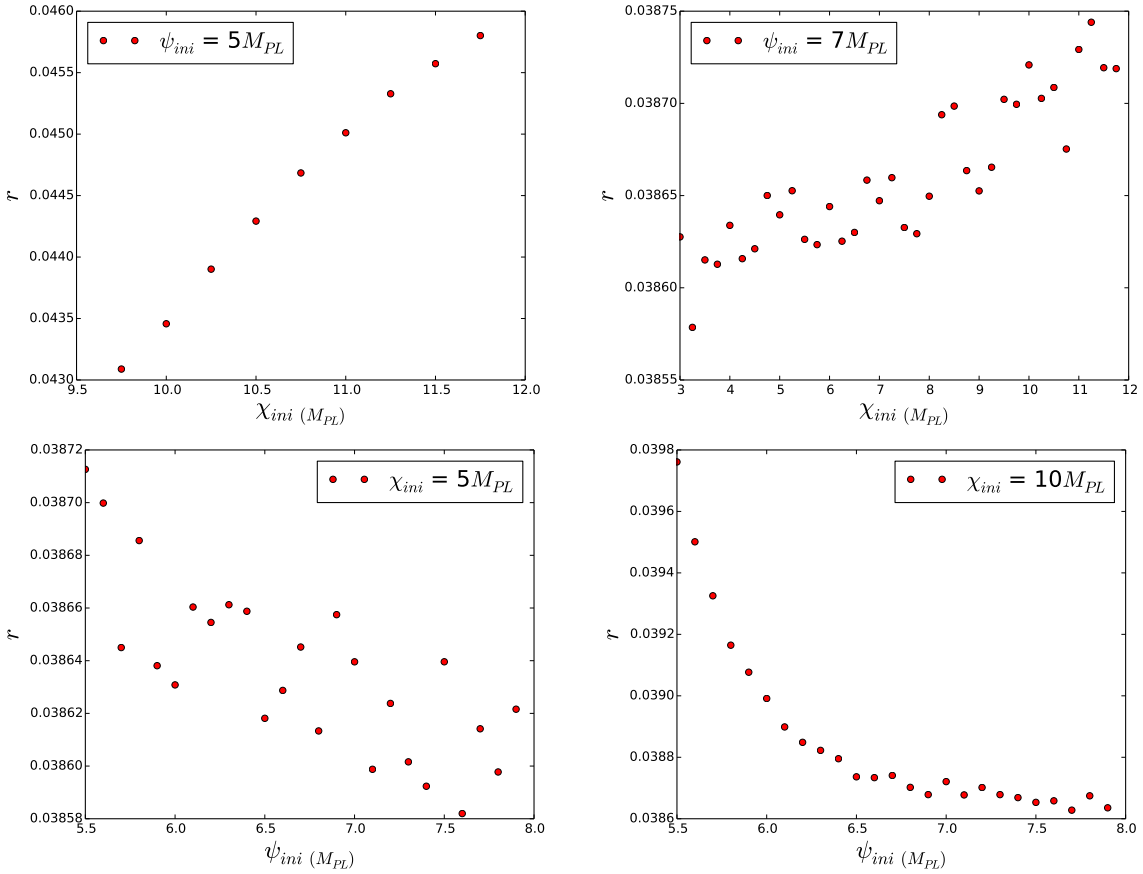

Figure 3.2: Predictions for the tensor-to-scalar ratio r under changes in the starting values of the inflationary fields. The top two subplots show the tensor-to-scalar ratio for ψ_{ini} constant at 5 M_{PL} on the left and 7 M_{PL} on the right, with varying χ_{ini} in the range $\{3 : 12\}M_{PL}$. The bottom two subplots show the tensor-to-scalar ratio for χ_{ini} constant at 5 M_{PL} on the left and 10 M_{PL} on the right, with varying ψ_{ini} in the range $\{5.5 : 8\}M_{PL}$.

Change in Spectral Index and Perturbation Amplitude at Pivot Point

We now look at how the predictions for the spectral index and the amplitude at the pivot scale $k_0 = 0.05\ Mpc^{-1}$ change when the starting values of the fields are varied and we compare them to the Planck 2015 [20] results:

$$\begin{aligned} n_s &= 0.9682 \pm 0.0062, \quad n_s \in [0.9620, 0.9744], \\ 10^9 A_s &= 2.23 \pm 0.16, \quad 10^9 A_s \in [2.07, 2.39]. \end{aligned} \tag{3.56}$$

We consider the range of initial values of the fields $\psi_{\rm ini},\ \chi_{\rm ini} \in \{1 : 10\} M_{PL}$. We find that for runs with starting values in this range, the spectral index is in the observationally allowed region by Planck 2015 results. We also find that the changes in n_s are small and tend to be below or just of the order of the latest observational accuracy, of $\mathcal{O}(10^{-5})$, as can be seen in the left hand side panels of Figure 3.3 and Figure 3.4. The changes in A_s with different initial conditions for the field values are very small relative to the observational accuracy, staying consistently under 5%. We note that the for this part of the analysis we are not interested in the absolute value of the amplitude, as we are only trying to understand the robustness of the predictions under these changes.

Note that in the figures showing the variation in the perturbation amplitude, the y-axis shows different ranges of values for the amplitude; the lower the value of $\chi_{\rm ini}$, the bigger the apparent scatter in the plot. That is because the field χ has a smaller effect on the trajectory relative to the field ψ, when they have equal masses, as can be seen by looking at the potential of our model (3.4), where ψ contributes more to the potential energy.

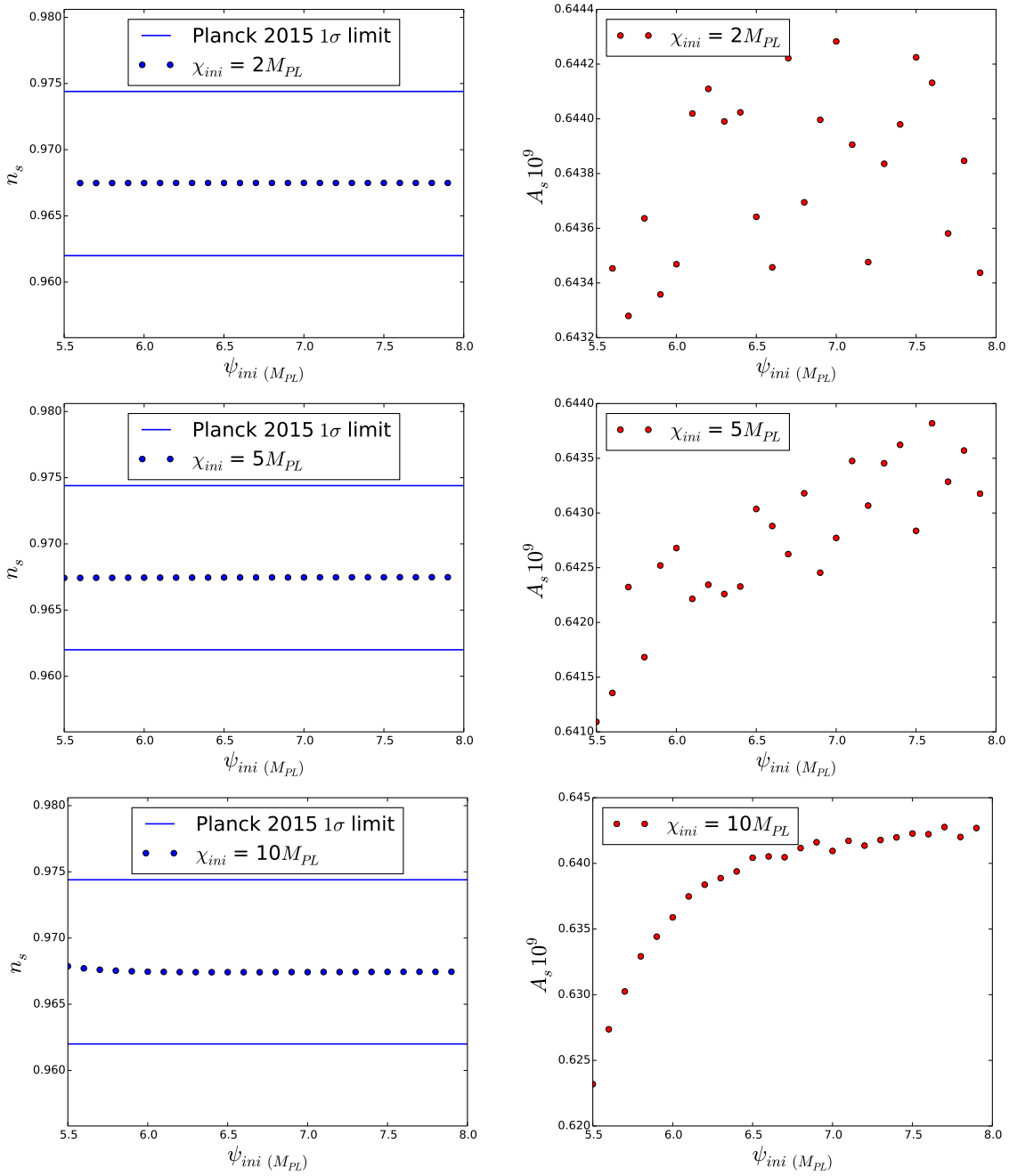

Figure 3.3: The change in the spectral index n_s (left hand side subplots) and in the amplitude A_s at the pivot point $k = 0.05\ Mpc^{-1}$ (right hand side subplots), for fixed values of $\chi_{\rm ini}$ and varying $\psi_{\rm ini}$. The solid lines on the left hand side plots of the spectral index represent the Planck 2015 1 σ limits on n_s. The top 2 panels show the predictions for $\chi_{\rm ini} = 2\ M_{PL}$ in both n_s and A_s at the pivot scale, the middle 2 panels going down show the predictions for $\chi_{\rm ini} = 5\ M_{PL}$ and the bottom 2 panels show the predictions for $\chi_{\rm ini} = 10\ M_{PL}$.

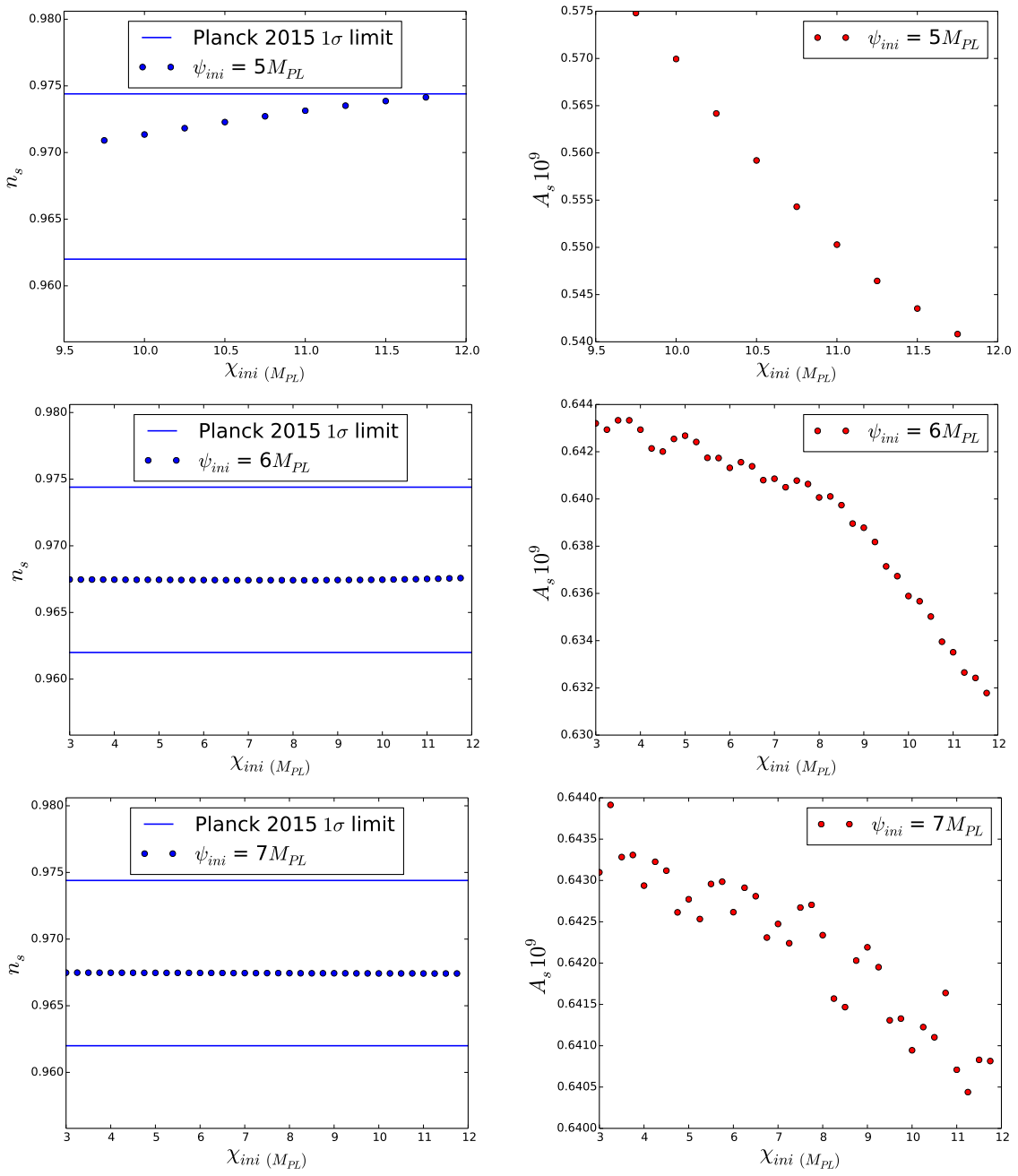

Figure 3.4: The change in the spectral index n_s (left hand side subplots) and in the amplitude A_s at the pivot point $k = 0.05\ Mpc^{-1}$ (right hand side subplots), for fixed values of $\psi_{\rm ini}$ and varying $\chi_{\rm ini}$. The solid lines on the left hand side plots of the spectral index represent the Planck 2015 1 σ limits on n_s. The top 2 panels show the predictions for $\psi_{\rm ini} = 5\ M_{PL}$ in both n_s and A_s at the pivot scale, the middle 2 panels going down show the predictions for $\psi_{\rm ini} = 6\ M_{PL}$ and the bottom 2 panels show the predictions for $\psi_{\rm ini} = 7\ M_{PL}$.

3.2.2 Varying Field Mass and Mass Ratio

Having looked at how the predictions in the model change when varying the initial conditions for the fields and keeping the masses fixed, we now want to understand how the predictions for the tensor-to-scalar ratio r, the spectral index n_s and amplitude of the power spectrum A_s at the pivot scale $k = 0.05\ Mpc^{-1}$ change when we vary the masses of the fields. We will keep the initial conditions $\psi_{\text{ini}} = 6\ M_{PL}$ and $\chi_{\text{ini}} = 3\ M_{PL}$ and alter the two mass parameters, namely the mass of the χ field, m_χ and the mass ratio $R_m = m_\psi/m_\chi$.

We consider mass ratios $R_m \in [0.15, 10]$ for values of $m_\chi \in [10^{-7}, 10^{-4}]M_{PL}$. We show in Figure 3.5 how changing the mass m_χ and the ratio of the masses R_m affects the background trajectory, by looking at $m_\chi = 10^{-5.5}M_{PL}$ and $m_\psi < m_\chi$, $m_\psi = m_\chi$ and $m_\psi > m_\chi$. If the field χ is heavier than the field ψ, then it will run towards its minimum faster than ψ. If the two fields have the same mass, then they both reach their minimum at approximately the same time, when the slow-roll parameters also approach 1. For the case when ψ is much heavier than χ, inflation ends before the field χ has a chance to reach its minimum, leading to the possibility of double-inflation [56].

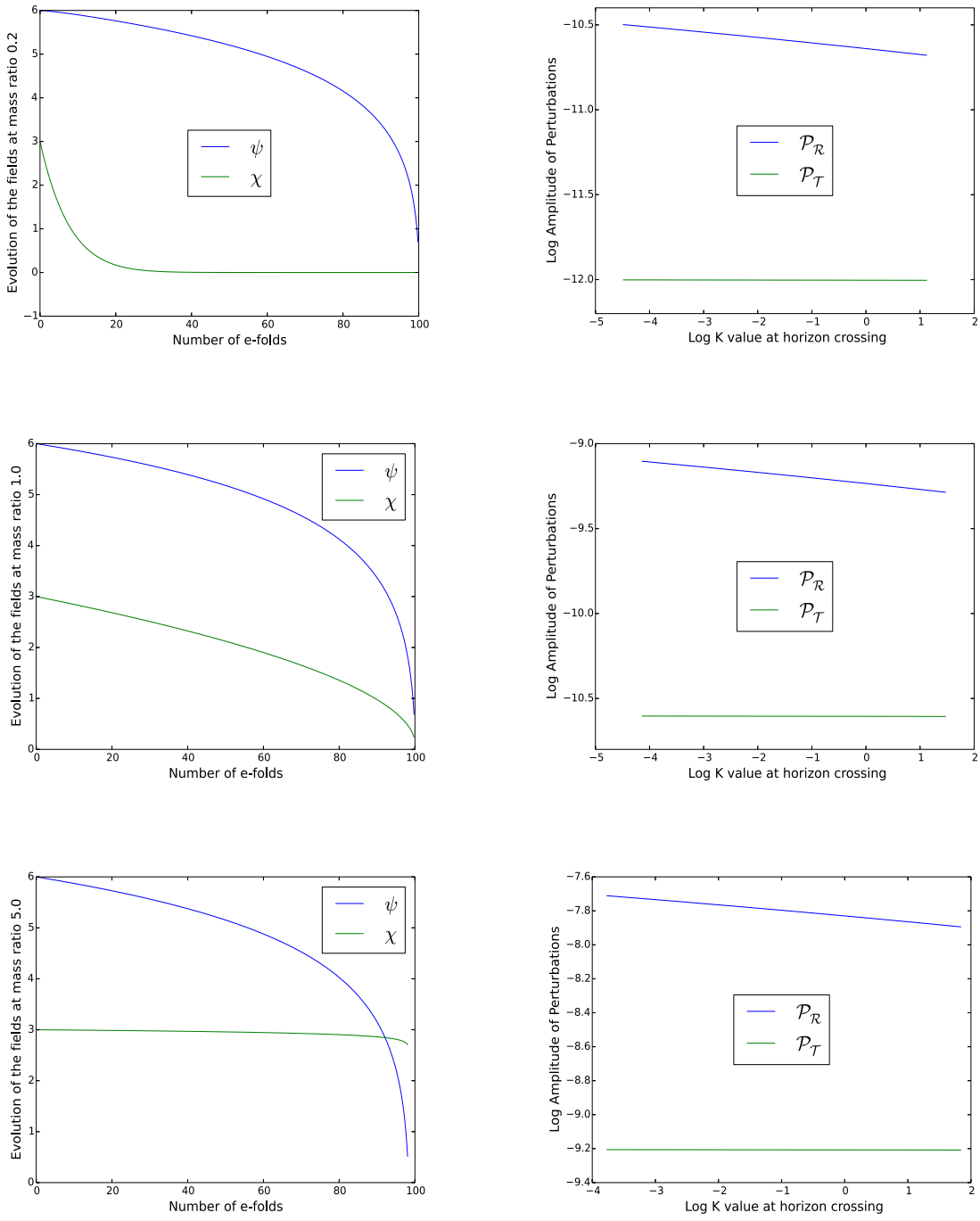

Figure 3.5: Field trajectories and corresponding scalar power spectra for runs with the same field starting conditions, $\psi_{\rm ini} = 6\ M_{PL}$ and $\chi_{\rm ini} = 3\ M_{PL}$, for a mass $m_\chi = 10^{-5.5} M_{PL}$ and varying the mass ratio R_m. The top row shows the case $R_m = 0.2$, or $m_\psi < m_\chi$, the next row down shows $R_m = 1.0$, or $m_\psi = m_\chi$ and the bottom row shows $R_m = 5.0$, or $m_\psi > m_\chi$. The power spectra plots illustrate the qualitative behaviour in these three cases; the numerical values hold no significance for our analysis.

The extended Starobinsky model we are considering gives predictions consistent with observational Planck 2015 results, however they are sensitive to the masses of the fields. We would like to note how the predictions compare to the 2013 results; we want to use this as an argument as to how robust our choice of model is when comparing it to observational data.

As such, we mark the regions which predict the spectral index n_s and amplitude A_s to be consistent with the Planck 2013 results [57]. We considered mass ratios $R_m \in [0.15, 10]$, for values of $m_\chi \in [10^{-7}, 10^{-4}]$. The results are summarised in the table below:

$m_\chi(M_{PL})$	$m_\psi(M_{PL})$
$10^{-4.5}$	$[0.179, 0.180] \bigcup [0.190, 0.191] \times 10^{-4.5}$
$10^{-6.0}$	$[5.70, 6.00] \times 10^{-6.0}$

Table 3.1: Table illustrating regions of the field mass parameter space which yield values of n_s and A_s compatible with the constraints given by the Planck 2013 data as referred to in [57].

In Figure 3.6, the black lines mark the 2013 Plank 2σ limits on the value of n_s, and it can be seen that the predictions of our model are on the upper limit of those results. The size of the range for R_m varies in order of magnitude as well, as can be seen from Table 3.1, with the variation in R_m of $\mathcal{O}(10^{-3})$ for $m_\chi = 10^{-4.5} M_{PL}$ and R_m of $\mathcal{O}(10^{-1})$ for $m_\chi = 10^{-6} M_{PL}$. For the Planck 2013 case, we are at the limits of the numerical accuracy in trying to find cases for which the predictions for both n_s and A_s are in agreement with the 2013 observational results.

For the Planck 2015 limits, we find runs that give observationally viable predictions for both n_s and A_s, as can be seen in Figure 3.6.

The Planck predictions for A_s do not change between the two rounds of analysis from the Planck collaboration. As can be seen from Figure 3.7, for every choice of

mass ratio R_m, there exists a range of values of m_χ which place the predictions for the amplitude of the scalar power spectrum within the observational limits. The same can be said for the tensor-to-scalar ratio r, which is predicted to be small and stays below 0.053 in the range of masses and mass ratios considered, as can be seen in Figure 3.8.

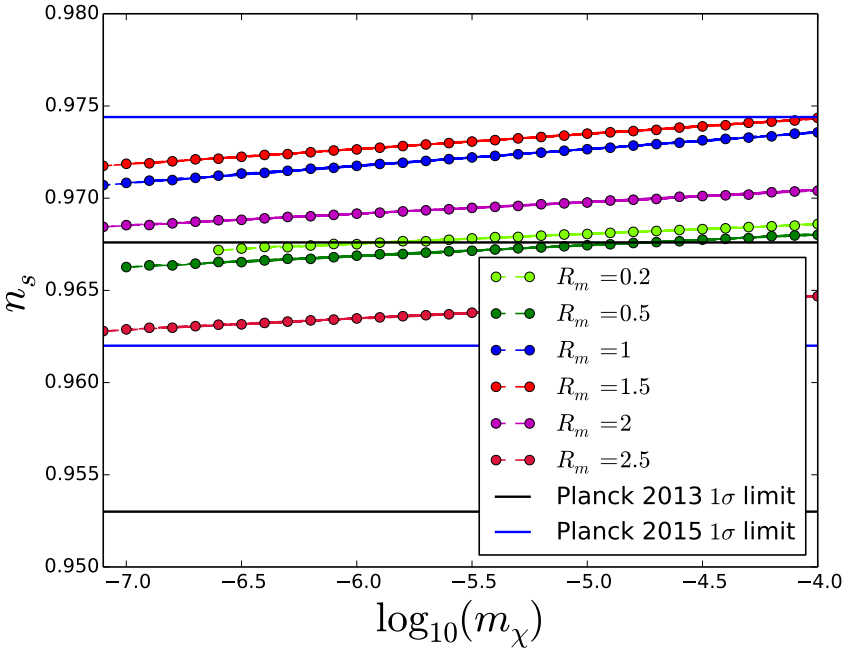

Figure 3.6: The change in spectral index n_s with change in m_χ and ratio R_m. The solid blue lines represent the Planck 2015 1 σ limit on the value of the spectral index. The solid black lines represent the Planck 2013 1 σ limit on the value of the spectral index. The coloured lines mark predictions from runs with the same value of R_m and different choices of m_χ.

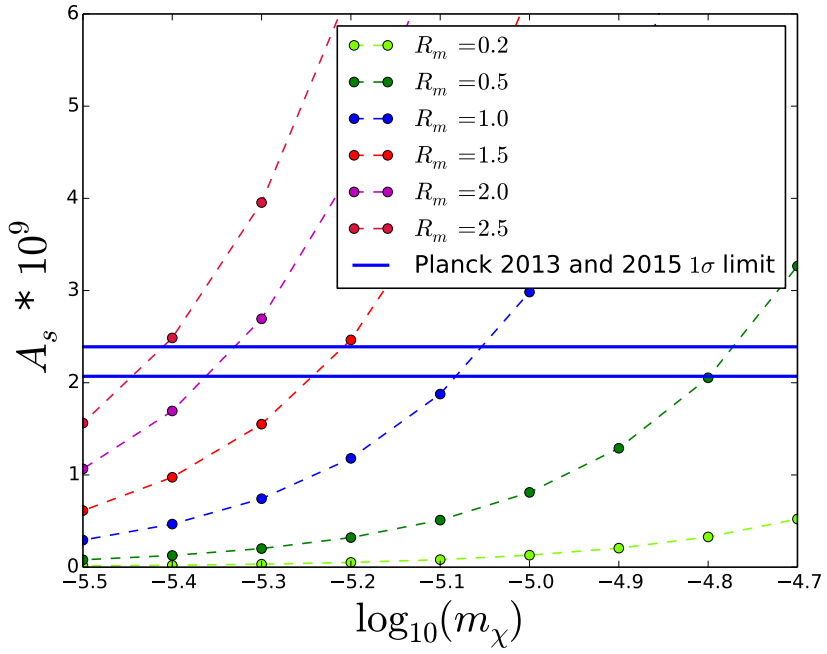

Figure 3.7: The change in amplitude of the power spectrum with change in m_χ and ratio R_m. The solid blue lines represent the Planck 2013 and 2015 1 σ limit on the value of the amplitude of the scalar power spectrum. The coloured lines mark predictions from runs with the same value of R_m and different choices of m_χ. As can be seen, for any choice of mass ratio R_m considered, there is a mass range for m_χ which gives predictions of A_s in agreement with observation.

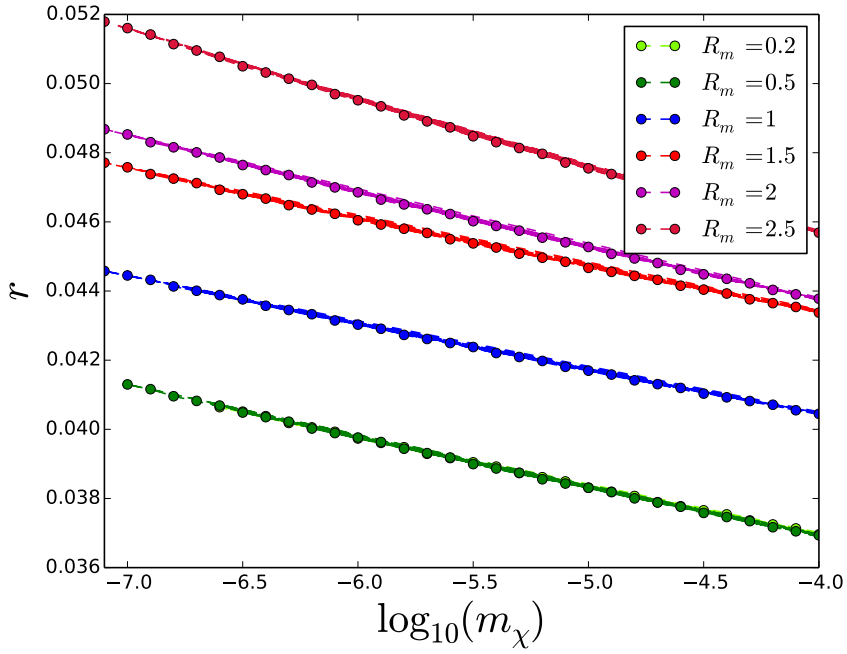

Figure 3.8: The change in tensor-to-scalar ratio with change in m_χ and ratio R_m. The coloured lines mark predictions from runs with the same value of R_m and different choices of m_χ.The tensor-to-scalar ratio stays below 0.053 for the range considered.

3.3 Summary of the Starobinsky Model Extension

The simplest extension to the Starobinsky model we have analysed in this Chapter was found to be stable under changes to conditions of the initial starting values of the fields in the considered range, $\psi_{\rm ini},\ \chi_{\rm ini} \in \{1, 10\}M_{PL}$. The predictions for the tensor-to-scalar ratio, spectral index and amplitude of the scalar power spectrum at a pivot scale of $k_0 = 0.05\ Mpc^{-1}$ vary little with the changes in initial field conditions. The spectral index stays consistently within the Planck 2015 allowed region and the amplitude of the power spectrum varies by a maximum of 5%. The tensor-to scalar ratio stays consistently below 0.053.

When changing the mass scales of the model, we observe a higher variation in predictions for observables than in the case of varying initial field conditions. In the considered range, with mass ratios $R_m \in \{0.15 : 10\}$ and $m_\chi \in \{10^{-7} : 10^{-4}\}$, the predictions for the spectral index are consistently within the Planck 2015 allowed range. The strongest constraint on the model comes from the prediction for the amplitude of the power spectrum. We have shown that for any given choice of mass ratio R_m considered, we can find a mass range for m_χ, such that the predictions for A_s are within the Planck allowed range. Again the predictions for the expected values of the tensor-to-scalar ratio are small and below 0.053 in the cases analysed.

It is also very important to note that the extension to the Starobinsky model considered in this chapter is in much better agreement with the Planck 2015 results, than the Planck 2013 results. This highlights the importance of understanding the dynamics of this model, for future model building of inflationary models and possibly embedding this model in a fundamental theory.

Chapter 4

Fine-Structure of Power Spectra in Two-Field Inflationary Models

In this chapter we will discuss at the running of the spectral index $\alpha_s = \frac{dn_s}{d\ln k}$ and the running of the running $\beta_s = \frac{d\alpha_s}{d\ln k}$ defined in (1.108) and (1.109) respectively. The most recent Planck collaboration analysis [20] places the Starobinsky model as the most favoured model in the $n_s - r$ plane. We will investigate the fine-structure of the power spectrum in the extended Starobinsky model in Chapter 3 and see how the predictions compare to observation. We will also consider other models with non-canonical kinetic terms and a model with a potential motivated by supergravity.

The interest in investigating the power spectrum beyond n_s was raised by recent observational studies of the CMB, which present large values for α_s and β_s [58], [59]. In [59] the constraints on the running are given by $\alpha_s = 0.011 \pm 0.010$ and $\beta_s = 0.027 \pm 0.013$ at a pivot scale of $k = 0.05 Mpc^{-1}$. In other words, β_s is positive in the 2σ limit and it appears to be larger than α_s. Not all cosmological models would predict such a hierarchy and work has been done to understand what kinds of models would

predict such running of the spectral index and running of the running [60]. There are a relatively limited number of studies looking at the running [61], [62], [63], [64] or the running of the running [58], [65].

We will discuss the semi-analytical approach in [60] and compare its predictions to those given by numerical fits on the power spectrum to second-order in slow-roll, obtained from the method in [47]. We will then present our predictions for two-field models of the running of the spectral index α_s and the running of the running β_s.

4.1 The Semi-Analytical Approach

Following the approach defined in [60] we work on models of General Relativity gravity with a scalar field Lagrangian P, depending on two fields ϕ^I with kinetic terms $X^{JK} = \frac{1}{2} g^{\mu\nu} \left(\partial\phi^J/\partial x^\mu\right) \left(\partial\phi^K/\partial x^\nu\right)$, with $I, K, J = 1, 2$.

The action for this system is:

$$S = \int d^4x\sqrt{-g} \left[\frac{1}{2}R + P\left(\phi^I, X^{JK}\right)\right]. \tag{4.1}$$

We recall the definition of the n^{th} order Hubble-flow parameters as defined in (1.58):

$$\begin{aligned} \epsilon_0 &= -\frac{\dot{H}}{H^2} \\ \epsilon_{n+1} &= \frac{\dot{\epsilon}_n}{H\epsilon_n}, \end{aligned} \tag{4.2}$$

where H is the expansion rate during inflation and the dot denotes the derivative with respect to cosmic time. We work in the slow-roll regime, where the slow-roll parameters defined in (4.2) are assumed to be very small ($\epsilon_n \ll \mathcal{O}(1)$) and not to vary much in time.

Under these assumptions, the power spectrum $\mathcal{P}_{\mathcal{R}}$ (3.41) of the curvature perturbation $\mathcal{R}$ at horizon crossing is to leading order [66], [67]:

$$\mathcal{P}_{\mathcal{R}*} \simeq \frac{H^2}{8\pi^2 \epsilon_0 c_s}, \tag{4.3}$$

where $*$ refers to horizon crossing where $c_s k = aH$ and c_s is the speed of sound of the adiabatic perturbation, related to the energy density and pressure by:

$$c_s^2 = \frac{\dot{p}}{\dot{\rho}}. \tag{4.4}$$

We further define the following slow-roll parameters [66], [67]:

$$\begin{aligned} s_0 =& \frac{\dot{c}_s}{H c_s}, \\ s_{n+1} =& \frac{\dot{s}_n}{H s_n}, \end{aligned} \tag{4.5}$$

which we assume to be small as well. At horizon crossing, the spectral index n_s, the running of the spectral index α_s and the running of the running β_s, in the lowest order slow-roll approximation, are:

$$(n_s^* - 1) \equiv \frac{d \ln \mathcal{P}_{\mathcal{R}}}{d \ln k}|_{c_s k = aH} \simeq -\frac{d \ln \mathcal{P}_{\mathcal{R}}}{dN}|_{c_s k = aH} \simeq -2\epsilon_0 - \epsilon_1 - s_0, \tag{4.6}$$

$$\alpha_s^* \equiv \frac{dn_s}{d \ln k}|_{c_s k = aH} \simeq -2\epsilon_0 \epsilon_1 - \epsilon_1 \epsilon_2 - s_0 s_1, \tag{4.7}$$

$$\beta_s^* \equiv \frac{d\alpha_s}{d \ln k}|_{c_s k = aH} \simeq -2\epsilon_0 \epsilon_1 (\epsilon_1 + \epsilon_2) - \epsilon_1 \epsilon_2 (\epsilon_2 + \epsilon_3) - s_0 s_1 (s_1 + s_2). \tag{4.8}$$

As one can see, at horizon crossing, $n_s - 1$ is linear in the slow-roll parameters, whereas α_s is quadratic and β_s is cubic in the slow-roll parameters. As such there should be a hierarchy that $n_s - 1 > \alpha_s > \beta_s$. In single field inflation, these results stay true after horizon crossing. In contrast, in two field models, such as the extended

Starobinsky model we considered in Chapter 3, this hierarchy might no longer hold true, because entropy perturbations in general source the curvature perturbations outside the horizon.

Therefore, on super-horizon scales, we must study isocurvature modes. We use the transfer function formalism of [48] where the total power spectrum at the end of inflation is related to the horizon crossing spectrum:

$$\mathcal{P}_{\mathcal{R}} = \mathcal{P}_{\mathcal{R}*}\left(1 + \mathcal{T}^2_{\mathcal{R}S}\right) \equiv \frac{\mathcal{P}_{\mathcal{R}*}}{\cos^2\Theta}. \tag{4.9}$$

$\mathcal{T}_{\mathcal{R}S}$ is the transfer function describing the effect of entropy perturbations on the growth of $\mathcal{R}$ and the transfer angle is:

$$\Theta = \tan^{-1}\mathcal{T}_{\mathcal{R}S}. \tag{4.10}$$

The transfer angle parametrises the superhorizon evolution and allows us to relate the value of n_s, α_s and β_s to their horizon crossing values. Using (4.6) through to (4.9) we find the values of the spectral index, the running and the running of the running at the end of inflation:

$$\begin{aligned}(n_s - 1) =& \frac{d\ln\mathcal{P}_{\mathcal{R}*}}{d\ln k} + \frac{d\ln(1+\mathcal{T}^2_{\mathcal{R}\mathcal{S}})}{d\ln k} \\ \simeq& (n_s^* - 1) + \frac{1}{H_*}\frac{d\ln(1+\mathcal{T}^2_{\mathcal{R}\mathcal{S}})}{dt_*}\end{aligned} \tag{4.11}$$

$$\alpha_s \simeq \alpha_s^* + \frac{1}{H_*^2}\frac{d^2\ln(1+\mathcal{T}^2_{\mathcal{R}\mathcal{S}})}{dt_*^2} \tag{4.12}$$

$$\beta_s \simeq \beta_s^* + \frac{1}{H_*^3}\frac{d^3\ln(1+\mathcal{T}^2_{\mathcal{R}\mathcal{S}})}{dt_*^3}. \tag{4.13}$$

In order to relate the perturbations in the early universe to those at later cosmic time, we need to understand the superhorizon evolution. At superhorizon scales, due to local energy conservation, the curvature perturbation $\mathcal{R}$ remains constant for

adiabatic perturbations [68]. Although entropy perturbations can generate curvature perturbations, purely adiabatic perturbations cannot generate entropy perturbations on superhorizon scales. Thus the time dependence of adiabatic and entropy perturbations on superhorizon scales can be modelled by [48]:

$$\begin{aligned} \dot{\mathcal{R}} &\simeq AH\mathcal{S} \\ \dot{\mathcal{S}} &\simeq BH\mathcal{S}, \end{aligned} \tag{4.14}$$

where A and B are model-dependent couplings.

The solution to these equations can be obtained by integrating (4.14) written as:

$$\begin{pmatrix} \mathcal{R} \\ \mathcal{S} \end{pmatrix} = \begin{pmatrix} 1 & \mathcal{T}_{\mathcal{RS}} \\ 0 & \mathcal{T}_{\mathcal{SS}} \end{pmatrix} \begin{pmatrix} \mathcal{R} \\ \mathcal{S} \end{pmatrix}^{*}, \tag{4.15}$$

with the transfer functions:

$$\mathcal{T}_{\mathcal{SS}}(t) = \exp\left(\int_{t^*}^{t} B(t)H(t)dt\right), \tag{4.16}$$

$$\mathcal{T}_{\mathcal{RS}}(t) = \int_{t^*}^{t} A(t)H(t)\mathcal{T}_{\mathcal{SS}}(t)dt. \tag{4.17}$$

Using this form we can evaluate the time derivatives of the transfer functions:

$$\begin{aligned} \dot{\mathcal{T}}_{\mathcal{RS}} &\simeq -H_*(A_* + B_*\mathcal{T}_{\mathcal{RS}}), \\ \ddot{\mathcal{T}}_{\mathcal{RS}} &\simeq H_*^2(A_*B_* + B_*^2\mathcal{T}_{\mathcal{RS}}), \\ \dddot{\mathcal{T}}_{\mathcal{RS}} &\simeq -H_*^3(A_*B_*^3 + B_*^3). \end{aligned} \tag{4.18}$$

With the definition of the transfer angle (4.10) and diverse trigonometric relations, we can show that:

$$n_s \simeq n_s^* - 2\sin(2\Theta)A_* + 2B_*\sin^2\Theta, \tag{4.19}$$

$$\alpha_s \simeq \alpha_s^* + 2\cos\Theta(A_*\cos\Theta + B_*\sin\Theta)(A_*\cos(2\Theta) + B_*\sin(2\Theta)), \tag{4.20}$$

$$\begin{aligned} \beta_s \simeq \beta_s^* &- 2\cos\Theta(A_*\cos\Theta + B_*\sin\Theta)(B_*\cos(2\Theta) - A_*\sin(2\Theta))\cdot \\ &\cdot (A_* + 2A_*\cos(2\Theta) + 2B_*\sin(2\Theta)). \end{aligned} \tag{4.21}$$

For models with actions:

$$S = \int d^4x\sqrt{-\tilde{g}}\left[\frac{\tilde{R}}{2} + X^{\phi\phi} + e^b X^{\chi\chi} - V(\phi,\chi)\right], \tag{4.22}$$

we have $c_s = 1$. Expressions for A and B are given by [60] and [69]:

$$A \simeq -2\eta_{\sigma s} - \epsilon_{b\chi}\sin^2\theta, \tag{4.23}$$

$$B \simeq (\eta_{\sigma\sigma} - \eta_{ss}) - 2\epsilon_0 - \frac{1}{2}\epsilon_{b\chi}(1 + \sin^2\theta - \sin\theta\cos\theta), \tag{4.24}$$

with $\cos\theta = \dot{\phi}/\dot{\sigma}$, $\sin\theta = e^b\dot{\chi}/\dot{\sigma}$ with $\dot{\sigma}^2 = \dot{\phi}^2 + \dot{\chi}^2 e^{2b}$,

$$\epsilon_{b\chi} = 2\frac{V_\chi b_\phi}{V} \tag{4.25}$$

and $\eta_{\sigma\sigma}$, η_{ss} and $\eta_{\sigma s}$ are as defined in (3.22).

We are now in the position to evaluate the power spectra in a number of models.

4.2 A Numerical Method

We introduce a second method to evaluate the running of the spectral index and the running of the running. We perform a numerical fit to the power spectrum evaluated to second order in slow-roll as presented in Section 3.1.2 in the previous chapter. We evaluate the fit to the parametrisation of the power spectrum introduced in (1.107), which we recall here:

$$\mathcal{P}_\mathcal{R} = A_s\left(\frac{k}{k_0}\right)^{n_s - 1 + \frac{\alpha_s}{2}\log\frac{k}{k_0} + \frac{\beta_s}{6}(\log\frac{k}{k_0})^2}, \tag{4.26}$$

with n_s, α_s and β_s are free parameters in the fit, which will be evaluated for a horizon crossing value of $k_0 = 0.05 Mpc^{-1}$.

For the numerical fit we use two modules from independent Python libraries; from the Scipy package [70] we use "optimization.curve_fit()" and from Numpy [71]

"numpy.polyfit". We find that the results predicted with the two methods are in agreement up to order $\mathcal{O}(10^{-6})$, so for the rest of the chapter we will use the numerical values predicted by the Scipy fitting module to discuss the model predictions for α_s and β_s. To make the presentation of the results easier in the following section, we introduce the parameter $e_m = \log_{10} m$, which is the base 10 logarithm of the mass m in the model.

The semi-analytical method is based on the slow-roll approximation and ignores higher order contributions to the power spectrum. In order to make accurate predictions about the running of the spectral index and the running of the running, this proves to be insufficient, as we will discuss later in this chapter.

4.3 Simplest Extension to Starobinsky and Modifications

We begin with a Lagrangian that looks like the extended Starobinsky model in the Einstein frame, but make the modification $\alpha \to \alpha_m$, where $\alpha_m \neq \frac{1}{\sqrt{6}}$. In other words, the action is written as:

$$S_E = \int d^4x\sqrt{-\tilde{g}}\left[\frac{\tilde{R}}{2\kappa} - \frac{\tilde{g}^{\mu\nu}}{2}(\tilde{\nabla}_\mu\psi)(\tilde{\nabla}_\nu\psi) - \frac{1}{2}\tilde{g}^{\mu\nu}e^{2b}(\tilde{\nabla}_\mu\chi)(\tilde{\nabla}_\nu\chi) - V\right], \tag{4.27}$$

with:

$$V = \frac{(1-e^{2b})^2}{8\kappa^2\mu} + \frac{1}{2}m^2e^{4b}\chi^2, \tag{4.28}$$

where the parameter b is now given as:

$$b(\psi) = -\alpha_m\psi. \tag{4.29}$$

We relate the mass of the scalaron ψ to the potential by:

$$\mu = \frac{\alpha_m^2}{m_\psi^2}. \tag{4.30}$$

We will look at models with different values of α_m and analyse the effect changing the masses of the fields has on the values of the running α_s and the running of the running β_s. We will focus on models whose predictions for the spectral index n_s and the amplitude A_s are within the Planck 2015 accepted range.

4.3.1 Changing α_m and Mass Ratios R_m

In this subsection, we will analyse three scenarios by chosing $\alpha_m = \alpha = 1/\sqrt{6}$, $\alpha_m = 0.1\alpha$ and $\alpha_m = 2\alpha$. We are interested in finding combinations of mass scales for the two fields, m_χ and $R_m = m_\psi/m_\chi$, which predict values of n_s and A_s in the Planck 2015 tolerance. For those cases we will show what the predictions for the running α_s and the running of the running β_s are. We fix the initial conditions of the fields at $\psi_{ini} = 5M_{PL}$ and $\chi_{ini} = 16M_{PL}$. In Figures 4.1, 4.2 and 4.3 we show the results for the choice of model $\alpha_m = \alpha$. Figure 4.1 illustrates the behaviour of the amplitude of the power spectrum A_s under changing m_χ and R_m. We observe how with increase in mass m_χ, the relative change in the value of the amplitude for increasing mass ratio R_m grows. For all masses m_χ, in Figure 4.1a, the values of R_m in reverse order from the top are $2.5, 2, 1.5, 1, 0.5, 0.2$. This behaviour is important, because as we will see later, for certain models, there are no values of both A_s and n_s in the Planck 2015 accepted range. Figure 4.2a illustrates the behaviour of the spectral index n_s under changing m_χ and R_m. For all values of m_χ in $m_\chi \in \{10^{-4.7} : 10^{-5.6}\}\ M_{PL}$ and $R_m \in \{0.15 : 2.5\}$, the predictions for the spectral index are in the Planck 2015 3 σ limits. Figure 4.2b shows the values of n_s for runs which predict both n_s and A_s in the Planck 2015

accepted range. In Figure 4.3 we see the predictions of this model for the running of the spectral index and the running of the running. The predictions show that there are choices of mass and mass ratio which lead to an inverted hierarchy, where $\beta_s > \alpha_s$. There are also runs which predict a positive β_s. These results are favoured by the analysis on the Planck 2015 data done by [59], and we show that the predictions on the fine-structure of the power spectrum from the extension to the Starobisnky model are in agreement with observation. In Figures 4.4 and 4.5 we show the results for the choice of model $\alpha_m = 0.1\alpha$, for masses m_χ and R_m which give predictions for A_s and n_s in the Planck 2015 accepted range. Figure 4.5 illustrates the behaviour of the running of the spectral index and the running of the running. The predictions show that $\alpha_s < 0$ and $\beta_s > 0$, although $|\beta_s| < |\alpha_s|$.

Figures 4.6 and 4.7 illustrate the results for the choice of model $\alpha_m = 2\alpha$, for masses m_χ and R_m which give predictions for A_s and n_s in the Planck 2015 accepted range. Figure 4.7 showes the behaviour of the running of the spectral index and the running of the running. The predictions are that $\alpha_s < 0$ and $\beta_s < 0$ with this choice of model.

To summarise, in the Starobinsky model with a scalar field, as we increase α_m, we are suppressing the dynamics of the field χ and we are closer to the single field regime, where the hierarchy of the runnings is as expected. As we decrease α_m, the field χ plays a more important role in the inflationary dynamics. We observe positive values of α_s in the case $\alpha_m = 0.1\alpha$ and $\beta_s > 0$ in the case $\alpha_m = \alpha$. We will proceed to discuss the behaviour of other two field models.

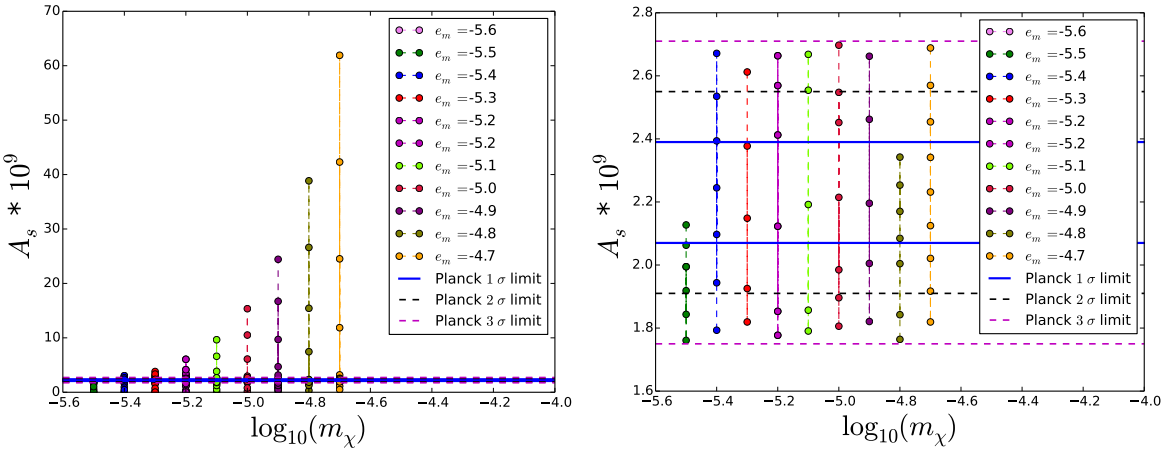

(a) A_s for $R_m \in \{0.2, 0.5, 1, 1.5, 2, 2.5\}$ (b) A_s for Planck accepted range

Figure 4.1: Predictions for the amplitude of the power spectrum in the extended Starobinsky model for the choice $\alpha_m = \alpha = 1/\sqrt{6}$. The initial starting conditions for all runs are $\psi_{ini} = 5\ M_{PL}$ and $\chi_{ini} = 16\ M_{PL}$. The left hand side figure presents the evolution of A_s with respect to changing mass scales $m_\chi = 10^{e_m} \in \{10^{-4.7} : 10^{-5.6}\}\ M_{PL}$ and $R_m \in \{0.2, 0.5, 1, 1.5, 2, 2.5\}$. We note the power law evolution of A_s with respect to changing m_χ for a given choice of R_m, e.g. the top points represented in Figure 4.1a correspond to $R_m = 2.5$. The right hand side figure contains a wider range of choices for R_m for the same range on m_χ. We only show the runs with prediction for A_s in the Planck 2015 3 σ limits.

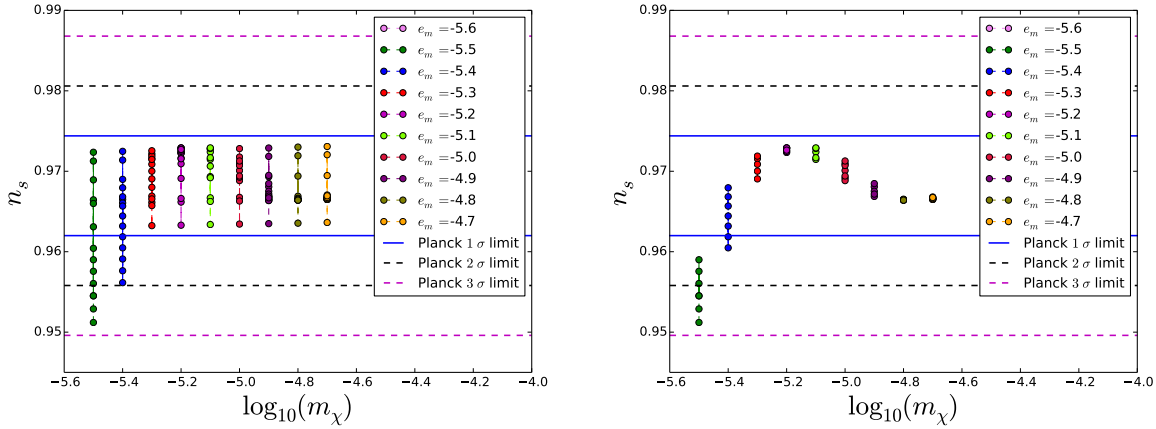

(a) n_s for wide range (b) n_s for Planck accepted range

Figure 4.2: Predictions for the spectral index in the extended Starobinsky model for the choice $\alpha_m = \alpha = 1/\sqrt{6}$. The initial starting conditions for all runs are $\psi_{ini} = 5\ M_{PL}$ and $\chi_{ini} = 16\ M_{PL}$. The left hand side figure presents the evolution of n_s with respect to changing mass scales $m_\chi = 10^{e_m} \in \{10^{-4.7} : 10^{-5.6}\}\ M_{PL}$ and R_m varying between 0.2 and 2.5. The predictions for n_s in this model are consistently in the Planck 2015 accepted range. The right hand side figure contains only the choices of R_m and m_χ which predict the amplitude of the power spectrum A_s in the Planck 2015 3 σ limits.

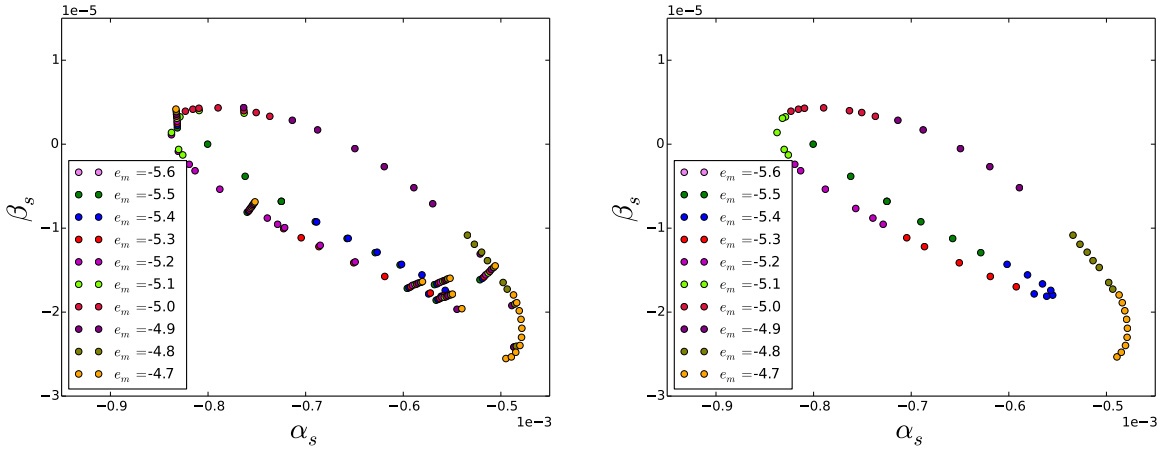

(a) α_s and β_s for wide range

(b) α_s and β_s for Planck accepted range

Figure 4.3: Predictions for the running of the spectral index α_s and the running of the running β_s in the extended Starobinsky model for the choice $\alpha_m = \alpha = 1/\sqrt{6}$. The initial starting conditions for all runs are $\psi_{ini} = 5\ M_{PL}$ and $\chi_{ini} = 16\ M_{PL}$. The left hand side figure presents the values of α_s and β_s for all the runs with mass scales $m_\chi = 10^{e_m} \in \{10^{-4.7} : 10^{-5.6}\}\ M_{PL}$ and $R_m \in \{0.2 : 2.5\}$. The right hand side figure contains only the results from runs where both A_s and n_s are in the Planck 2015 3 σ limits. For this choice of model, there are choices of m_χ and R_m which lead to positive predictions for β_s and cases where $\beta_s > \alpha_s$, which are favoured by the Planck 2015 measurements.

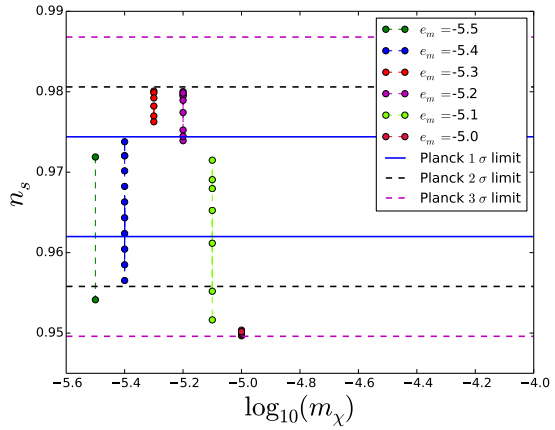

(a) n_s for the choice $\alpha_m = 0.1\alpha$

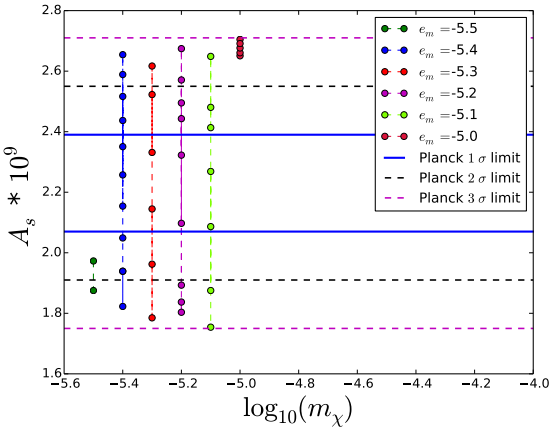

(b) A_s for the choice $\alpha_m = 0.1\alpha$

Figure 4.4: Predictions for the spectral index and amplitude of the power spectrum in the extended Starobinsky model for the choice $\alpha_m = 0.1\alpha$. The initial starting conditions for all runs are $\psi_{ini} = 5\ M_{PL}$ and $\chi_{ini} = 16\ M_{PL}$. The left hand side figure presents the values of n_s for runs with mass scales $m_\chi = 10^{e_m} \in \{10^{-4.7} : 10^{-5.6}\}\ M_{PL}$ and $R_m \in \{0.2 : 2.5\}$. Both figure contain the predictions for cases where both A_s and n_s are in the Planck 2015 3 σ limits.

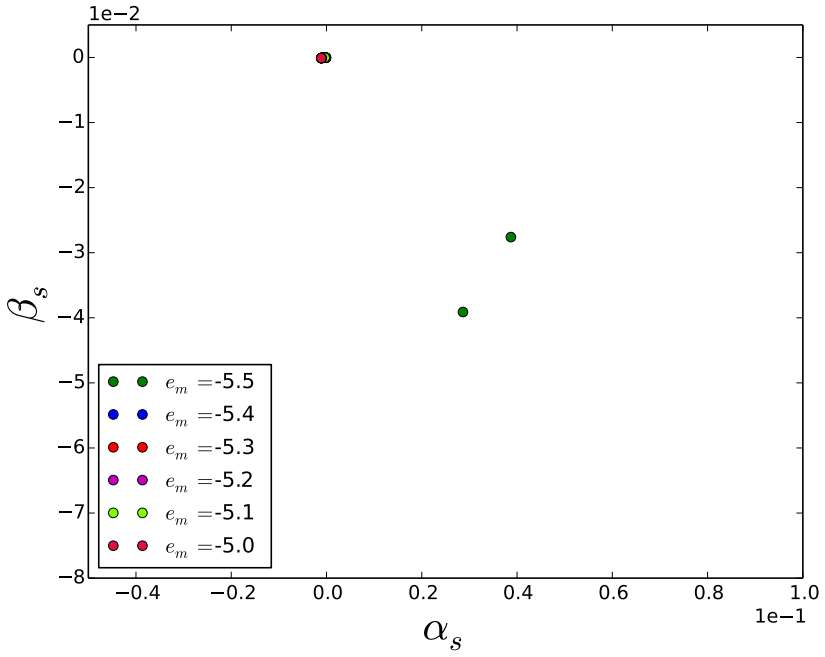

Figure 4.5: Predictions for the running of the spectral index α_s and the running of the running β_s in the extended Starobinsky model for the choice $\alpha_m = 0.1\alpha$. The initial starting conditions for all runs are $\psi_{ini} = 5\ M_{PL}$ and $\chi_{ini} = 16\ M_{PL}$. The values of α_s and β_s are shown for runs with mass scales $m_\chi = 10^{e_m} \in \{10^{-4.7} : 10^{-5.6}\}\ M_{PL}$ and $R_m \in \{0.2 : 2.5\}$. The results are for runs where both A_s and n_s are in the Planck 2015 3 σ limits.

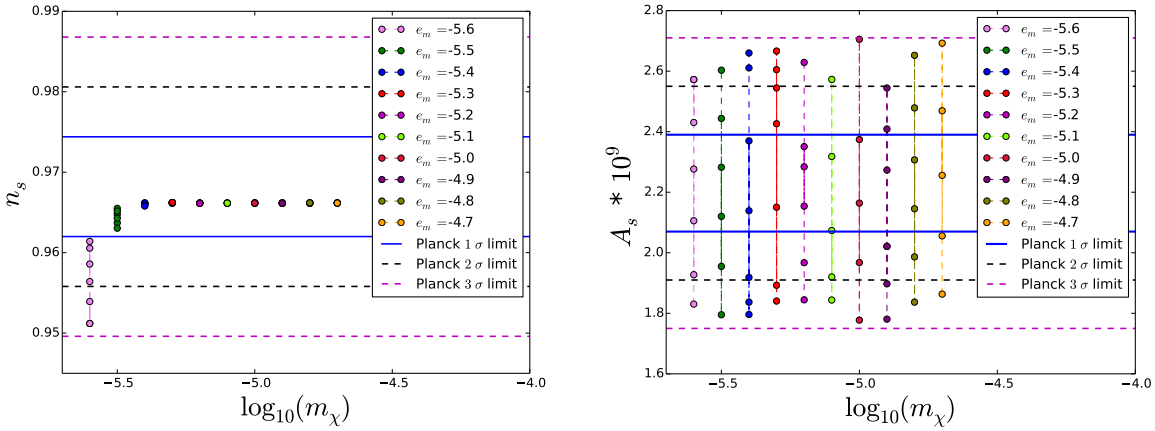

(a) n_s for the choice $\alpha_m = 2\alpha$ (b) A_s for the choice $\alpha_m = 2\alpha$

Figure 4.6: Predictions for the spectral index and amplitude of the power spectrum in the extended Starobinsky model for the choice $\alpha_m = 2\alpha$. The initial starting conditions for all runs are $\psi_{ini} = 5\ M_{PL}$ and $\chi_{ini} = 16\ M_{PL}$. The left hand side figure presents the values of n_s for runs with mass scales $m_\chi = 10^{e_m} \in \{10^{-4.7} : 10^{-5.6}\}\ M_{PL}$ and $R_m \in \{0.2 : 2.5\}$. Both figure contain the predictions for cases where both A_s and n_s are in the Planck 2015 3 σ limits.

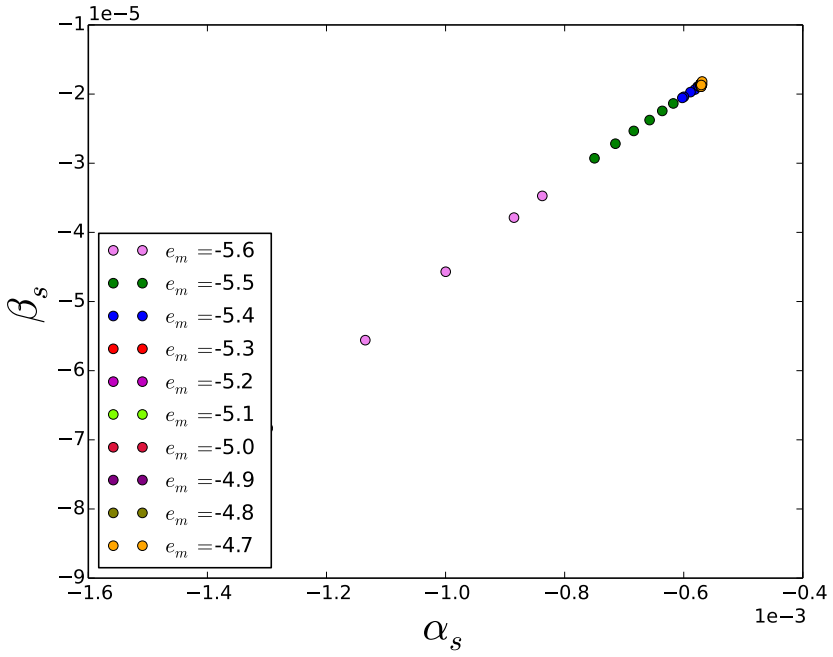

Figure 4.7: Predictions for the running of the spectral index α_s and the running of the running β_s in the extended Starobinsky model for the choice $\alpha_m = 2\alpha$. The initial starting conditions for all runs are $\psi_{ini} = 5\ M_{PL}$ and $\chi_{ini} = 16\ M_{PL}$. The values of α_s and β_s are shown for runs with mass scales $m_\chi = 10^{e_m} \in \{10^{-4.7} : 10^{-5.6}\}\ M_{PL}$ and $R_m \in \{0.2 : 2.5\}$. The results are for runs where both A_s and n_s are in the Planck 2015 3 σ limits.

4.4 Two Field Models with Chaotic Potential

We are interested in the action:

$$S_E = \int d^4x\sqrt{-\tilde{g}}\left[\frac{\tilde{R}}{2\kappa} - \frac{\tilde{g}^{\mu\nu}}{2}(\tilde{\nabla}_\mu\psi)(\tilde{\nabla}_\nu\psi) - \frac{1}{2}\tilde{g}^{\mu\nu}e^{b_\psi}(\tilde{\nabla}_\mu\chi)(\tilde{\nabla}_\nu\chi) - V\right], \tag{4.31}$$

with:

$$V = \frac{2}{2}m_\psi^2\psi^2 + \frac{1}{2}m_\chi^2\chi^2 \tag{4.32}$$

and

$$b(\psi) = -\alpha_m\psi. \tag{4.33}$$

This is similar to the action in (4.27), with a different choice of potential. The dynamics of the field χ are still affected by the field ψ, but the potential is quadratic for both fields. We analyse three cases, where $\alpha_m = 0.2$, $\alpha_m = -0.2$ and $\alpha_m = 1$, we keep the choice of initial conditions for the field values fixed and vary the value of m_χ and of the ratio $R_m = \frac{m_\psi}{m_\chi}$. We consider only values of initial conditions that give predictions of the spectral index n_s and amplitude of the power spectrum A_s which are in the Planck 2015 3 σ limits. The masses we use in the numerical runs are $m_\chi \in \{10^{-5.5}, 10^{-5.4}, 10^{-5.3}, 10^{-5.2}, 10^{-5.1}, 10^{-5.0}, 10^{-4.9}, 10^{-4.8}, 10^{-4.7}\}$ and mass ratios $R_m \in \{0.1 : 2.5\}$.

4.4.1 Changing α_m and Mass Ratio R_m

In Figures 4.8 and 4.9 we consider the first case $\alpha_m = 0.2$. The initial conditions are $\psi_{ini} = 30\ M_{PL}$ and $\chi_{ini} = 10\ M_{PL}$ and for given values of m_χ, we choose the ratio $R_m \in \{0.1 : 4.5\}$ such that the predicted values of n_s and A_s are in agreement with the Planck 2015 results. In Figures 4.10 and 4.11 we present the results for the second case $\alpha_m = -0.2$, with initial conditions of the fields $\psi_{ini} = 5M_{PL}$ and

$\chi_{ini} = 16 M_{PL}$ and mass in the range $m_\chi \in \{10^{-4.7} : 10^{-5.5}\}\ M_{PL}$, with the mass ratios in $R_m \in \{0.1 : 4.5\}$. Finally, in Figures 4.12 and 4.13 we present the results for the third case with the parameter choice $\alpha_m = -1$, with initial starting values of the fields $\psi_{ini} = 30 M_{PL}$ and $\chi_{ini} = 10 M_{PL}$ and masses for the fields, $m_\chi \in \{10^{-5.5} : 10^{-5.3}\}\ M_{PL}$ and $R_m \in \{0.1 : 4.5\}$. All the parameter choices are such that the predictions for n_s and A_s are in agreement with Planck 2015 3σ limits. In all of the cases considered for this model we found $|\alpha_s| > |\beta_s|$, so no inverted hierarchy was observed. All the predictions for α_s and β_s were found to be slightly negative, but still in the 3σ limit calculated in [59].

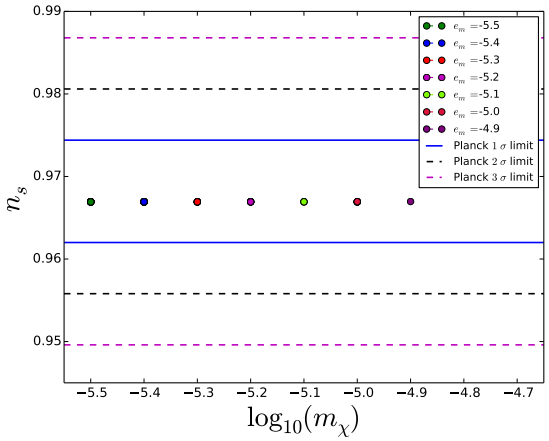

(a) n_s for the choice $\alpha_m = 0.2$

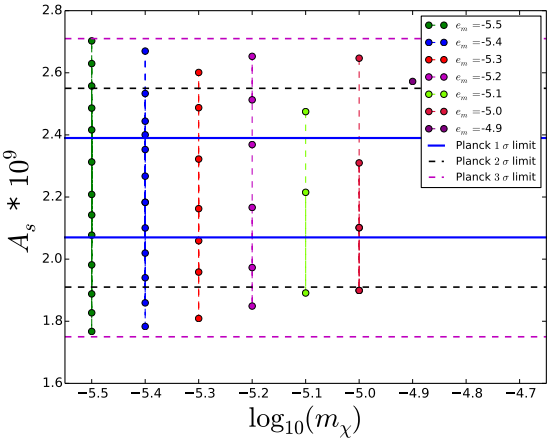

(b) A_s for the choice $\alpha_m = 0.2$

Figure 4.8: Predictions for the spectral index and amplitude of the power spectrum for the chaotic potential with the parameter choice $\alpha_m = 0.2$. The initial starting conditions for the numerical simulations are $\psi_{ini} = 30\ M_{PL}$ and $\chi_{ini} = 10\ M_{PL}$. The figures present the values of n_s on the left and A_s on the right for runs with mass in the range $m_\chi = 10^{e_m} \in \{10^{-4.7} : 10^{-5.5}\}\ M_{PL}$ and mass ratio in $R_m \in \{0.2 : 2.5\}$. Both figures contain the predictions for cases where both A_s and n_s are in agreement with the Planck 2015 results.

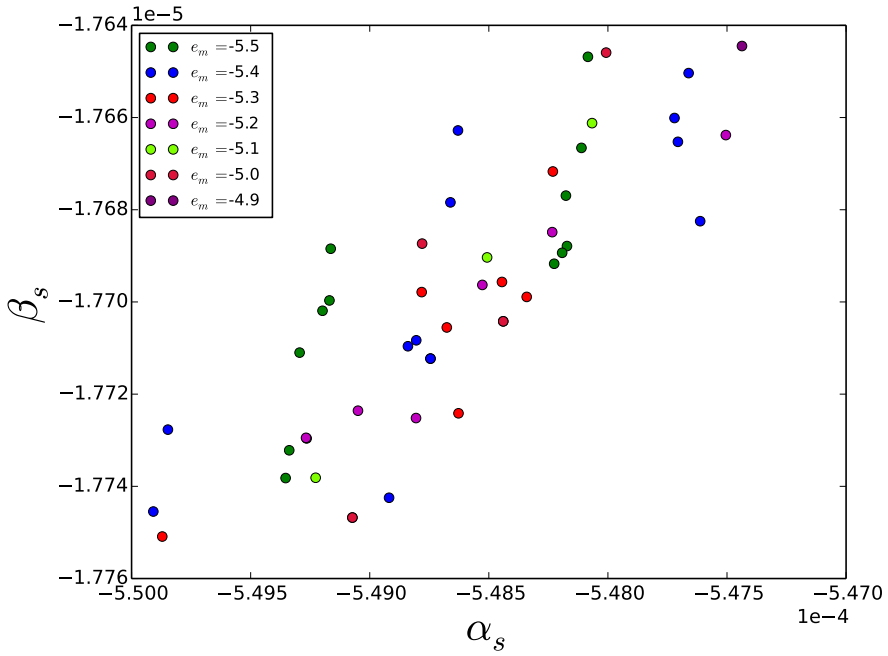

Figure 4.9: Predictions for the running of the spectral index α_s and the running of the running β_s for the chaotic potential with the parameter choice $\alpha_m = 0.2$. The initial starting conditions for the numerical simulations are $\psi_{ini} = 30\ M_{PL}$ and $\chi_{ini} = 10\ M_{PL}$. The values of α_s and β_s are shown for runs with mass scales $m_\chi = 10^{e_m} \in \{10^{-5.5} : 10^{-4.9}\}\ M_{PL}$ and $R_m \in \{0.2 : 2.5\}$. The predictions are for cases where both A_s and n_s agreement with the Planck 2015 results. We find $\alpha_s < 0$ and $\beta_s < 0$.

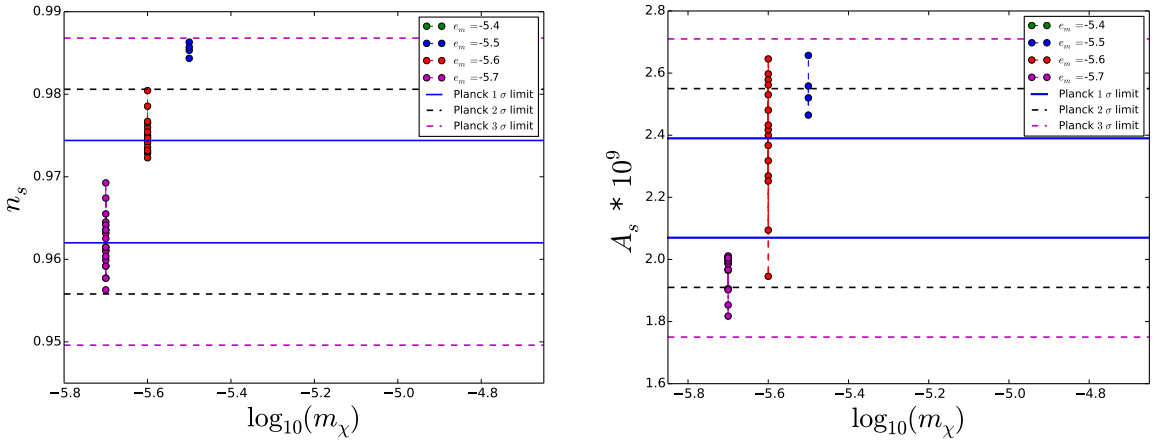

(a) n_s for the choice $\alpha_m = -0.2$ (b) A_s for the choice $\alpha_m = -0.2$

Figure 4.10: Predictions for the spectral index and amplitude of the power spectrum for the chaotic potential with the parameter choice $\alpha_m = -0.2$. The initial starting conditions for the numerical simulations are $\psi_{ini} = 5M_{PL}$ and $\chi_{ini} = 16M_{PL}$, with mass scales $m_\chi = 10^{e_m} \in \{10^{-5.7} : 10^{-5.5}\}\ M_{PL}$ and $R_m \in \{0.1 : 4.5\}$. Both figures contain the predictions for cases where both A_s and n_s are in agreement with the Planck 2015 results.

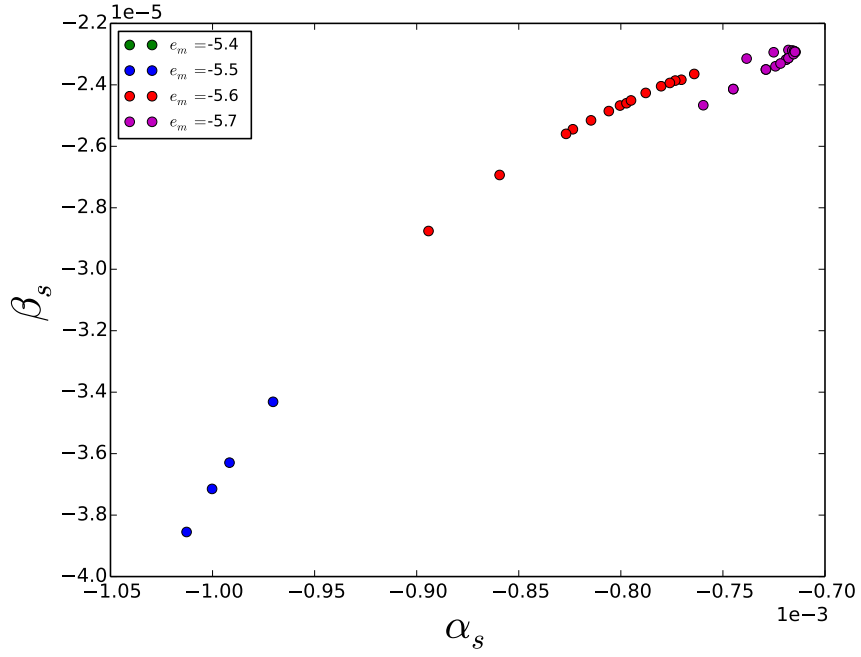

Figure 4.11: Predictions for the running of the spectral index α_s and the running of the running β_s for the chaotic potential with the parameter choice $\alpha_m = -0.2$. The initial starting conditions for the numerical simulations are $\psi_{ini} = 5M_{PL}$ and $\chi_{ini} = 16M_{PL}$. The values of α_s and β_s are shown for runs with mass scales $m_\chi = 10^{e_m} \in \{10^{-5.7} : 10^{-5.5}\}\ M_{PL}$ and $R_m \in \{0.1 : 4.5\}$. The predictions are for cases where both A_s and n_s agreement with the Planck 2015 results. We find $\alpha_s < 0$ and $\beta_s < 0$.

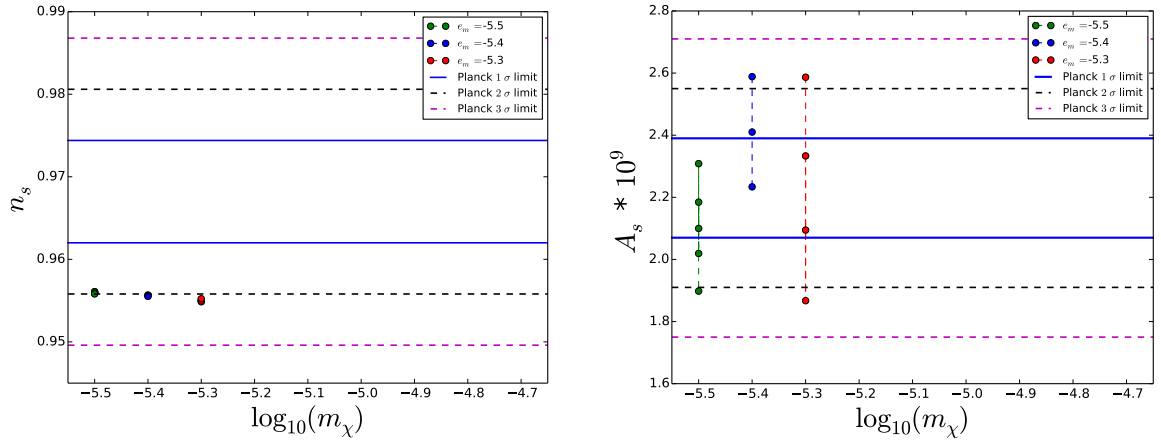

(a) n_s for the choice $\alpha_m = -1$ (b) A_s for the choice $\alpha_m = -1$

Figure 4.12: Predictions for the spectral index and amplitude of the power spectrum for the chaotic potential with the parameter choice $\alpha_m = -1$. The initial starting conditions for the numerical simulations are $\psi_{ini} = 30M_{PL}$ and $\chi_{ini} = 10M_{PL}$. The figures present the values of n_s on the left and A_s on the right for runs with mass in the range $m_\chi = 10^{e_m} \in \{10^{-5.5} : 10^{-5.3}\}\ M_{PL}$ and $R_m \in \{0.1 : 3.5\}$. Both figures contain the predictions for cases where both A_s and n_s are in agreement with the Planck 2015 results.

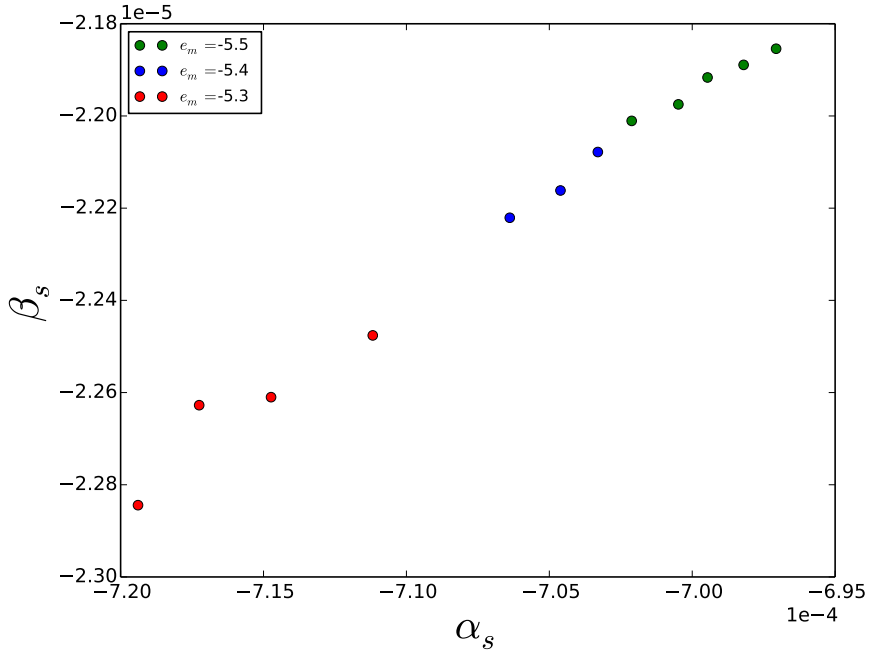

Figure 4.13: Predictions for the running of the spectral index α_s and the running of the running β_s for the chaotic potential with the parameter choice $\alpha_m = -1$. The initial starting conditions for the numerical simulations are $\psi_{ini} = 30M_{PL}$ and $\chi_{ini} = 10M_{PL}$. The values of α_s and β_s are shown for runs with mass scales $m_\chi = 10^{e_m} \in \{10^{-5.5} : 10^{-5.3}\}\ M_{PL}$ and $R_m \in \{0.1 : 3.5\}$. The predictions are for cases where both A_s and n_s agreement with the Planck 2015 results. We find $\alpha_s < 0$ and $\beta_s < 0$.

4.5 A Supergravity Motivated Model

The final model we are interested in was proposed in [72] and its action can be derived from supergravity. Like the extension to Starobinsky inflation that we have considered in 4.3, it is a two field model, where one field has a non-canonical kinetic term.

$$S_E = \int d^4x\sqrt{-\tilde{g}}\left[\frac{\tilde{R}}{2\kappa} - \frac{\tilde{g}^{\mu\nu}}{2}(\tilde{\nabla}_\mu\psi)(\tilde{\nabla}_\nu\psi) - \frac{1}{2}\tilde{g}^{\mu\nu}e^{2\sqrt{\frac{2}{3}}\psi}(\tilde{\nabla}_\mu\chi)(\tilde{\nabla}_\nu\chi) - V\right], \quad (4.34)$$

with:

$$V = \frac{3}{4}m^2\left(1 - e^{-\sqrt{\frac{2}{3}}\psi}\right)^2 + \frac{1}{2}m^2\chi^2. \quad (4.35)$$

There is only one mass scale in this model, m, so we will analyse the behaviour of the running of the spectral index α_s and the running of the running β_s under changes to conditions of the initial starting values of the fields, $\psi_{ini} \in \{6 : 13\}\ M_{PL}$ and $\chi_{ini} \in \{0.8 : 3.5\}\ M_{PL}$.

Following the same analysis as in the previous sections, we present in Figure 4.14 the predictions for n_s and A_s, for numerical runs with initial starting values of the fields in the ranges $\psi_{ini} \in \{6 : 13\}\ M_{PL}$ and $\chi_{ini} \in \{0.8 : 3.5\}\ M_{PL}$. The mass is $m \in \{10^{-5.5} : 10^{-5.2}\}\ M_{PL}$. All the parameter choices are such that the predictions for n_s and A_s are in agreement with Planck 2015 3σ limits. As can be seen in Figure 4.15, for the range we have analysed, this model predicts α_s and β_s as negative and $|\beta_s| < |\alpha_s|$, however it is still in the 3 σ limit of [59].

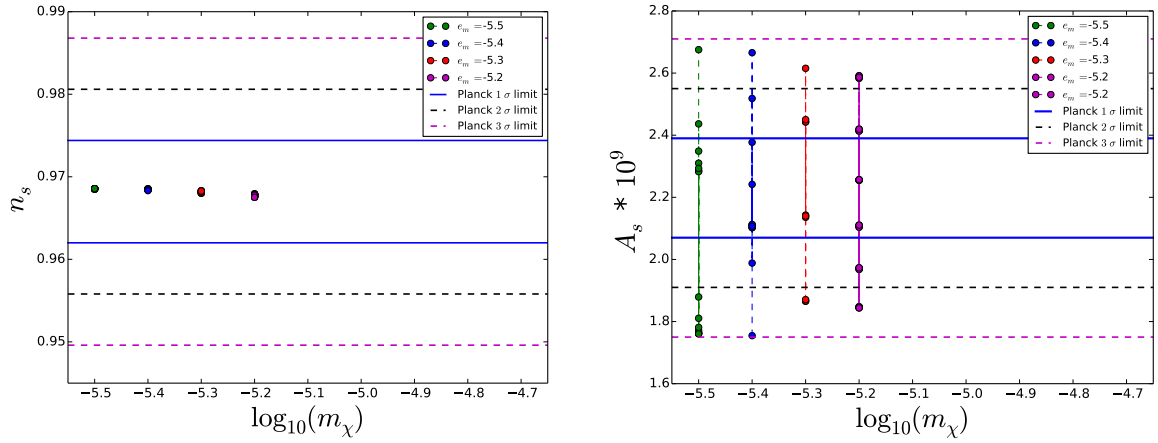

(a) n_s for the choice $\alpha_m = -1$ (b) A_s for the choice $\alpha_m = -1$

Figure 4.14: Predictions for the spectral index and amplitude of the power spectrum in a supergravity embedded model. The changes to changes to the initial starting values of the fields are in the range $\psi_{ini} \in \{6 : 13\}\ M_{PL}$ and $\chi_{ini} \in \{0.8 : 3.5\}\ M_{PL}$. The left hand side figure presents the values of n_s for runs with mass scales $m = 10^{e_m} \in \{10^{-5.5} : 10^{-5.2}\}\ M_{PL}$. Both figure contain the predictions for cases where both A_s and n_s are in the Planck 2015 3 σ limits.

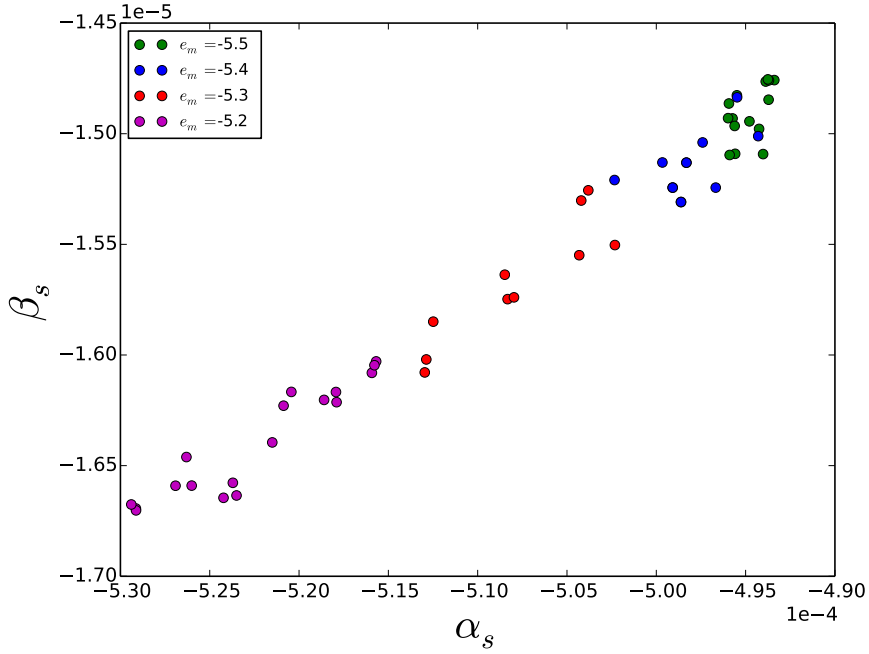

Figure 4.15: Predictions for the running of the spectral index α_s and the running of the running β_s in a supergravity embedded model. The changes to changes to the initial starting values of the fields are in the range $\psi_{ini} \in \{6 : 13\}\ M_{PL}$ and $\chi_{ini} \in \{0.8 : 3.5\}\ M_{PL}$. The figure presents the values for runs with mass scales $m = 10^{e_m} \in \{10^{-5.5} : 10^{-5.2}\}\ M_{PL}$. The runs presented give predictions for cases where both A_s and n_s are in the Planck 2015 3 σ limits.

4.5.1 Comparing the Two Methods

We compare the predictions for n_s, α_s and β_s using two methods. In the first, we use the semi-analytic method presented in Section 4.1 to evaluate the values of the running of the spectral index α_s and of the running of the running β_s. In the second, we perform a numerical fit to the power spectrum evaluated to second order in slow-roll as discussed in Section 3.1.2.

We analyse the Supergravity motivated potential introduced in (4.34), where we find that the predictions for the running of the spectral index α_s and the running of the running β_s are not consistent between the two methods. To illustrate, we present in Table 4.1 the numerical results.

n_s	n'_s	α_s	α'_s	β_s	β'_s
0.9685	0.9685	$-4.99 \cdot 10^{-4}$	$7.69 \cdot 10^{-5}$	$-1.48 \cdot 10^{-5}$	$4.29 \cdot 10^{-4}$

Table 4.1: The predictions for the spectral index, the running of the spectral index and the running of the running in the Supergravity motivated model with a scalar field, for a choice of initial conditions $\psi_{ini} = 12\ M_{PL}$, $\chi_{ini} = 3\ M_{PL}$, with mass $m = 10^{-5.5}\ M_{PL}$. We denote the semi-analytical method predictions by n'_s, α'_s and β'_s. The numerical fit predictions are marked as n_s, α_s and β_s. The predictions for α_s and α'_s have opposite signs. The absolute values of α_s and α'_s are an order of magnitude different. The same is true for β_s and β'_s.

Our analysis of the chaotic potential with action (4.31) for $\alpha_m < 0$, confirms a similar pattern, whereby the predictions from the two methods for α_s can vary in sign and the same holds true for β_s.

We have shown that the numerical fit to the power spectrum evaluated to second order in slow-roll [47] does not always agree with the semi-analytical method introduced in Section 4.1, as we have discussed is the case for the Supergravity motivated model in Table 4.1. This means that for precise calculations, we have to go beyond the first order slow-roll approximation [60]. To improve the accuracy of the predictions,

one has to go to higher order in the approximations, in order to make predictions that can compare to data in the area of precision cosmology, as was also noted in [50] and [47].

4.6 Conclusions to the Study on the Fine-Structure of the Power Spectrum

We have looked at three different classes of models, the first an extension of Starobinsky inflation with a scalar field, the second a two-field model with chaotic potential and the third a supergravity embedded model. We have only observed positive values of α_s and β_s in the Starobinsky extension models. Although the results in [59] are not of a high-enough level of accuracy to exclude any of the models considered, they raise an interesting question about the hierarchy of the running of the spectral index α_s and the running of the running β_s and whether, as observational accuracy improves, these parameters could help discriminate between inflationary models. We have found that the semi-analytical method in [60] does not predict values in agreement with the numerical fit to the power spectrum evaluated to second order in slow-roll. Future work could explore the method to higher order.

Chapter 5

Preheating and Reheating in the Simplest Extension to the Starobinsky Model

In the previous chapters we have discussed what happens in two field models during inflation and what the predictions are at the end of inflation. In this Chapter we want to understand the behaviour of the fields and their decay at the end of inflation. After inflation, as the fields reach the minimum value of their potential, the Universe is in a state of very low temperature. A successful theory of inflation needs to be able to then 'reheat' the Universe to a temperature high enough for the subsequent phases of the Universe's evolution to occur. To present the theory of reheating and preheating, we follow the structure in [38]. Other reviews on the theory of reheating can be found in [76], [77], [78].

The first models of reheating were proposed by [73] and [74]. Reheating is explained as particle production caused by the decay of the inflaton fields near the minimum of

their effective potential. The inflaton fields oscillate near the minimum of the potential, but they experience the damping effect of the Hubble expansion. While the fields oscillate around the minimum of their potential, they decay into other particles. The process finishes when most of the energy of the fields has been converted into new particles. The equilibrium temperature at that stage is called the reheating temperature T_{reh}.

In this chapter we discuss the two main mechanisms for reheating the Universe after inflation, namely perturbative reheating and parametric resonance, and apply them to the extended Starobinsky model.

5.1 Theory of Reheating

5.1.1 Perturbative Reheating

We will briefly discuss the theory of perturbative reheating in the case of single field inflation. Let us consider the inflaton ϕ to be a collection of scalar particles with a finite probability of decaying, which couples to scalars ψ and fermions χ in the Lagrangian, with interaction defined as :

$$\mathcal{L}_{int} = -\nu\sigma\phi\psi^2 - h\phi\bar{\chi}\chi, \tag{5.1}$$

where σ has dimensions of mass and ν and h are dimensionless couplings (see [74], [75]). In the case of the inflaton being much heavier than the particles it decays into, the decay rates are :

$$\begin{aligned} \Gamma_{\phi\to\psi\psi} &= \frac{\nu^2\sigma^2}{8\pi m_\phi}, \\ \Gamma_{\phi\to\chi\bar{\chi}} &= \frac{h^2 m_\phi}{8\pi} \end{aligned} \tag{5.2}$$

Until $\Gamma > H$ the expansion of the Universe will not allow a thermal distribution to be reached, meaning there is an upper limit on the temperature after inflation. Solving for the temperature $\Gamma_{tot} = \Gamma_{\phi\to\psi\psi} + \Gamma_{\phi\to\chi\bar{\chi}} = H = (8\pi\rho/3M_{PL})^{1/2}$ with the assumption that all the energy density ρ of the universe is in the form of relativistic matter with $\rho = g_*\pi^2T^4/30$, where g_* is the effective number of massless degrees of freedom, we get the reheating temperature, T_{reh}:

$$T_{reh} \simeq 0.2\left(\frac{100}{g_*}\right)^{1/4}\sqrt{\Gamma_{tot}M_{PL}}. \tag{5.3}$$

The temperature changes if there are massive matter species, since the relationship between H and T is modified.

The CMB imposes another constraint, coming from the amplitude of anisotropies, which are kept low, provided that $m_\phi \sim 10^{-6}M_{PL}$.

To reiterate, after inflation finishes and the slow-roll parameters ϵ and η are of order one, the inflaton is at the minimum of its potential and it begins to oscillate around the minimum, damped by the expansion of the Universe. As it reaches a certain model dependent threshold, the inflaton decays into particles which behave like the beginning of the Hot Big Bang model. That is one of the requirements of model building, having a hot dense universe at the end of inflation; there are two main mechanisms which are used to describe this effect, namely perturbative reheating and parametric resonance.

5.1.2 Theory of Perturbative Reheating

The inflaton oscillates around the minimum value of its potential and the coherent oscillations can be considered as a collection of independent scalar particles. If these scalars can couple to other particles, the inflaton can decay perturbatively into lighter particles. The decay is described by an effective decay rate Γ_ϕ. Reheating - particle

production - only starts when the decay rate is about the same value as the Hubble parameter, $\Gamma_\phi \propto H$. The majority of the inflaton energy is in the $k = 0$ mode. In models with potentials that have a minimum, the energy oscillates coherently in space.

Consider the massive, chaotic inflation potential:

$$V(\phi) = \frac{1}{2} m_\phi^2 \phi^2 \tag{5.4}$$

At its minimum of $\phi = 0$ the inflaton will execute oscillations damped due to the expansion of the Universe:

$$\phi(t) = \bar{\phi}(t) \sin(m_\phi t), \quad \bar{\phi}(t) = \frac{M_{PL}}{\sqrt{3\pi} m_\phi t}. \tag{5.5}$$

The amplitude of the inflaton oscillations $\bar{\phi}(t)$ decreases in time. Inflation ends when the slow-roll parameter $\eta = 1$ and is approximately at $\phi_f = M_{PL}/2\sqrt{\pi}$. The initial amplitude for the oscillations of the field ϕ is slightly smaller than ϕ_f [76].

The system behaves classically to first approximation, so the inflaton can be treated as a classical external force acting on the quantum fields χ and ψ.

As the inflaton changes with time, so do the effective masses of the fields χ and ψ, which in turn leads to a non-adiabatic excitation of the field fluctuations by parametric resonance. Then the picture of the inflaton as a large collection of statistically independent particle breaks down.

So consider the system where the inflaton only couples to a scalar ψ through an interaction term :

$$L_{int} = \frac{1}{2} g^2 \phi^2 \psi^2, \tag{5.6}$$

where g is a dimensionless coupling. This describes the process of two ϕ particles decaying into two ψ particles. We will asume for simplicity that the inflaton potential

does not depend on the particles it will decay into, so the potential of the system is:

$$V_{eff}(\phi,\psi) = V(\phi) + \frac{1}{2}g^2\phi^2\psi^2 \tag{5.7}$$

The effective mass of the ψ particle is:

$$m^2_{\psi,eff} = \frac{\partial V_{eff}(\phi,\psi)}{\partial \psi^2} = g^2\phi^2(t). \tag{5.8}$$

Neglecting metric perturbations, the Fourier modes of the ψ field then obey the following Klein-Gordon equation:

$$\ddot{\psi}_k + 3H\dot{\psi}_k + \left[\frac{k^2}{a^2} + g^2\phi^2(t)\right]\psi_k = 0, \tag{5.9}$$

with $m_{\psi,eff}$ playing the role of mass in equation (5.9).

Equation (5.9) resembles a damped harmonic oscillator with a time-dependent mass. The frequency in that case is :

$$\omega_k = \left[k^2/a^2 + g^2\phi^2(t)\right]^{1/2} \tag{5.10}$$

and if it only varies slowly with time, then the solution to the equation can be approximated to that in which ω_k is constant, namely the solutions $\psi_k(t)$ do not grow, in a physical interpretation - there is no production of ψ particles. If the effective mass $m_{\psi,eff}$ changes rapidly in time, the WKB analysis breaks down. To quantitatively describe the two regimes, we define the dimensionless ratio :

$$R_a = \frac{\dot{\omega}_k}{\omega_k^2} \tag{5.11}$$

When $|R_a| << 1$, the particle number n_k is an adiabatic invariant, i.e. no particles are produced. When $|R_a| >> 1$, the particle number increases, in other words we observe particle production. We define n_k, the comoving occupation number of bosons in mode k as in [76], as the ratio of the total energy and the energy per particle ω_k. The total

energy is the sum of the kinetic energy $\frac{|\dot{\Psi}_k|^2}{2}$ and the potential energy $\omega_k^2\Psi_k^2 - \frac{\omega_k}{2}$, where the latter term is due to the zero state of the quantum system.

$$n_k = \frac{\omega_k}{2}\left(\frac{|\dot{\Psi}_k|^2}{\omega_k^2} + \Psi_k^2\right) - \frac{1}{2}, \tag{5.12}$$

where $\Psi_k = a^{3/2}\psi_k$ is the amplitude of the mode.

Looking at the dimensionless ratio R_a, defined in (5.11), and at the definition of the frequency in (5.10), we can approximate for the regime of long wavelengths with $k/aH << 1$ and with the effective mass defined in (5.8) given by the interaction term introduced in (5.6), the following:

$$R_a = \frac{\dot{\omega}_k}{\omega_k^2} = \frac{g^2\phi(t)\dot{\phi}(t)}{(k^2/a^2 + g^2\phi^2(t))^{32}} \approx \frac{\dot{\phi}}{g^2\phi^2} \approx \frac{m_\phi}{g^2\phi} \tag{5.13}$$

As the inflaton ϕ oscillates after inflation has ended, R_a diverges at every oscillation, when $\phi \to 0$; this means there is an explosion of particle production at every oscillation of the inflaton.

5.2 Reheating in the extension to the Starobinsky model

We now turn our attention to the extended Starobinsky model. The theory presented so far relies on *a*) the theory of General Relativity for the background expansion and *b*) on a single field decay. As shown in [79], the decay rates of the scalaron field are suppressed by a factor of $1/M_{PL}^2$. We will find that in the extended Starobinsly model, the dominant decay channel is the χ decay. Nevertheless, as we will show, the scalaron affects the background evolution and hence the efficiency of reheating and preheating. We will discuss the processes in both the Einstein and Jordan frames.

5.2.1 Perturbative Reheating

We start by recalling the action of the theory in the Jordan frame (3.1):

$$S_J = \int d^4x\sqrt{-g}\frac{1}{2\kappa}\Big[R + \mu\kappa R^2\Big] + \int d^4x\sqrt{-g}\Big[-\frac{1}{2}g^{\mu\nu}\nabla_\mu\chi\nabla_\nu\chi - \frac{1}{2}m^2\chi^2\Big] + S_{J\ Other}, \tag{5.14}$$

where $S_{J\ Other}$ contains information about the other energy forms in the Universe, which in the case we consider are matter particles that the field χ can decay into.

We have calculated the equations of motion for this action in (2.3) and we rewrite them here:

$$F(R)R_{\mu\nu} - \frac{1}{2}f(R)g_{\mu\nu} - \nabla_\mu\nabla_\nu F(R) + g_{\mu\nu}\Box F(R) = \kappa T^M_{\mu\nu}, \tag{5.15}$$

where $F(R) = \partial f(R)/\partial R$ and the trace of the equations of motion in (2.4), which is:

$$3\Box F(R) + F(R)R - 2f(R) = \kappa T, \tag{5.16}$$

where T is the trace of $T^M_{\mu\nu}$. If we perform a redefinition, we can rewrite (5.16) as the equation of a new scalar field $\phi = F(R) = 1 + 2\mu R$, with a potential defined by:

$$V_\phi = \frac{dV}{d\phi} = \frac{1}{3}(2f(R) - \phi R) = \frac{R}{3} = \frac{\phi - 1}{6\mu} \tag{5.17}$$

and a mass given by $m^2_\phi = V_{\phi\phi} = 1/6\mu$.

The equation of motion for ϕ becomes:

$$\Box\phi = V_\phi + \frac{\kappa}{3}T. \tag{5.18}$$

Using the fact that we are working in an FRW space-time, with $ds^2 = -dt^2 + a^2(t)d\mathbf{x}^2$ and the identity $\Box F(R) = \frac{1}{\sqrt{-g}}\partial_\mu(\sqrt{-g}g^{\mu\nu}\partial_\nu F(R))$, we find the equation of motion of ϕ to be:

$$\ddot{\phi} + 3H\dot{\phi} + V_\phi = \frac{\kappa}{3}(\rho_\chi - 3p_\chi), \tag{5.19}$$

where $\rho_\chi = \frac{1}{2}\dot{\chi}^2 + \frac{1}{2}m_\chi^2\chi^2$ and $p_\chi = \frac{1}{2}\dot{\chi}^2 - \frac{1}{2}m_\chi^2\chi^2$. The time evolution of H is governed by:

$$\begin{aligned} \dot{H} &= \frac{R}{6} - 2H^2 = \frac{\phi - 1}{12\mu} - 2H^2, \\ H^2 &= \frac{\kappa}{3\phi}\rho - \frac{f - \phi R}{6\phi} - \frac{\dot{\phi}}{\phi}H. \end{aligned} \tag{5.20}$$

The field equation for the field χ is:

$$\ddot{\chi} + 3H\dot{\chi} + m_\chi^2\chi = -\Gamma\dot{\chi} \tag{5.21}$$

and we have denoted the decay rate of χ into radiation by Γ. The equation for radiation is:

$$\dot{\rho}_r = -4H\rho_r + \Gamma\dot{\chi}^2, \tag{5.22}$$

where ρ_r is the radiation produced in the decay of χ.

As mentioned earlier, we use the fact that χ dominates the reheating process at the end of inflation. Therefore there are no decay terms introduced in the evolution equation for ϕ. In the Jordan frame ϕ influences the evolution of the Hubble parameter H. However, we want that both fields oscillate when they reach their minimum, so we will only look at cases where the mass ratios of the two fields m_ϕ/m_χ are $\mathcal{O}(1)$.

To understand the effect of perturbative reheating in our model, we will look at three quantities:

- The reheating temperature is defined by:

$$\rho_r = \frac{\pi^2}{30}g_{\text{dof}}T_{reh}^4, \tag{5.23}$$

  where $g_{\text{dof}} \approx 100$ is the number of relativistic degrees of freedom.

- The duration of the reheating phase $\Delta N = N_{er} - N_{ei}$.

- The e-fold averaged equation of state $w_{\rm Nav}$ is defined as follows

$$w_{\rm Nav} = \frac{1}{N_{er} - N_{ei}} \int_{N_{ei}}^{N_{er}} w dN \ , \tag{5.24}$$

where the subscripts 'ei' denotes the time at the end of inflation and 'er' the time at the end of reheating; w is the total equation of state, defined by

$$-\frac{\dot{H}}{H^2} = \frac{3}{2}(1+w) \ . \tag{5.25}$$

It can be shown that [80]:

$$w_{\rm Nav} \ = \ \frac{2}{3}\frac{1}{\Delta N} \ln\left(\frac{H_{ei}}{H_{er}}\right) - 1 \ . \tag{5.26}$$

To find the predictions we are interested in, we numerically integrate equations (5.19-5.22). We impose the condition that inflation last longer than 50 e-folds and integrate from the beginning of inflation until the end of the reheating phase, when the field χ has completely decayed into radiation such that $\rho_r a^4 = constant$ (5.22). Numerically, we define the end of reheating when $\rho_r/(\rho_\chi + \rho_r) > 0.9$. The choice of parameters is motivated by our previous work [1], presented in Chapter 3, chosen such that the inflationary predictions in our model are in agreement with the Planck 2015 data [20].

The numerical results for three choices of parameters are compiled in Table 5.1. As it can be seen, increasing m_ϕ relative to m_χ, which makes the R^2 corrections become less important, leads to a slight increase in the reheating temperature and the duration of reheating. On the other hand, decreasing m_ϕ and therefore increasing the importance of the R^2 correction, decreases the reheating temperature and shortens the reheating period. This can be understood physically by noting that, for $m_\phi < m_\chi$, χ will approach its minimum faster than ϕ. As a result, any radiation produced

m_ϕ/m_χ	$m_\chi(M_{PL})$	$T_{re}(GeV)$	$w_{\rm Nav}$	ΔN
1.5	$5.89 \cdot 10^{-6}$	$2.11 \cdot 10^{13}$	0.0416	5.17
1	$8.51 \cdot 10^{-6}$	$8.72 \cdot 10^{12}$	0.0066	4.95
0.9	$9.33 \cdot 10^{-6}$	$5.47 \cdot 10^{12}$	0.0998	4.86

Table 5.1: Reheating predictions for allowed values for m_ϕ and m_χ. Here we set $\Gamma = 10^{-3} m_\chi$. $\Delta N = N_{er} - N_{ei}$ is the duration of the reheating phase. The end of reheating is defined to be the time when $\rho_r/(\rho_\chi + \rho_r) > 0.9$.

by the decay of χ would be diluted away by the expansion of the universe as it is affected by the ϕ field. We illustrate the evolution of the fields in Fig. 5.1, where we choose identical initial conditions for three simulations with different mass ratios, i.e., $m_\phi < m_\chi$, $m_\phi = m_\chi$ and $m_\phi > m_\chi$. In our following analysis we fix the value of the decay rate $\Gamma = 10^{-3} m_\chi$.

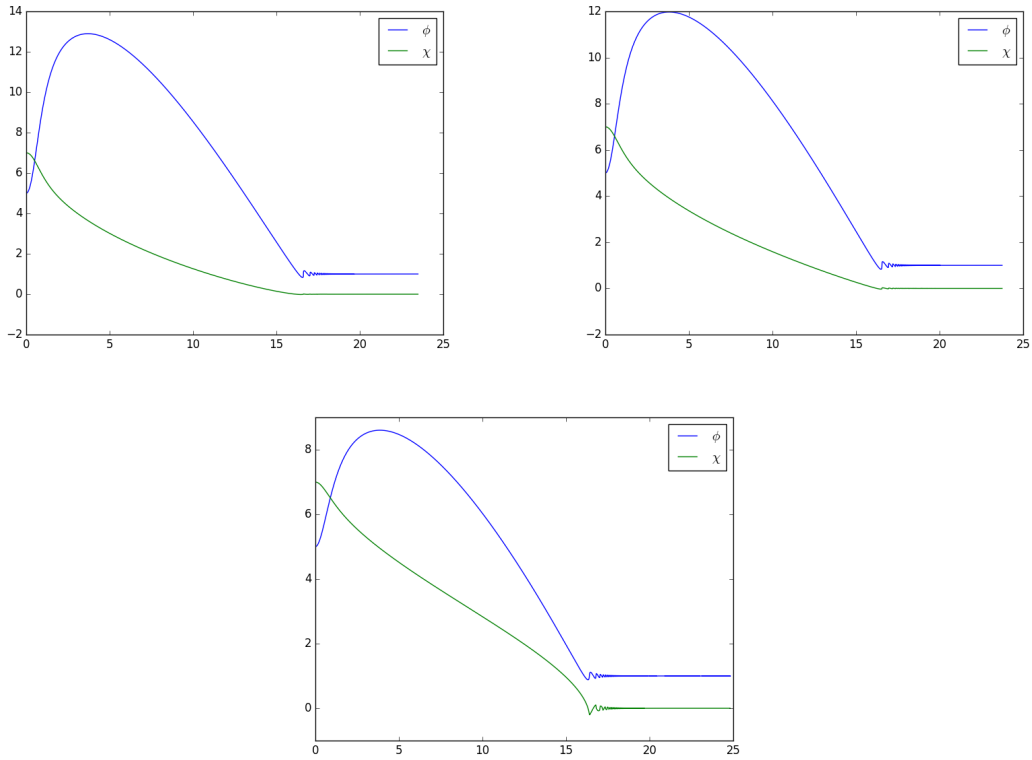

Figure 5.1: Inflationary trajectories for different mass ratios with identical initial conditions. On the top left, we show the case for $m_\chi > m_\phi$, on the top right $m_\chi = m_\phi$ and on the bottom $m_\chi < m_\phi$.

In summary, we have found that the more important the R^2 corrections are at the end of inflation relative to the contribution from the χ-field, the lower the reheating temperature and the shorter the reheating period.

5.2.2 Parametric Resonance

We turn now our attention to preheating in the extended Starobinsky model. We begin our analysis in the Jordan frame.

The view from the Jordan frame

We add an additional scalar field σ, which interacts directly with the χ field via a four-leg interaction term, so that the full action is given by

$$\begin{aligned} S = \frac{1}{2\kappa}\int d^4x\sqrt{-g}\Big[R+\mu R^2\Big] + \int d^4x\sqrt{-g} \quad \cdot \\ \cdot\Big[-\frac{1}{2}g^{\mu\nu}\partial_\mu\chi\partial_\nu\chi - \frac{1}{2}g^{\mu\nu}\partial_\mu\sigma\partial_\nu\sigma - \frac{1}{2}m_\chi^2\chi^2 - \frac{1}{2}m_\sigma^2\sigma^2 - \frac{1}{2}h^2\chi^2\sigma^2\Big]. \end{aligned} \tag{5.27}$$

The σ field is neglected during inflation, so we set its vacuum expectation value to be zero. The evolution of perturbations around the vacuum expectation value with momentum $\mathbf{k}$ obeys

$$\ddot{\sigma}_k + 3H\dot{\sigma}_k + \left(\frac{k^2}{a^2} + m_\sigma^2 + h^2\chi^2\right)\sigma_k = 0\,. \tag{5.28}$$

As is well known, in the standard Einstein gravity case, for certain values of k, parametric resonance can occur [81], resulting in an explosive growth of the particle number density n_k, given by

$$n_k = \frac{1}{2\omega_k}\left(|\dot{\sigma}_k|^2 + \omega_k^2|\sigma_k|^2\right) - \frac{1}{2}\,, \tag{5.29}$$

where $\omega_k^2 = (k/a)^2 + m_\sigma^2 + h^2\chi^2$.[1] We will now investigate whether this effect happens in the extended Starobinsky model.

We numerically integrate the equations for two cases with different mass ratios m_ϕ/m_χ, whilst fixing $m_\chi = 1.3 \cdot 10^{-6} \mathrm{M_{PL}}$, $m_\sigma = 10^{-2} m_\chi$, $h = 5 \cdot 10^{-4}$ and $k = 5 \cdot 10^{-7}$. In the first case, we choose $m_\phi = 1.5 m_\chi$. The results are shown in the left panel of Fig. 5.2. Here, the ϕ field oscillates around $\phi_{\min} = 1$ $\mathrm{M_{PL}}$, but the amplitude is rather small and therefore the modifications to General Relativity due to the R^2 corrections are not significant. The field χ oscillates around 0, but with a much larger amplitude. As it can be seen, the particle number density n_k of particles with momentum k, grows rapidly. Because $\phi \approx 1$, the dynamics of the field χ is very close to that of General Relativity. There are only minor deviations, due to the small oscillations of ϕ around 1 $\mathrm{M_{Pl}}$, affecting slightly the evolution of the expansion rate H.

In the second case, we choose $m_\phi = m_\chi$. The results are shown in the right panel of Figure 5.2. In this case, the field ϕ oscillates around $\phi_{\min} = 1$ $\mathrm{M_{Pl}}$ with a much larger amplitude, whereas the χ field oscillates around 0 with a smaller amplitude. As a consequence, the modifications to General Relativity are more important in this case, with the expansion rate H behaving in an unconventional way and showing oscillatory behaviour, due to the oscillations of the ϕ field, see eq. (5.20). As a result, the number density n_k in this second case does not exhibit much growth.

In summary, we have found that preheating is much less efficient if the R^2 corrections are large at the end of inflation. We attribute this to the impact of these corrections to the evolution of the expansion rate H, which in turn affects the evolution of χ.

[1] The equation above is justified by $n_k = \rho_k/\omega_k$, where ω_k is the energy of the harmonic oscillator with mode k and $\rho_k = \left(|\dot{\sigma}_k|^2 + \omega_k^2 |\sigma_k|^2\right)/2 - \frac{1}{2}\omega_k$ is the energy density with subtracted ground state energy $\omega_k/2$.

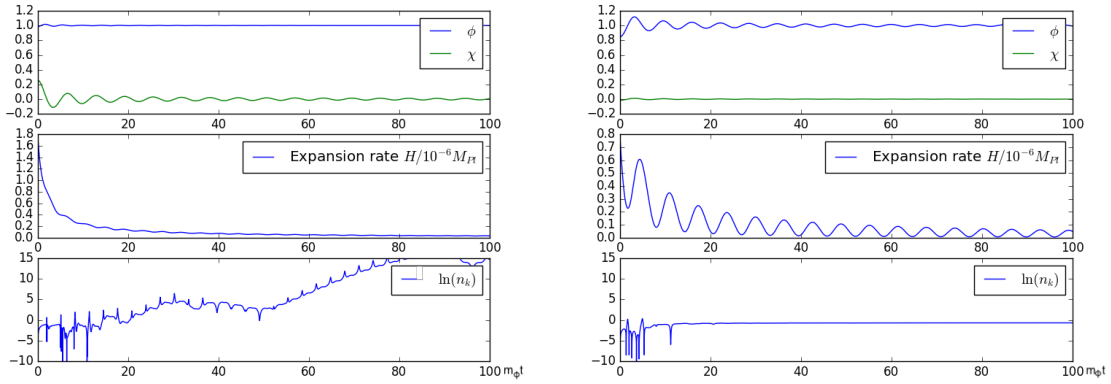

Figure 5.2: Preheating for mass ratio $m_\phi/m_\chi = 1.5$ (left) and $m_\phi/m_\chi = 1.0$ (right). The upper panels show the evolution of ϕ and χ at the end of inflation, the middle panels show the evolution of the expansion rate H and the lower panels show the particle number n_k, defined in eq. (5.29). We have chosen a value of k where we are in a band of instability. As it can be seen, the mass ratio affects the evolution of n_k significantly.

The view from the Einstein frame

The same question can be looked at in the Einstein frame, where the contributions from corrections to Einstein gravity affect the system through the altered kinetics of the fields. Whereas in the Jordan frame the field ϕ has to be displaced from its minimum value $\phi = 1M_{PL}$ for the Hubble parameter to be modified, as can be seen from eq. (5.20), in the Einstein frame that is no longer the case.

The conformal transformation to the Einstein frame is presented in Section 2.3 by considering $\tilde{g}_{\mu\nu} = e^{2\psi/\sqrt{6}} g_{\mu\nu}$, with $\psi = \sqrt{\frac{3}{2\kappa}} \ln(1 + 2\mu R)$ defined in (3.19). Then, choosing

$$g_{\mu\nu} = \text{diag}\left(-1, a^2(t), a^2(t), a^2(t)\right) \tag{5.30}$$

$$\tilde{g}_{\mu\nu} = \text{diag}\left(-1, a_E^2(t_E), a_E^2(t_E), a_E^2(t_E)\right) \ , \tag{5.31}$$

with $dt_E = e^{\psi/\sqrt{6}} dt$, the expansion rate in the Jordan frame $H = \dot{a}/a$ is related to the

expansion rate in the Einstein frame H_E, by

$$H_E \equiv \frac{1}{a_E}\frac{da_E}{dt_E} = e^{-\psi/\sqrt{6}}\left(H + \frac{1}{\sqrt{6}}\dot{\psi}\right) , \tag{5.32}$$

where the dot represents a derivative with respect to t. The equations of motion for the fields are :

$$\psi'' + 3H_E\psi' + V_\psi = -\frac{1}{\sqrt{6}}e^{-2\psi/\sqrt{6}}\chi'^2 , \tag{5.33}$$

$$\chi'' + (3H_E - \frac{2}{\sqrt{6}}\psi')\chi' + e^{2\psi/\sqrt{6}}V_\chi = 0 , \tag{5.34}$$

where the prime denotes the derivative with respect to t_E, $V_\psi = \partial V/\partial\psi$ and $V_\chi = \partial V/\partial\chi$. The Friedmann equation has the standard form in the Einstein frame. It is consistent to neglect the expansion of space (i.e. to set $H_E = 0$) and have both fields evolving. In this case the evolution of both fields are coupled via the kinetic terms. In addition, the masses of the χ– and σ–fields become ψ–dependent as well as the coupling h, which transforms as $h \to \tilde{h} = he^{-\psi/\sqrt{6}}$ and similarly for m_χ and m_σ. The evolution of the ψ–field, which encodes the modifications of gravity in the Einstein frame, affects the evolution of the χ–field in two ways. Firstly, χ acts as a source for the oscillations of the ψ–field. Secondly, an oscillatory ψ–field results in oscillations of the effective masses for χ and σ as well we as the coupling h. This is a very different situation from the one studied in [82], where the masses and couplings were not functions of ψ. In our model, if the amplitude of ψ is not negligible immediately after inflation, the equation for the perturbations of σ can no longer be written in Mathieu or Whittaker form and parametric resonance is mitigated.

5.3 Conclusion on Preheating Reheating

In this chapter we studied the periods of reheating and preheating in a simple extension of the Starobinsky inflationary model. The choices of parameters in this chapter are such that the predictions for the primordial power spectrum are consistent with the Planck 2015 data, as presented in Chapter 3. We considered the two most efficient ways of reheating in this model, namely perturbative reheating and parametric resonance, in order to better understand the implications to later stages in the evolution of the Universe of having matter fields present during inflation.

In the case of reheating, the mass m_ϕ of the scalar degree of freedom associated with the R^2 correction has an effect on the reheating temperature and the duration of reheating. As the corrections to Einstein gravity are made less important by increasing m_ϕ, the reheating temperature increases and the duration of reheating is longer. The influence is small for the parameter values we have considered, however it is of importance when comparing the theory to data. The change in the duration of reheating will affect the relation between the e-fold number and the wavenumber k of the physical scales, as can be seen from (1.68). The contribution is small, but not negligible.

In the case of preheating, we find that larger corrections to Einstein gravity at the end of inflation, result in less efficient particle production. The corrections affect the evolution of the expansion rate in the Jordan frame, which in turn affects the dynamics of the χ field. We also considered the situation from the perspective of the Einstein frame; the ψ-field, which encodes the corrections to Einstein gravity, couples in the Einstein frame to the χ and σ-fields. Specifically, the masses and couplings of χ and σ become ψ-dependent and the oscillating behaviour of ψ influences particle production.

We have shown that modifications of gravity have an effect in the reheating phase

of the evolution of the Universe and these modifications due to corrections to gravity have to be taken properly into account when comparing the theory to data.

Chapter 6

Conclusions

The theory of inflation offers an elegant solution to some questions about observational facts the Universe. There are numerous models of inflation, as we mention in Chapter 1. In recent years, the accuracy of observational measurements has improved and a large number of models have been ruled out by observations. The Starobinsky model is one of the favoured models by the latest Planck results, predicting a nearly flat power spectrum and a small tensor-to-scalar ratio. We were interested in investigating the robustness of these results and how the predictions would change if we allow the dynamics of inflation to be co-driven by an additional scalar field.

We outlined the theory for General Relativity and Inflation in Chapter 1. What followed in Chapter 2 was an analysis of the Starobinsky model, where an R^2 term is added to the Ricci scalar in the Einstein-Hilbert action. We showed that the modification to General Relativity can be redefined with the help of a conformal transformation and the action was shown to take the form of the standard Einstein-Hilbert action with an additional scalar field called the scalaron. We showed that for inflation lasting ~ 50 e-folds, the predictions for the value of the spectral index in the Starobinsky model,

are ~ 0.96, which is in the range favoured by the 2015 observational results from the Planck collaboration.

In Chapter 3 we analysed what we refer to as the simplest extension to the Starobinsky model, a model which adds a μR^2 correction to the Einstein-Hilbert action and an additional scalar field, we denote by χ. To simplify the calculations we performed a conformal transformation and field redefinition to go from the Jordan frame to the Einstein frame, where the action takes the form of standard General Relativity with two scalar fields, one describing the contributions of the μR^2 correction, which we called ψ, and the other, the χ field, which acquires a non-standard kinetic term in this frame. We found that the predictions for the spectral index, amplitude of the power spectrum and tensor-to-scalar ratio in this model do not vary much under changes to conditions for the initial starting values of the fields. When we varied the masses of the fields, m_χ and m_ψ, we observed a more significant variation in predictions. The strongest constraint on the model comes from the value of the amplitude of the power spectrum. We have shown that for any given choice of mass ratio $R_m = m_\psi/m_\chi$ considered, we can find a mass range for m_χ, such that the predictions for A_s and n_s are within the Planck allowed range. The tensor-to-scalar ratio is predicted to be small, for the masses considered.

In Chapter 4 we investigated the running of the spectral index $\alpha_s = \frac{dn_s}{d\ln k}$ and the running of the running $\beta_s = \frac{d\alpha_s}{d\ln k}$ in a number of inflationary models. We did this with the help of two different numerical fits from the Scipy library on the evaluation of the power spectrum to second order in slow-roll defined in Chapter 3. We started by analysing the extended Starobinsky model, which was the focus of Chapter 3. We found that there are choices of masses of the fields ψ and χ, that predict a positive

running of the running β_s for a negative running of the spectral index α_s , as can be seen in Figure 4.3, whilst also predicting a spectral index and amplitude of the power spectrum in agreement with the Planck 2015 results. We proceeded to investigate the effects of altering the action by changing the value of the parameter $b(\psi)$. We found that reducing the parameter by a factor of 10 resulted in negative β_s and positive α_s; when we increased $b(\psi)$ by a factor of 2, we found negative values for both α_s and β_s. In all cases considered the absolute value of the running of the spectral index is of higher order than the absolute value of the running of the running. We also included in our analysis a model motivated by supergravity and models which have two scalar fields, ψ and χ, where the latter has a non-standard kinetic term, with potential $\frac{1}{2}m_\psi^2 + \frac{1}{2}m_\chi^2$. Our results show that α_s and β_s are both negative in these models and that $\mathcal{O}|\alpha_s| > \mathcal{O}|\beta_s|$. We have demonstrated that the Starobinsky model with a scalar field and its modifications can predict positive values for either α_s or β_s whilst predicting values for n_s and A_s which are in agreement with Planck 2015 results. The analysis on the Planck CMB data [59] seems to favour models which predict positive β_s at the 2σ confidence level and we have shown that the extended Starobinsky model can give such predictions.

In Chapter 5 we studied the end of inflation in the extended Starobinsky theory. We were interested in particular in reheating and preheating. We found that the scalaron mass inhibits the rise in temperature caused by the additional inflationary field's decay. The duration of reheating is not negligible, which is an important result for comparing theoretical predictions to data. The scalaron was also shown to affect the efficiency of particle production at the end of perturbative reheating.

Following the results from Chapter 4, we would be interested in developing the first

order approximation in the analytical calculation to include higher order corrections to the power spectrum and understand how the predictions for the running of the spectral index and the running of the running would change. Current observational results are approaching levels of accuracy which need to be met from a theoretical model building perspective as well. It would also be of interest to explore further modifications of the $b(\psi)$ parameter in the Starobinsky model with a scalar field, to see if one can match the numerical predictions for α_s and β_s from Planck.

The original Starobinsky model predictions are in good agreement with the observational CMB results form Planck 2015. The work presented in this thesis shows that the predictions of the Starobinsky model with a scalar field present during inflation are in a favoured position with respect to observational data. The model proves to be very robust, even under the addition of a new matter species. What we have shown is also the relevance of higher order corrections to slow-roll and to the structure of the power spectrum in this model. Lastly, we have discussed how the scalaron affects the period immediately after inflation. We hope that this work will be relevant to inflationary model building and possibly embedding the model into a more fundamental theory.

Appendix A

Conformal Transformations

We define a conformal transformation as rescaling of the metric tensor at each point in the space-time:

$$\tilde{g}_{\mu\nu} = \Omega^2 g_{\mu\nu} \quad \rightarrow \sqrt{-\tilde{g}} = \Omega^4 \sqrt{-g}, \tag{A.1}$$

where $\Omega = \Omega(x)$ is a nonvanishing regular function. These transformations change the the norm of space-like and time-like vectors, whilst leaving light cones unchanged and not disturbing the causal structure of the space. Using the definition in (1.3) we see that the Christoffel coefficients change under a conformal transformations as:

$$\tilde{\Gamma}^{\alpha}_{\beta\gamma} = \Gamma^{\alpha}_{\beta\gamma} + \Omega^{-1}\left(\delta^{\alpha}_{\beta}\nabla_{\gamma}\Omega + \delta^{\alpha}_{\gamma}\nabla_{\beta}\Omega - g_{\beta\gamma}\nabla^{\alpha}\Omega\right). \tag{A.2}$$

We can calculate the change in the Ricci tensor using its definition in (1.4) on a space of dimension $n = 4$:

$$\begin{aligned}\tilde{R}_{\alpha\beta} =& R_{\alpha\beta} - 2\nabla_{\alpha}\nabla_{\beta}(\ln\Omega) - g_{\alpha\beta}g^{\delta\gamma}\nabla_{\delta}\nabla_{\gamma}(\ln\Omega) + 2\nabla_{\alpha}(\ln\Omega)\nabla_{\beta}(\ln\Omega) - \\ & - 2g_{\alpha\beta}g^{\delta\gamma}\nabla_{\delta}(\ln\Omega)\nabla_{\gamma}(\ln\Omega).\end{aligned} \tag{A.3}$$

The transformed Ricci scalar is:

$$\begin{aligned}\tilde{R} &= \tilde{g}^{\alpha\beta}\tilde{R}_{\alpha\beta} \\ &= \Omega^{-2}\left[R - 6\Box(\ln\Omega) - 6\frac{g^{\alpha\beta}\nabla_\alpha\Omega\nabla_\beta\Omega}{\Omega^2}\right] \\ &= \Omega^{-2}\left[R - \frac{6\Box\Omega}{\Omega}\right]\end{aligned} \tag{A.4}$$

$$R = \Omega^2\tilde{R} + 6\tilde{g}^{\mu\nu}\Omega(\tilde{\nabla}_\mu\tilde{\nabla}_\nu\Omega) - 12\tilde{g}^{\mu\nu}(\tilde{\nabla}_\mu\Omega)(\tilde{\nabla}_\nu\Omega). \tag{A.5}$$

The conformal transformation will affect not only the gravitational part of the action, but also any other scalars that exist in the theory. For example, let us consider a scalar field χ of mass m_χ with action:

$$S_\chi = \int d^4x\sqrt{-g}\Big[-\frac{1}{2}g^{\mu\nu}\nabla_\mu\chi\nabla_\nu\chi - \frac{1}{2}m_\chi^2\chi^2\Big]. \tag{A.6}$$

Under the conformal transformation in (A.1) it becomes:

$$S_\chi = \int d^4x\sqrt{-\tilde{g}}\big[-\frac{1}{2}\tilde{g}^{\mu\nu}\Omega^{-2}(\tilde{\nabla}_\mu\chi)(\tilde{\nabla}_\nu\chi) - \frac{1}{2}m_\chi^2\Omega^{-4}\chi^2\big]. \tag{A.7}$$

Bibliography

[1] C. van de Bruck and L. E. Paduraru, Phys. Rev. D **92** (2015) 083513 [arXiv:1505.01727 [hep-th]].

[2] C. van de Bruck, P. Dunsby and L. E. Paduraru, Int. J. Mod. Phys. D **26** (2017) no.13, 1750152 [arXiv:1606.04346 [gr-qc]].

[3] A. Einstein, *Sitzungsber.Preuss.Akad.Wiss.Berlin (Math.Phys.)*, vol. 1915, pp. 844–847, 1915.

[4] A. Einstein, *Annalen Phys.*, vol. 49, pp. 769–822, 1916.

[5] A. Einstein, Sitzungsber. Preuss. Akad. Wiss. Berlin (Math. Phys.) **1917** (1917) 142.

[6] U.J.J. Le Verrier, *Comptes Rendus*, vol. 49, pp. 379–383, 1859.

[7] A. Einstein, Sitzungsber. Preuss. Akad. Wiss. Berlin (Math. Phys.) **1915** (1915) 831.

[8] R. V. Pound and J. L. Snider, Phys. Rev. Lett. **13** (1964) 539.

[9] V. M. Slipher, *Proc.Am.Phil.Soc.*, vol. 56, pp. 403–409, 1917.

[10] E. Hubble, *Astrophys.J.*, vol. 64, pp. 321–369, 1926.

[11] E. Hubble, *Proc.Nat.Acad.Sci.*, vol. 15, pp. 168–173, 1929.

[12] G. Lemaitre, Annales Soc. Sci. Bruxelles A **47** (1927) 49 [Gen. Rel. Grav. **45** (2013) no.8, 1635].

[13] W. de Sitter, Mon. Not. Roy. Astron. Soc. **78** (1917) 3.

[14] G. Lemaitre, Nature **127** (1931) 706 [Gen. Rel. Grav. **43** (2011) 2929].

[15] G. Lemaitre, Gen. Rel. Grav. **29** (1997) 641 [Annales Soc. Sci. Bruxelles A **53** (1933) 51].

[16] G. Lemaître, "*Comptes Rendus de L'Academie des Sciences de Paris*, vol. 196, pp. 903–904, 1933.

[17] A. Friedmann, *Z.Phys.*, vol. 10, pp. 377–386, 1922.

[18] A. Friedmann, *Zeitschrift fur Physik*, vol. 21, pp. 326–332, Dec. 1924.

[19] A. A. Penzias and R. W. Wilson, *Astrophys.J.*, vol. 142, pp. 419–421, 1965.

[20] P. A. R. Ade *et al.* [Planck Collaboration], Astron. Astrophys. **594** (2016) A13 [arXiv:1502.01589 [astro-ph.CO]].

[21] R. H. Dicke, P. J. E. Peebles, P. G. Roll and D. T. Wilkinson, Astrophys. J. **142** (1965) 414.

[22] R. A. Alpher, H. Bethe and G. Gamow, Phys. Rev. **73** (1948) 803.

[23] R. K. Sachs and A. M. Wolfe, Astrophys. J. **147** (1967) 73 [Gen. Rel. Grav. **39** (2007) 1929].

[24] G. F. Smoot *et al.* [COBE Collaboration], Astrophys. J. **396** (1992) L1.

[25] E. L. Wright *et al.*, Astrophys. J. **396** (1992) L13.

[26] G. Hinshaw *et al.* [WMAP Collaboration], Astrophys. J. Suppl. **208** (2013) 19 [arXiv:1212.5226 [astro-ph.CO]].

[27] A. H. Guth, Phys. Rev. D **23** (1981) 347.

[28] A. D. Linde, *Phys.Lett.*, vol. B108, pp. 389–393, 1982.

[29] A. D. Linde, *Phys.Lett.*, vol. B129, pp. 177–181, 1983.

[30] A. Albrecht and P. J. Steinhardt, Phys. Rev. Lett. **48** (1982) 1220.

[31] A. A. Starobinsky, Phys. Lett. **91B** (1980) 99.

[32] A. D. Linde, Phys. Lett. B **175** (1986) 395.

[33] D. Langlois, Lectures given at Conference: C03-08-04, p.235-278 Proceedings, hep-th/0405053.

[34] J. Martin, C. Ringeval and V. Vennin, Phys. Dark Univ. **5-6** (2014) 75 [arXiv:1303.3787 [astro-ph.CO]].

[35] A. D. Linde, Phys. Rev. D **49** (1994) 748 [astro-ph/9307002].

[36] A. R. Liddle and S. M. Leach, Phys. Rev. D **68** (2003) 103503 [astro-ph/0305263].

[37] A. Riotto,ICTP Lect. Notes Ser. **14** (2003) 317 [hep-ph/0210162].

[38] B. A. Bassett, S. Tsujikawa and D. Wands, Rev. Mod. Phys. **78** (2006) 537 [astro-ph/0507632].

[39] V. N. Lukash, Sov. Phys. JETP **52** (1980) 807 [Zh. Eksp. Teor. Fiz. **79** (1980) 1601].

[40] D. H. Lyth, Phys. Rev. D **31** (1985) 1792.

[41] V. F. Mukhanov, H. A. Feldman and R. H. Brandenberger, Phys. Rept. **215** (1992) 203.

[42] A. De Felice and S. Tsujikawa, Living Rev. Rel. **13** (2010) 3 [arXiv:1002.4928 [gr-qc]].

[43] T. P. Sotiriou and V. Faraoni, Rev. Mod. Phys. **82** (2010) 451 [arXiv:0805.1726 [gr-qc]].

[44] L. Sebastiani and R. Myrzakulov, Int. J. Geom. Meth. Mod. Phys. **12** (2015) no.9, 1530003 [arXiv:1506.05330 [gr-qc]].

[45] H. A. Buchdahl, Mon. Not. Roy. Astron. Soc. **150** (1970) 1.

[46] M. Giovannini, "A primer on the physics of the cosmic microwave background," Singapore, Singapore: World Scientific (2008) 488.

[47] C. van de Bruck and M. Robinson, JCAP **1408** (2014) 024 [arXiv:1404.7806 [astro-ph.CO]].

[48] D. Wands, N. Bartolo, S. Matarrese and A. Riotto, Phys. Rev. D **66** (2002) 043520 [astro-ph/0205253].

[49] C. Gordon, D. Wands, B. A. Bassett and R. Maartens, Phys. Rev. D **63** (2001) 023506 [astro-ph/0009131].

[50] A. Avgoustidis, S. Cremonini, A. C. Davis, R. H. Ribeiro, K. Turzynski and S. Watson, JCAP **1202** (2012) 038 [arXiv:1110.4081 [astro-ph.CO]].

[51] Z. Lalak, D. Langlois, S. Pokorski and K. Turzynski, JCAP **0707** (2007) 014 [arXiv:0704.0212 [hep-th]].

[52] V. F. Mukhanov, Sov. Phys. JETP **67** (1988) 1297 [Zh. Eksp. Teor. Fiz. **94N7** (1988) 1].

[53] M. Sasaki, Prog. Theor. Phys. **76** (1986) 1036.

[54] P. Peter, J.P. Uzan, "Primordial Cosmology ," OUP Oxford, ISBN-13: 978-0199665150.

[55] A. R. Liddle and D. H. Lyth, "Cosmological inflation and large scale structure," Cambridge, UK: Univ. Pr. (2000) 400.

[56] S. Gottlober, V. Muller and A. A. Starobinsky, Phys. Rev. D **43** (1991) 2510.

[57] P. A. R. Ade *et al.* [Planck Collaboration], Astron. Astrophys. **571** (2014) A16 [arXiv:1303.5076 [astro-ph.CO]].

[58] M. Escudero, H. Ramrez, L. Boubekeur, E. Giusarma and O. Mena, JCAP **1602** (2016) no.02, 020 [arXiv:1509.05419 [astro-ph.CO]].

[59] G. Cabass, E. Di Valentino, A. Melchiorri, E. Pajer and J. Silk, Phys. Rev. D **94** (2016) no.2, 023523 [arXiv:1605.00209 [astro-ph.CO]].

[60] C. van de Bruck and C. Longden, Phys. Rev. D **94** (2016) no.2, 021301 [arXiv:1606.02176 [astro-ph.CO]].

[61] S. Gariazzo, O. Mena, H. Ramrez and L. Boubekeur, Phys. Dark Univ. **17** (2017) 38 [arXiv:1606.00842 [astro-ph.CO]].

[62] M. Peloso, L. Sorbo and G. Tasinato, JCAP **1406** (2014) 040 [arXiv:1401.7136 [astro-ph.CO]].

[63] J. Garcia-Bellido and D. Roest, Phys. Rev. D **89** (2014) no.10, 103527 [arXiv:1402.2059 [astro-ph.CO]].

[64] K. Kohri and T. Matsuda, JCAP **1502** (2015) 019 [arXiv:1405.6769 [astro-ph.CO]].

[65] M. Bojowald, G. Calcagni and S. Tsujikawa, JCAP **1111** (2011) 046 [arXiv:1107.1540 [gr-qc]].

[66] J. Garriga and V. F. Mukhanov, Phys. Lett. B **458** (1999) 219 [hep-th/9904176].

[67] D. Langlois, S. Renaux-Petel, D. A. Steer and T. Tanaka, Phys. Rev. D **78** (2008) 063523 [arXiv:0806.0336 [hep-th]].

[68] D. Wands, K. A. Malik, D. H. Lyth and A. R. Liddle, Phys. Rev. D **62** (2000) 043527 [astro-ph/0003278].

[69] F. Di Marco and F. Finelli, Phys. Rev. D **71** (2005) 123502 [astro-ph/0505198].

[70] E. Jones, E. Oliphant, P. Peterson, et. al. "SciPy: Open Source Scientific Tools for Python, 2001-," http://www.scipy.org/ .

[71] E. Oliphant, "A guide to NumPy,' USA: CreateSpace Independent Publishing Platform , USA 2015 ISBN:151730007X 9781517300074.

[72] J. Ellis, M. A. G. Garcia, D. V. Nanopoulos and K. A. Olive, JCAP **1408** (2014) 044 [arXiv:1405.0271 [hep-ph]].

[73] L. F. Abbott, E. Farhi and M. B. Wise, Phys. Lett. **117B** (1982) 29.

[74] A. D. Dolgov and A. D. Linde, Phys. Lett. **116B** (1982) 329.

[75] A. D. Linde, Contemp. Concepts Phys. **5** (1990) 1 [hep-th/0503203].

[76] L. Kofman, A. D. Linde and A. A. Starobinsky, Phys. Rev. D **56** (1997) 3258 [hep-ph/9704452].

[77] R. Allahverdi, R. Brandenberger, F. Y. Cyr-Racine and A. Mazumdar, Ann. Rev. Nucl. Part. Sci. **60** (2010) 27 doi:10.1146/annurev.nucl.012809.104511 [arXiv:1001.2600 [hep-th]].

[78] V. Mukhanov, "Physical Foundations of Cosmology," ISBN: 9780521563987.

[79] D. S. Gorbunov and A. G. Panin, Phys. Lett. B **700** (2011) 157 [arXiv:1009.2448 [hep-ph]].

[80] C. van de Bruck, K. Dimopoulos and C. Longden, Phys. Rev. D **94** (2016) no.2, 023506 [arXiv:1605.06350 [astro-ph.CO]].

[81] L. Kofman, A. D. Linde and A. A. Starobinsky, Phys. Rev. Lett. **73** (1994) 3195.

[82] J. Lachapelle and R. H. Brandenberger, JCAP **0904** (2009) 020 [arXiv:0808.0936 [hep-th]].

[83] T. P. Sotiriou, Thesis SISSA, Trieste INFN, Trieste [arXiv:0710.4438 [gr-qc]].

[84] JOUR 1844, Monthly Notices of the Royal Astronomical Society December 13, 1844 6(11):136.